UNIVERSITY OF BIRMINGHAM

Preparation and Testing of Catalysts for Fuel Upgrading

By

ISMAILA MUDI

A thesis submitted to
The University of Birmingham
for the degree of
DOCTOR OF PHILOSOPHY

School of Chemical Engineering
College of Engineering and Physical Science
University of Birmingham
October2023

Abstract

In this study, biochar which is a by-product of pyrolysis was used as a support to develop robust, novel, and renewable Ni/biochar catalyst for hydrodeoxygenation (HDO) of bio-oil and its model oxygenate organic compounds, such as vanillin and furfural. Through chemical treatment with H_2SO_4 (sulfuric acid) and KOH (potassium hydroxide), the textural and physicochemical features of the biochar support were modified to increase mass transfer and active metal dispersion. The catalysts were characterised by a range of physical and chemical techniques. The catalysts were used in the HDO of vanillin, hydrogenation of furfural, and the HDO of bio-oil itself using a 100 mL Parr reactor, catalyst loading 0.4–0.8 g, temperature 100°C to 150°C, hydrogen (H_2) pressures of 30 to 50 bar, and a stirring rate of 1000 rpm. The three catalysts were tested for the HDO of vanillin, a typical oxygenate phenolic compound found in bio-oil, into creosol. Over the unmodified 15wt% Ni/biochar catalyst, vanillin conversion of up to 97% with 91.17% selectivity to p-creosol was achieved; in addition to being extremely selective and active for p-creosol, which can be used as a future biofuel, the catalyst was stable for four successive experimental cycles. Chemical treatments of the biochar support increased its physicochemical characteristics, which led to a better catalytic performance in terms of vanillin conversion and p-creosol production in the sequence Ni/biochar(H_2SO_4) > Ni/biochar (KOH) > Ni/biochar, which is the same order of specific surface area and mesoporosity increase. The kinetics of liquid-phase furfural hydrogenation into 2-methylfuran also was studied using 15wt% Ni/biochar(H_2SO_4) catalyst. The results demonstrate that at 1000 rpm stirring rate and 106 µm catalyst particle size, both external and intraparticle mass transport constraints were insignificant, ensuring kinetically controlled experiments. Three plausible Langmuir–Hinshelwood-Hougen-Watson (LHHW) kinetic type models, competitive (Model I), with a competitive adsorption site (Model II) and a non-competitive adsorption site (Model III), were screened based on the fact that an R^2 value greater

than 99% demonstrated that the experimental data were satisfactorily fit to the model. Based on the correlation coefficient of more than 99% between experimental and predicted rates, the best fit is model III, which is a dual-site adsorption mechanism involving furfural adsorption as well as hydrogen dissociative adsorption and surface reactions. It was found that when the sulfuric acid treatment duration of the biochar used to prepare Ni/biochar(H_2SO_4) catalyst increased from 3 to 9 hours, the conversion of furfural and the yield of 2-methyl furan increased. In addition to the hydrogen present in the solution, the competitive adsorption of furfural and vanillin for the catalyst active sites limits the conversion due to hydrogenation and HDO in a binary model compounds process. The conversion of furfural via hydrogenation was substantially greater than HDO of vanillin in the binary system of model compounds. Based on the results of four successive experimental studies, the developed Ni/biochar(H_2SO_4) catalyst proved remarkable stability in terms of furfural conversion (96%) and 2-methylfuran yield (54%) at the 4^{th} experiment compared to 99% and 57% for the 1^{st} experiment. In terms of the bio-oil itself, HDO catalytic upgrading of bio-oil decreased oxygenates from 13.02% (crude bio-oil) to 8.3% (commercial TK-341 catalyst) and 5.93% (sulfided Ni/biochar(H_2SO_4) catalyst. Whilst the hydrocarbon components of the upgraded bio-oil can be summarised as thus: 90.39% (commercial TK-341 catalyst) and 93.56% (sulfided Ni/biochar(H_2SO_4) catalyst) catalytic upgrading was accomplished, compared to 71.26% for the crude bio-oil. Thus, the developed 15wt% Ni/biochar(H_2SO_4) catalyst demonstrated superior performance than the commercial TK-341 catalyst in this investigation. This can be attributed to the enhanced mesopores, and surface of the biochar support treated with sulfuric acid.

Dedication

This research work is dedicated to my beloved parent late Mal. Tanimu Danjumma and Hajiya Habiba Suleman and to all the innocent men, women and children who are victims of wars across the world. This work is also specially dedicated to Petroleum Technology Development Fund (PTDF), Nigeria and the University of Birmingham for their financial support.

Acknowledgement

All praise is due to Allah (S.W. A) The provider and most generous. Oh Allah, I thank you for giving me the fortitude and vigor to endure all the challenges encountered during this research work.

My profound appreciation and gratitude go to Prof. Joseph Wood for his guidance, suggestions, and supervision throughout the period of my research work. I would also like to thank June Callison, Lisa Allen, and Sining Chen from Harwell Research Complex and Dr. Miloud Ouadi and Marcin Sajdak of Birmingham Energy Innovation Centre for their collaborations and help with catalyst characterization and HDO of bio-oil respectively.

My appreciation also goes to Dr. Abarasi Hart for helping with proof reading.

I wish to express my gratitude to Zoe Simon, Chyntol Kanhimbe and Jonathan Goldfinch from school of chemical engineering, university of Birmingham and John Wedderburn from Metallurgy and Materials, University of Birmingham for their technical support.

I would like to convey my heartfelt appreciation to my parents, late Malam Tanimu Danjumma and Hajiya Habiba Suleman for their prayers and support.

My sincere gratitude to Aunty Ni'ima, Aunty Mero, Uncle Abdullahi Suleman, Uncle Yusuf Mudi and Uncle Sani Mudi. I also acknowledge Petroleum Technology Development Fund (PTDF), Nigeria for their financial support.

Table of Contents

List of Figures

List of Tables

Nomenclature

Abbreviation	Meaning
HDO	Hydrodeoxygenation
TCR	Thermochemical conversion
KOH	Potassium hydroxide
H_2SO_4	Hydrogen tetraoxosulfate (vi)
CO_2-TPD	Carbondioxide temperature programmed desorption
H_2-TPR	Hydrogen temperature programmed reduction
SEM	Scanning electron microscopy
EDX	Energy dispersive X-ray
XRF	X-ray fluorescence spectroscopy
TGA	Thermogravimetric analysis
FT-IR	Fourier-transform-infrared spectroscopy
HPLC	High perfomance liquid chromatography
r_0	Initial reaction rate
R	Reaction rate
R_{gas}	Universal gas constant
N	Effectiveness factor
Φ	Thiele modulus
N_A	Avogadro's number
W	Catalyst loading
L	Characteristic length of spherical catalyst particle
C_H	Dissolved Hydrogen concentration in solvent
C_{SB}	Concentration of substrate
K_S	Surface reaction constant
K_H	Hydrogen adsorption constant
K_{SB}	Substrate adsorption constant
C_p	Desired product concentration
R	Rate of reaction
A_{bs}	Absorbance
A	Pre-exponential factor
ε	Molar extinction coefficient
B	Length
V	Quantity of gas adsorbed
P_0	Saturated pressure of adsorbate
P	Equilibrium pressure of adsorbate
P_{eq}	Equilibrium pressure of adsorptive nitrogen
V_m	Quantity of gas absorbed
S	Area of adsorbed N_2 gas molecules
M_V	Molar volume of gas adsorbed
r_k	Radius of curvature of the adsorptive condensed in the pore
r_p	cylindrical radius

Ta	thickness of adsorbed film
2θ	Diffraction angle
D	Lattice spacing
Λ	Wavelength
M_p	Mass of product
M_r	Mass of reactant
E_a	Activation energy
K	Rate constant
C	Concentration
N	Order of reaction

Chapter One

Introduction

1.1 Background

Modern society heavily relies on transportation for economic and social development, making it the major contributor of carbon dioxide (CO_2) emissions. As fossil fuels such as crude oil reserves deplete, the need for an alternative transportation fuel source becomes increasingly evident. Additionally, the increasing concerns of global warming, climate change, and peak oil caused by the continued use of petroleum-based fuels drive the development of renewable and sustainable alternatives. The abundance of lignocellulosic biomass on earth, coupled with the fact that it is bio-renewable, has made it a promising alternative to fossil fuels [1]. Biomass can be converted into bio-oil, which can then be upgraded over a heterogeneous catalyst to produce biofuels and chemicals. This is the concept and upgrading methodology that the present research study focuses on.

In recent years, both industry and academia have been focusing on the possibility of upgrading lignocellulosic biomass-derived bio-oils to partially replace crude oil as transportation fuels [2]. Through its CO_2 neutrality, lignocellulosic biomass-derived bio-oils would help to minimize the dependence on petroleum-based fuels, as well as mitigate emissions of carbon dioxide that cause global warming. However, bio-oils are a complex mixture of numerous oxygenated organic compounds, regardless of lignocellulosic biomass origin. As a result, their transition to liquid hydrocarbon biofuels must incorporate oxygen removal to make them compactible with engines. Additionally, the benefit of biomass feedstock for bio-oil production is that it contains lower quantities of sulfur, nitrogen, and metals than fossil oils and is sustainable and widely available. It is also currently only biomass that can be used to produce

liquid biofuels for existing transportation infrastructure as a renewable source of hydrocarbons and chemicals.

Bio-oil can be produced from lignocellulosic biomass via hydrothermal liquefaction and pyrolysis [2-4]. The produced bio-oils have certain undesirable features for fuel applications, generally due to the oxygenate organic compounds, which includes poor heating value (less than 50% of that of conventional oils), immiscibility with petroleum-based fuels, thermal and chemical instability, high density and viscosity, corrosiveness, and other drawbacks [2,5,6]. It is highly recommended to upgrade bio-oil with deoxygenation steps, which reduce the oxygen content, to improve their stability and miscibility with conventional fuels [7]. Two main routes to achieve this have been proposed, based on laboratory studies and industrial experience: hydrodeoxygenation (HDO) and zeolite catalytic cracking, which are well established refinery technologies.

Hydroprocessing (i.e., hydrodesulfurisation (HDS), hydrodenitrogenation (HDN) and hydrotreatment), which includes removing heteroatoms (such as S, O, and N) from crude oil refined products and hydrogenating olefins by hydrogen addition, can be applied in the catalytic upgrading of pyrolysis bio-oil [8]. The HDS and HDN of petroleum products with negligible oxygen content is well recognised processes, so the mechanistic pathways for removing sulfur and nitrogen have been established in extensive studies[9-11]. By reducing oxygenated species and increasing hydrocarbon content in the upgraded bio-oil, catalytic upgrading produces an oil that is more stable, less viscous, and less corrosive than its original pyrolysis bio-oil. In contrast, despite studies on bio-oil and its model compounds, HDO reactions with considerable oxygenates (e.g., carboxylic acids, furans, aldehydes, ketones, alcohols, esters, phenols, ethers, and carbohydrates) have not been well understood. To gain a better understanding of HDO mechanisms, several lab-scale studies have been conducted with different oxygenate model compounds present in bio-oil.

As petroleum derived feedstocks are the primary source of most chemicals globally, building a similar flexibility into the bio-oils market by dedicating part of their production to chemical manufacturing has obvious economic benefits. In fact, integrated biofuel, chemical, and energy production is a basic characteristic of biorefineries [3]. As hydrogen at moderate temperatures (300–600°C) reacts with bio-oil over a heterogeneous catalyst, oxygen is removed, which leads to the formation of water in HDO[12]. Since bio-oil is a multi-component mixture of a variety of oxygenates (aldehydes, ketones, phenolics, carboxylic acids, etc.) with varying sizes and shapes, there is a need to design a heterogeneous catalyst with appropriate pore structure to improve diffusion and high surface to enhance dispersion of active metals for hydrogen activation[13].

To enhance the quality of bio-oil and improve H/C ratio, a hydrodeoxygenation (HDO) process is needed to remove oxygen in the form of water, carbon dioxide, and carbon monoxide. Considering the complex and multicomponent nature of bio-oil, a first step was taken to understand how to develop robust catalysts and elucidate reaction mechanisms through the study of model compounds. The majority of HDO research works have focused on model compounds representing bio-oil, while most recent works have focused on developing advanced catalysts [14-17]. Experimental studies using various oxygenated model compounds have contributed to better understanding of HDO reaction mechanisms. It was especially challenging to explore efficient catalysts and related reaction mechanisms in bio-oils due to the complexity of the components and the repolymerization of phenolic compounds in thermal environments [18].

As part of current research efforts, lignin model compounds (e.g., vanillin, guaiacol, etc.) and platform molecules like furfural are being used as reaction substrates to design and screen efficient catalysts. The insight gained from the performance of these catalysts with model compounds would provide the fundamental science for developing general catalysts for

HDO of actual bio-oil. As cleaved lignin largely consists of guaiacol and vanillin, these compounds have been extensively used to analyse HDO mechanisms in bio-oil [19-22]. The other commonly studied model compounds include furfural, benzoic acid, anisole, and acetic acid. In contrast to bio-oil, HDO of guaiacol and vanillin have demonstrated a much clearer product distribution [23-25], which helps explore HDO reaction networks and kinetic models development via mechanistic insights provided. Interestingly, a biofuel derived from the HDO of vanillin, 2-methoxy-4-methylphenol (i.e., p-creosol), is also considered an alternative to traditional fossil fuels [24]. Likewise, 2-methylfuran from the hydrogenation of furfural platform molecule is also a contender for replacement fuels[26].

HDO reactions have been achieved so far by using a wide variety of remarkable catalysts, such as noble metals and non-noble metals, which convert biomass derivative oxygenate model compounds and platform chemicals into biofuels and value-added products. Noble metal (e.g., Pd, Ru, Rh, Pt, etc) catalysts are scarce and expensive, limiting widespread application [27,28]. It has also been reported [29-33] that non-noble metal (e.g., Ni, Co, Cu, Mo, Fe, , etc.) catalysts, such as metal sulfides, carbides, phosphides, and nitrides, have been studied for HDO of oxygenate model compounds and to upgrade bio-oil. Due to a relatively low HDO activity, particularly in the HDO of phenols, high reaction temperatures and high metal loadings are usually required, resulting in coke deposition and deactivation when used at high temperatures [18,25].

Usually, porous materials provide support for HDO catalysts to ensure that catalytically active phases are dispersed widely. They include acidic supports (e.g., zeolite Al_2O_3, TiO_2, etc.), basic supports (e.g., ZrO_2, MgO, CaO, etc.) and neutral supports (e.g., activated carbon, SiO_2, etc.). However, the chemisorption of aromatic phenolic compounds and produced water from HDO reactions usually deactivate most of these support materials [34]. Thus, HDO of bio-oil remains one of the most challenging processes to industrialise, due

to the lack of robust, inexpensive, and non-noble metal catalysts. Therefore biochar, one of the products of biomass pyrolysis, could be recycled for use as a catalyst support, potentially making HDO a more economical method of upgrading bio-oil [35].

The term biochar refers to a type of charcoal derived by pyrolysing biomass. It is important to note that fresh biochar, which is derived from biomass via pyrolysis, has certain constraints in chemical composition and pore structure [36], which limit mass transport during HDO reactions. Thus, without post-pyrolysis activation treatment either physically (i.e., steam or gas) or chemically (i.e., base or acid), the pristine biochar has poor catalytic properties based on its morphology and porosity [37,38]. By synthesising mesoporous biochar as a catalyst support, catalysis can be enhanced by providing greater surface area and pore size, which would improve the dispersion of active metal and acid properties (the rich oxygen-containing functional groups (e.g., -COOH) on the biochar surface).

In this study, the mesoporosity of biochar is enhanced through chemical activation and modification using suitable alkali (KOH) and acid (H_2SO_4). By decomposing oxygen-containing compounds, removing pore-clogging tar, and forming new functional groups, post-treatment of biochar with acids or bases promotes pores formation [36]. The oxygen-containing functional groups on the surface of biochar support material has been considered as Bronsted acid sites, which is known to promote the cleavage of C-O bond of biomass derivatives oxygenate model compounds [18]. In addition to abstracting the oxygen from the phenolics, moderately oxygenophilic catalysts, such as Ni metal can easily remove oxygen-containing functional groups easily with active hydrogen [18]. There has been a comprehensive report describing the catalytic practices and challenges of biochar in the field of catalysis[38]. Biochar, along with liquid bio-oil and gases, is one of the products of pyrolysis of biomass. Through physical and chemical modification, biochar can be tailored to offer specific textural properties such as high surface area and mesoporosity, in addition to being renewable and easy to prepare.

Furthermore, functional groups on the surface of biochar could improve active metal dispersion via metal-support interaction, while the engineered mesopores in biochar allow the substrate and hydrogen to access the active metal more readily during HDO.

Biochar support has been reportedly used by Nguyen et al. [39] for the HDO of bio-oil from microalgae. The purpose of this research is to study the use of Ni/biochar for HDO of selected bio-oil model compounds (vanillin and furfural), test the HDO of TCR bio-oil and study the effect of chemical modification of the biochar as catalyst support through its incorporation into HDO process. Potentially this support could improve the overall economics of upgrading bio-oil, in contrast to previous studies that used activated carbon, silica, or alumina as catalyst support with noble metal or bimetallic catalysts. The hydrogenation mechanism of Ni-based catalysts, with preferential saturation of aromatic rings, is similar to that of Pd and Pt-based catalysts, which have attracted much attention due to their high activity in HDO reactions. Also, among transitional metals, Ni is the fourth most abundant after Ti, Fe, and Zr[25]. Hence, nickel (Ni) was chosen as the active metal phase in the catalyst design with biochar as support material. The novelty of this work is development of robust and sustainable catalyst for HDO of vanillin, a bio-oil model compound, into p-creosol. It is also tested for the hydrogenation of furfural into 2-methylfuran, a potential biofuel, and consequently applied in catalytic upgrading of bio-oil itself.

1.2 Aim and objectives

Ultimately, the aim of this research work is to design and develop novel, efficient and renewable cheap catalysts for hydrodeoxygenation (HDO) of bio-oil model compounds and bio-oil itself. This is based on biochar from pyrolysis of woody biomass and nickel as active metal phase. Specifically, to accomplish this aim the following objectives have been addressed:

1. To design and tune the pore structure, surface area, as well as other physicochemical properties of biochar produced via slow pyrolysis of woody biomass. To achieve mesoporosity via chemical activation of alkali (KOH) and acid (H_2SO_4). Specifically, to investigate:

- The impact of alkali and acid chemical activation methods on the biochar properties using different material characterisation techniques.
- The hypothesis that improved specific surface area and mesoporosity would enhance the dispersion of Ni nanoparticles, improve mass transport, and increase catalytic activity and selectivity.

2. Evaluate the performance of biochar with improved textural properties (i.e., specific surface area, mesoporous structure, and exposure of surface functional groups) on HDO of vanillin and hydrogenation of furfural with aim to increase selectivity towards biofuel products p-creosol and 2-methylfuranrespectively.

3. To establish the optimal conditions for HDO reaction and study the influence of processing variables based on the designed Ni/biochar catalyst by means of response-surface methodology.

4. Develop models to describe kinetics of furfural hydrogenation reaction into 2-methylfuran under tetralin solvent environment using the developed and chemically activated Ni/biochar catalyst. Specific details are:

- The investigation includes the effect of changes in reaction temperature, initial furfural concentration, catalyst loading, and hydrogen gas pressure on the rate of reaction.
- Analysis of the major product distributions and reaction pathways during the conversion of single model compounds, mixtures of model compounds, and bio-oil.
- Clarification of the nature of the active sites and investigation of the HDO reaction mechanism over the catalyst via kinetic modelling in order to improve the design of efficient bio-oil conversion systems.

5. Evaluate the HDO activity and performance of the developed and chemically activated Ni/biochar catalyst against an industrially used catalyst for bio-oil upgrading. This study is based on the extent of overall deoxygenation achieved by the catalysts.

1.3 Thesis layout

In this thesis, there are seven chapters, each devoted to a specific subject in the topic of the research. **Chapter One** provides the motivation and background that informed and justified the research work. Additionally, this chapter discusses knowledge gaps, and highlights series of objectives to accomplish the general aim of the research work. In **Chapter Two**, advances and state-of-the-art literature reviews on bio-oil, its method of production and upgrading are detailed. As part of the subdivisions, HDO catalysts are discussed as well as biochar as support for catalysts in the HDO of bio-oil model compounds. The experimental materials are covered in **Chapter Three**. This includes details of the materials such as bio-oil, solvents, organic compounds, and gases used, catalyst preparation, the experimental setup, and analytical instruments such as material characterisation and product quantification techniques used to carry out the investigation. The results of the developed catalyst characterisation are the subject matter presented and discussed in **Chapter Four**. **Chapter Five** presents the findings from the application of the developed catalysts in hydrodeoxygenation (HDO) of vanillin bio-oil model compound, including optimisation study and catalyst reusability test. In **Chapter Six**, hydrogenation of platform chemical furfural is presented and discussed, including results on kinetic modelling and actual bio-oil catalytic upgrading based on the developed catalyst. In the seventh **Chapter**, the conclusions based on key observations and findings from the results chapters (i.e., **Chapters Four, Five and Six**) are highlighted in brief, while future research areas are suggested and outlined as recommendations.

Chapter Two

Literature Review

2.1 Introduction

Owing to declining crude-oil reserves, rising demand for fuels globally, and increased climate concerns regarding the usage of fossil-based energies, technologies for biomass conversion into hydrocarbon fuels have received a lot of attention in recent times[40]. Lignocellulosic biomass is more abundant, renewable, sustainable, and less carbon-intense than fossil fuels for valorisation to biofuels and valuable chemicals. Lignocellulose is comprised of primary components cellulose (40-50%), hemicellulose (25-30%), and lignin(15-20%) [41]. Typically, bio-oil comprises water (15-30%), heavy lignin fractions (20%), and various organic compounds (50-65%), such as aldehydes, organic acids (i.e., carboxylic acids), ketones, alcohols, phenols, furans, methoxyphenols, sugar derivatives, and others. The content of bio-oil is determined by the kind of biomass feedstock and the pyrolysis conditions.

Gasification, pyrolysis, hydrothermal liquefaction, and hydrolysis are some of the most common methods of converting lignocellulosic biomass. Syngas can be generated by gasification of lignocellulosic biomass, while bio-oil and biochar can be produced by pyrolysis. As a result of its high acidity and high water and oxygenate contents, bio-oil obtained directly from pyrolysis has poor quality. A subsequent deoxygenation step, specifically hydrodeoxygenation (HDO), is essential for further upgrading the bio-oil. A summary of the markets for products derived from fast pyrolysis of biomass is shown in **Figure 2.1**. The crude bio-oil needs to be upgraded through further processes, like zeolite cracking and HDO, in order to reduce oxygenate content and increase energy density.

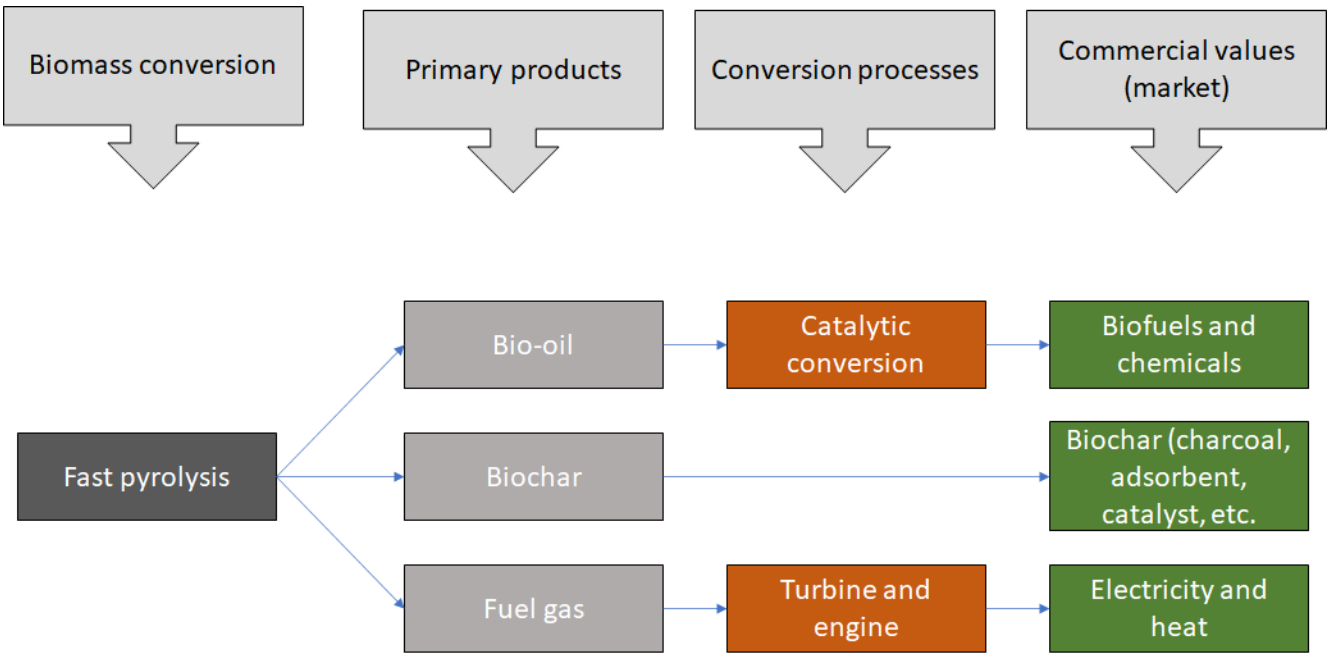

Fig. 2.1. Products and market for fast pyrolysis of biomass [3].

On the other hand, the biochar by-product from pyrolysis of lignocellulosic biomass can be recycled as a catalyst support for catalytic upgrading of the produced bio-oil via HDO. This approach promotes sustainability by closing the production loop and creates a circular economy. There are a number of special properties of biochar material, that makes it a catalyst support candidate, including its characteristic porosity, large specific surface area, rich surface functional groups, and trace mineral elements [42]. Through the use of biochar and chemical activation method applied in this study, the textural attributes will be tuned in order to improve mass transport and HDO catalytic performance.

Initially tested in the 1980s and 1990s, the catalysts typically used in bio-oil upgrading were based on sulfided NiMo or CoMo supported on alumina or aluminosilicate, and the process conditions were comparable to those employed in the hydrodenitrogenation (HDN) and hydrodesulfurisation (HDS)of petroleum fractions[3]. Hydroprocessing involves removing heteroatoms (e.g., S, N, and O) from crude oil and hydrogenating olefins via hydrogen addition, can be employed in catalytic upgrading of pyrolysis bio-oil [8]. By using hydrogen under high

pressure, HDO removes oxygen from bio-oil, resulting in a high-grade hydrocarbon oil product similar to crude oil [6]. The HDO reaction pathway has not been studied as extensively as nitrogen and sulfur removal because commonly studied petroleum crude oils do not contain oxygen like bio-oil. For HDO catalyst development and insight into reaction chemistry, simplified reactions involving bio-oil model compounds such as phenolic compounds (e.g., anisole, vanillin, and guaiacols), benzoic acid, and platform molecules like furfural have been investigated. This process involves hydrogenolysis of oxygen-containing compounds' C-O bonds (HDO) with the formation of water as the result. For oxygenated aromatic compounds (e.g., vanillin, furfural, anisole, guaiacol, etc.) two primary HDO reaction pathways have been reported: (1) hydrodeoxygenation of oxygenated substituents followed by aromatic ring hydrogenation and (2) aromatic ring hydrogenation followed by hydrodeoxygenation [8]. The advantage of choosing model compounds are that they simplify potentially complex reactions, reduce the number of chemical components and impurities in the system, highlight the structure and reactivity of the bio-oil components, analysis requirements and track the reaction route to the products [5,24]. Possible disadvantages include that the system is simplified, so competitive, deactivating or synergistic effects are not captured in the reactions.

In this chapter, the review of bio-oil and platform molecule production methods are discussed in order to create the perspective and the conceptual framework for undertaking this research work. Typical properties of bio-oil that necessitated the need for catalytic upgrading of bio-oil via HDO are also covered. As a result of the literature review, it was possible to get an understanding of the complexity of bio-oil and its multicomponent nature, which led to the study of model compounds as a way to develop a robust catalyst and elucidate the mechanisms of reaction. Thus, several phenolic model compounds of bio-oil, as well as platform molecule furfural, are presented and reviewed in detail. A review and discussion of reported catalysts and their support materials were conducted, which is aimed at providing a conceptual

framework for development of a robust and renewable catalyst for HDO of the model compounds and actual bio-oil. The HDO reaction processes of several types of catalysts, such as traditional sulfided HDS catalysts, noble metals, transition metals, phosphides, carbides, nitrides, non-precious metals, and bimetallic-based catalysts, are discussed. Consequently, the use of biochar and subsequent chemical modification prior to application as a catalyst support for HDO is presented.

2.2 Production of bio-oil

Most lignocellulosic biomass is composed of cellulose, hemicellulose, and lignin. These macromolecules are composed of carbon, hydrogen, and oxygen atoms. However, a small quantity of pectin, nitrogen compounds, and inorganic materials are also included. The largest component of lignocellulosic biomass is cellulose, which can be represented by $(C_6H_{10}O_5)_n$ (where, $n \approx 10{,}000$), formed by the β-1,4 glycosidic linkage of D-glucopyranose units. By dry weight, hardwoods contain 18–25% lignin while softwoods contain 25–35% lignin, consisting of methoxylated phenylpropanoid subunits [43]. To convert lignocellulosic biomass feedstocks directly into liquid bio-oil, two main processes have been developed: hydrothermal liquefaction (HTL) and both fast and slow pyrolysis [44,45].

Hydrothermal liquefaction (HTL) uses hot, pressurised water for sufficient time to break down the solid biopolymers' structure into primarily liquid components and convert it into liquid biocrude oil in a closed oxygen-free reactor [44,46,47]. This is illustrated using the block diagram in **Figure 2.2**. Temperatures of 250-380°C and working pressures ranging from 4 to 22 MPa are standard HTL processing conditions [44,46,47]. The biomass biopolymers undergo pyrolytic reactions at high temperatures, while liquid phase processing is sustained at this pressure range. It is essentially the process of pyrolysis of biomass in hot liquid water that

is responsible for HTL. Although HTL uses pyrolytic mechanisms, the bio-oil it produces is very different from fast pyrolysis bio-oil.

Depending on process temperature HTL can be classified into hydrothermal carbonization (< 250°C) with main product as hydrochar, hydrothermal liquefaction (250-380°C) resulting in the production of bio-oil, and hydrothermal gasification (> 380°C) in which syngas is produced [47]. Although HTL does not essentially involve a catalyst, in recent times substantial research and development has been reported on catalytic liquefaction to enhance hydrothermal processes. Physically, crude bio-oil generated using HTL is considerably more viscous than fast pyrolysis bio-oil, yet it is less dense [46].

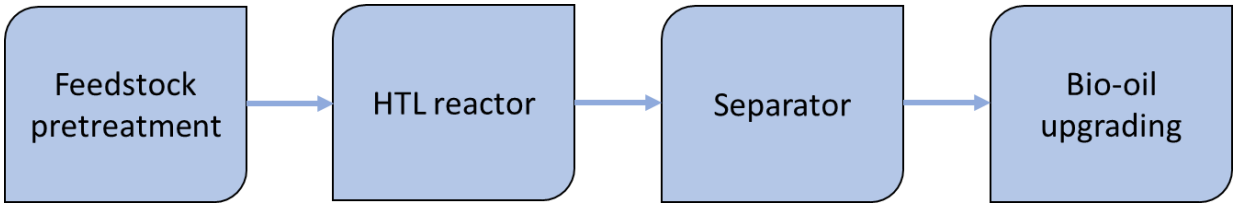

Figure 2.2. Block diagram of HTL of biomass to biocrude oil.

Bio-oil, biogas, biochar, and water-soluble matter are produced through HTL by depolymerizing lignocellulosic biomass [43]. The process factors that influence the quality and yield of biocrude oil from HTL include subcritical or supercritical water, temperature, and retention time at the operating temperature. This method lowers the cost of processing biomass since it does not require a drying stage. Under conditions of 300°C for 30 min, HTL of woody biomass (birchwood sawdust) with and without catalyst was studied[48]. The study compared the catalytic activities of KOH, $FeSO_4.7H_2O$, K_2CO_3, MgO, synthetic hydrotalcite, and ground colemanite (calcium borate mineral). With KOH, the bio-crude oil yield increased to around 40 wt%, more than double the HTL uncatalysed yield of about 18 wt%, while the solid residue yield decreased from 33 to 12wt%$FeSO_4$ and MgO showed the least catalytic activity for

biocrude oil yield among all catalysts studied. Conversely, high biomass slurry concentrations and higher operating pressures, both of which cause increased pumping challenges, are economic drivers for capital cost in HTL processes.

As a similar process to HTL, pyrolysis involves converting biomass into bio-oil, biochar, and other gases under an oxygen-free atmosphere at high temperatures (400-700°C). Biomass is thermally cracked into gases and vapours through pyrolysis, which operates in anaerobic conditions and provides a broad range of compounds [49]. As biomass decomposes very quickly, it generates mostly vapours and aerosols, as well as charcoal and gas, which are cooled and condensed to produce a dark brown homogeneous liquid bio-oil [3]. The pyrolysis can be slow or fast mode depending on the product of interest. Slow pyrolysis at a moderate heating rate is frequently used to maximise biochar yield, however the yield of bio-oil is much lower than that of fast pyrolysis. A fast pyrolysis process involves short residence times (usually less than 2 seconds), rapid heating rates, high temperatures, around 400-700°C, and low pressures (1-5 atm), in an oxygen-free environment. It is appropriate for transformation of low moisture-containing biomass (<10 wt. %) into bio-oil [45]. The gas yields increase as the fast pyrolysis temperature rises, whereas the char yields decrease. To reduce the oxygenates in the pyrolysis bio-oil, catalytic upgrading routes via a conventional method or in situ catalytic vapour cracking combined with fast pyrolysis can be applied. These upgrading schemes are illustrated diagrammatically in **Figure 2.3**. When biomass is fast pyrolysed, 60–75 wt% bio-oil, 15–25 wt% biochar, and 10–20 wt% non-condensable gases are produced [50].

(a)

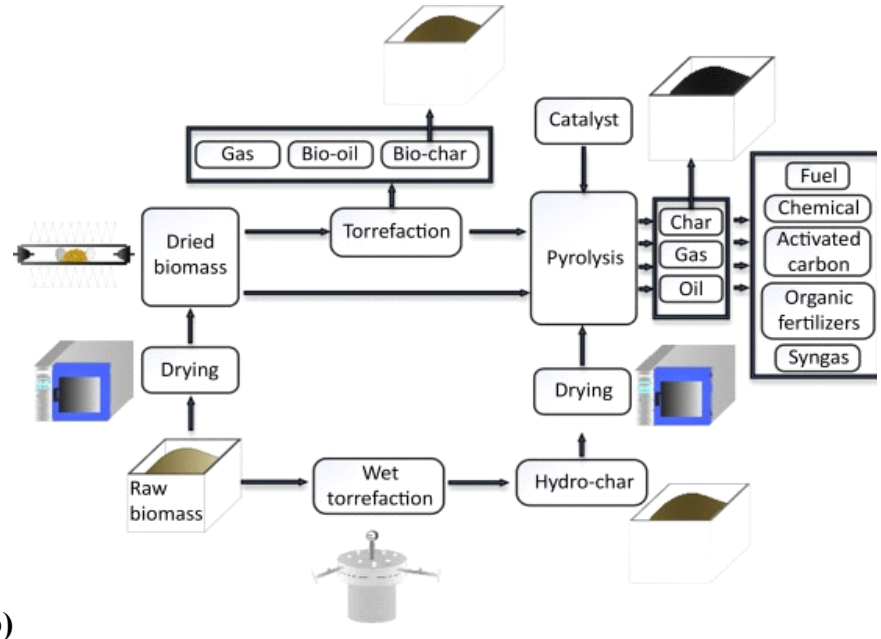

(b)

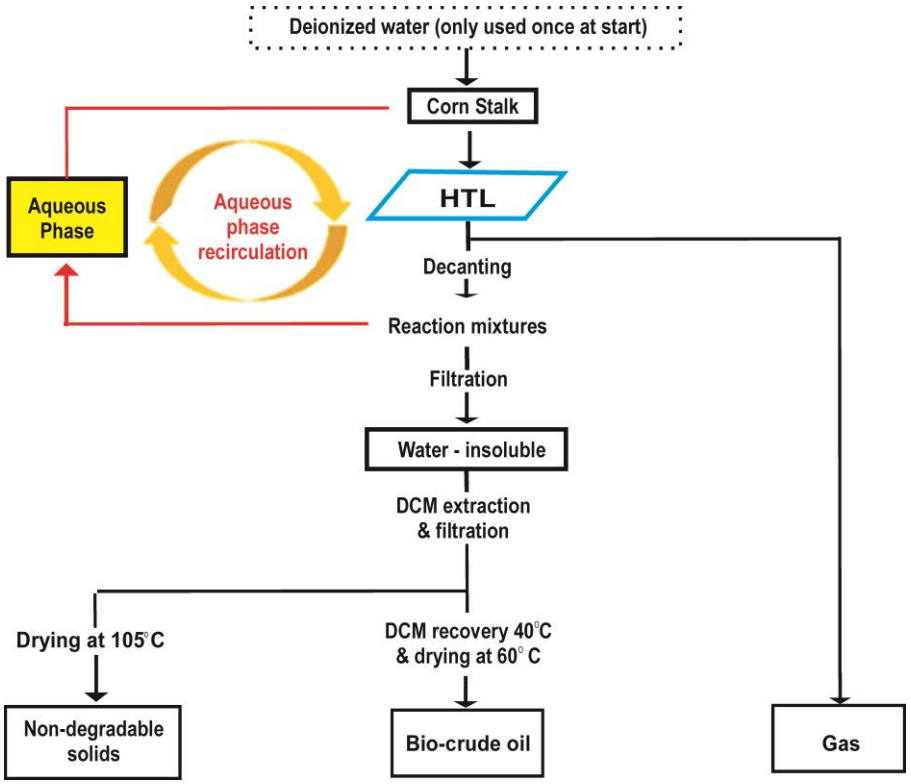

Figure 2.3.Process diagram of (a) fast pyrolysis for biomass [51] and (b) hydrothermal liquefaction of biomass for bio-oil production[52]

In comparison to petroleum crude oil with water content of less than 1%, that of pyrolysis bio-oil is significantly higher in the range of 15-30 wt%. However, pyrolysis has a lower capital cost than HTL, making it more commercially viable. Bio-oils produced via fast pyrolysis usually contain more oxygen, are more acidic, and have a lower heating value than those produced using HTL [2]. **Equation 2.1** shows the stoichiometric empirical formula for biomass conversion to bio-oil by pyrolysis [53].

$$CH_{1.46}O_{0.67} \rightarrow 0.71CH_{1.98}O_{0.76} + 0.21CH_{0.1}O_{0.15} + 0.08CH_{0.44}O_{1.23} \quad (2.1)$$

Biomass Bio-oil Biochar Gas

2.3 Bio-oil

Bio-oil is a viscous, dark brown, and free-flowing liquid containing highly oxygenated compounds with a smoky odour, derived from biomass via HTL and pyrolysis. The physical and chemical characteristics of bio-oil are commonly influenced by the biomass feedstock and synthesis conditions. The yield of bio-oil is significantly affected by production method and process conditions.

2.3.1 Properties of bio-oils

Due to the presence of organic acids (i.e., carboxylic acids compounds), crude bio-oils are acidic and reactive. Because of their high contents of oxygenates (e.g., phenolics, aldehydes, alcohols, ethers, and ketones) and organic acids (i.e., carboxylic acids), bio-oils are also unstable and immiscible with petroleum-based products like gasoline, diesel, and kerosene. Thus, bio-oil is an unstable multicomponent mixture. The mixture consist of polar organics (about 75 – 80 wt%) and water (about 20 – 25 wt%) [53]. The conversion of bio-oils into transportation fuels requires the removal of organic acids, the elimination or significant reduction of oxygenate content, and the improvement of hydrocarbon content. Typical properties and characteristics of bio-oil produced by fast pyrolysis are shown in **Tables 2.1** and

2.2. The cause and effect of bio-oil properties are clearly presented in **Table 2.2**. It has been reported that oxygen is present in over more than 300 compounds that have been identified in bio-oils due to the three key biomass building blocks (i.e., cellulose, hemicellulose, and lignin).

Table 2.1. Typical properties of crude bio-oil produced by fast pyrolysis of biomass[4,49]

Physical properties	**Typical value**
Water content	15 – 30 wt%
P^H	2.5
Specific gravity	1.2
C	54 -58 wt%
H	5.5 -7 wt%
O	35 - 40 wt%
N	0 -0.2 wt%
Viscosity (40°C and 25% water)	100 mPa.s
Solids (char) which also includes ash	0.2 -1
Vacuum distillation residue	Up to 50%
Heating value as produced	16 – 19 $MJ.kg^{-1}$

Table 2.2. Characteristics of pyrolysis bio-oil [3,49,53]

Property	Cause	Effect
Acidity or low pH	Organic acids (e.g., carboxylic acids) from biopolymer degradation	Corrosion of vessels and pipework
Ageing	Continuation of secondary reactions including polymerisation	Slow increase in viscosity from secondary reactions such as condensation. Potential phase separation.
Alkali metals (ash)	Virtually all alkali metals point to char. Incomplete solids separation. High ash feedstock.	Catalyst poisoning. Erosion and corrosion.
Biochar	Incomplete biochar separation.	Ageing of oil. Catalyst or bed blockage. Filter blockage. Sedimentation.
Chlorine	Contaminants in biomass feedstock	Catalyst poisoning in upgrading process.
Colour	Cracking of biopolymers and biochar	Discolouration of some products such as resins
Poor distillability	Reactive mixture of degradation of biomass	Bio-oil cannot be distilled – maximum 50% typically. Liquid begins to react at below 100°C and substantially decomposes above 100°C.
High viscosity	Chemical composition of bio-oil, water content, and aging.	High pumping cost. Gives high-pressure drop-in catalyst bed.
Low H/C ratio	Biomass has low H/C ratio	Upgrading to hydrocarbons is a challenge
Miscibility with hydrocarbons is very low	Highly oxygenated nature of bio-oils	Will not mix with any hydrocarbons so integration

		into a refinery is more difficult.
High oxygen content	Biomass composition has high oxygen	Non-miscibility with hydrocarbons. Poor stability and phase separation.
Phase separation/inhomogeneity	High water content in biomass. High ash in feedstock.	Inconsistency in handling, storage, and processing. Phase separation and poor mixing. Catalyst deactivation.

2.3.2 Composition of bio-oils

Bio-oil is a highly oxygenated mixture of compounds whose composition varies depending upon biomass feedstock, thermochemical conversion route and the processing conditions (heating rate, temperature, time, etc.) under which it is produced. Common oxygenate organic compounds found in bio-oils include carboxylic acids, alcohols, aldehydes, ketones, ethers, esters, phenols (e.g., guaiacol, vanillin, etc.), furans (e.g., furfural), and carbohydrates. The proportional amount of cellulose, hemicellulose, and lignin in the biomass used to produce bio-oil can vary depending on source, and so its oxygenated building components. Pyrolysis of cellulose- or hemicellulose-rich biomass feedstock yields lower molecular weight oxygenated molecules [5]. When biomass feedstock containing high lignin fractions is pyrolysed, the produced bio-oil is rich in phenolic compounds [4]. It is therefore very challenging and nearly impossible to completely characterize the bio-oil due to its multicomponent and complex nature. Bio-oil has been characterized using a variety of analytical techniques, including High Pressure Liquid Chromatography (HPLC), Gas Chromatography-Mass Spectrometry (GC-MS), Gel Permeation Chromatography (GPC), Nuclear Magnetic Resonance (NMR), and Fourier Transform Infrared (FTIR) spectroscopy. GC-MS is the most often used method for characterising bio-oil.

2.4 Methods of upgrading bio-oils and platform chemicals from lignocellulosic biomass

In order to improve the stability of biofuel along with its miscibility with conventional fuels, it is highly recommended to upgrade bio-oils with deoxygenation steps, which reduces the oxygen content by 30 – 50 wt%[7]. A variety of reactions have been employed to remove oxygen functionalities from oxygenate organic compounds domicile in biomass derived pyrolysis bio-oil over the past decades, they include hydrogenolysis, dehydration, hydrocracking, decarbonylation, hydrogenation, decarboxylation, polymerization, and hydrodeoxygenation (HDO) [6]. HDO involves reactions between bio-oil and hydrogen in the presence of a suitable catalyst. The process enriches the H/C ratio and in the end produces hydrocarbons from bio-oil, while rejecting oxygen in the form of water. Due to the large diversity of organic chemicals in the pyrolysis bio-oil, catalytic upgrading of bio-oil involves a complicated reaction network.

Zeolite catalytic cracking, hydrotreating, hydrocracking, esterification, emulsification, and steam reforming are some of the technologies developed and reported for upgrading bio-oil [54]. The deoxygenation of bio-oil can be catalysed by zeolites, such as HZSM-5, Y-zeolite, HY-zeolite, silica-alumina, US-Y, etc. as an alternative route known as zeolite cracking process. Catalytic upgrading of bio-oil by zeolite cracking is similar to fluid catalytic cracking (FCC), which also employs zeolites [2]. Due to the fact that hydrogen is not a requirement in this system, it is operated at atmospheric pressure, resulting in a large amount of carbon deposition and a very short catalyst lifetime [6]. Furthermore, because no external hydrogen is provided, it generally impacts on the hydrogen concentration of the upgraded oil resulting in a low H/C ratio. As a result of zeolite cracking, the oil produced is of a low grade, with heating values that are approximately 25% lower than those of crude oil [6]. A zeolite is a microporous material with a three-dimensional structure. A variety of processes underpin the zeolite cracking mechanism. General cracking processes reduce large hydrocarbons to smaller

fragments. While dehydration, decarboxylation, and decarbonylation are all involved in oxygen removal during zeolite cracking, with dehydration being the most common. Water, carbon monoxide, carbon dioxide, and short-chain acids are all forms through which oxygen is removed from bio-oil in catalytic cracking. Carbon dioxide (CO_2) and carbon monoxide (CO) are both harmful gases that result from these reactions and contribute to global warming [5].

Additionally, carbon losses during the process impact on H/C ratio and reduce the quality of the upgraded oil and often result in substantial catalyst deactivation. Since catalytic cracking does not require hydrogen and operates under atmospheric pressure, it is considered cost-effective, as it offers considerable economic and processing advantages over HDO. However, low hydrocarbon liquid product yields, considerable coking found during catalytic cracking of bio-oils, and poor fuel quality are all bottlenecks that must be addressed. The high temperature used in zeolite cracking contribute to high coke formation and catalyst deactivation. Although bio-oil can be upgraded with the zeolite catalytic cracking method for small oxygenates such as aldehydes and ketones, higher phenolic compounds are hard to deoxygenate because of their micropores [5]. Therefore, to handle phenolic compounds and benzoic acids with complex molecular structures, catalysts are required with a mesoporous structure to facilitate diffusion and access to active sites.

Alternatively, catalytic hydrodeoxygenation (HDO) of bio-oil is proposed. This method involves high temperatures, high hydrogen pressures, and heterogeneous catalysts. The deoxygenation reaction is generally believed to take place via two distinct routes: hydrogenation (HYD) and direct deoxygenation (DDO). The phenolic and benzoic acids model compounds within bio-oil are typically polycyclic aliphatic and aromatic in structure, with oxygen atoms as their main component. These compounds will benefit from hydrogenation of unsaturated bonds due to the presence of hydrogen in HDO. In bio-oil HDO, oxygen is eliminated as water, nitrogen is eliminated as ammonia, and large molecules are hydrogenated-

hydrocracked to produce gasoline and diesel range hydrocarbons. Thus, the presence of hydrogen in the HDO process results in lower formation of carbon dioxide and carbon monoxide than zeolite cracking method. However, the formation of water in HDO could cause catalyst deactivation depending on the interaction with the support material. Finally, the upgraded product of bio-oil HDO shows close similarities to crude oil properties. Hydrogen functions as a reducing agent in**equation 2.2**, which demonstrates the general HDO reaction [5].

$$CH_{1.4}O_{0.4} + 0.7\ H_2 \rightarrow -CH_2- + \quad 0.4H_2O \qquad (2.2)$$

Bio-oil upgraded oil water

On the other hand, a series of targeted chemical processing steps are applied to convert lignocellulosic biomass into platform molecules, which are intermediates for biofuels and value-added chemicals production. Lignocellulosic biomass-derived compounds can be accomplished via different catalytic routes such as catalytic depolymerization of biomass to sugars, hydrolysis, dehydration, oxidation, etc. to platform chemicals and biofuels products. The pathway from biomass to platform chemicals and biofuels is shown in **Figure 2.4**. An initial chemical processing step can produce four classes of platform molecules: sugars, dehydration products, polyols, and lignin monomers [1,55]. A variety of methods have been developed to produce more than 200 value-added compounds from lignocellulosic biomass [1]. Several platform chemicals have been produced from lignocellulosic biomass, including sugar alcohols, organic acids, furfural, and 5-HMF. Consequently, platform chemicals like furfural can be catalytic converted into biofuel (2-methylfuran) via hydrogenation. The kinetic model of the process is studied with Ni/biochar catalyst developed in this work.

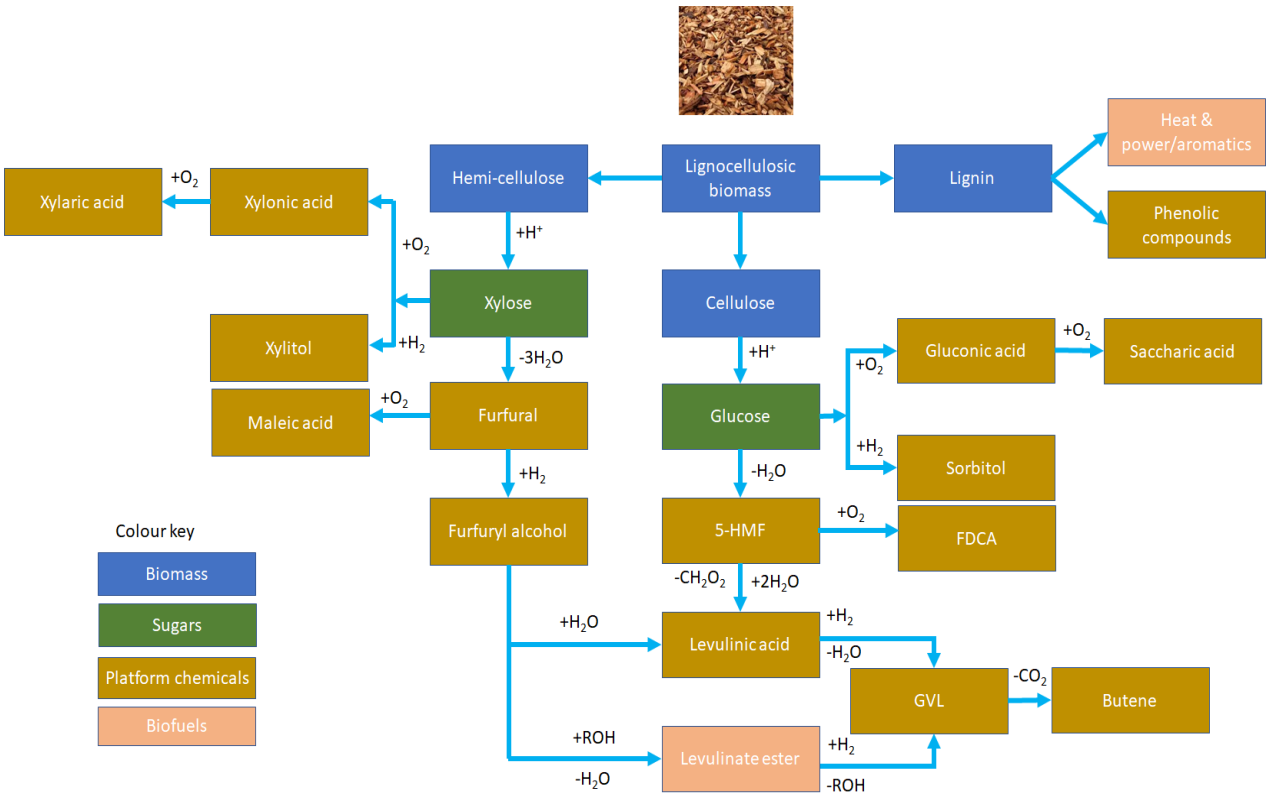

Figure 2.4. Schematic diagram of routes from biomass through sugars to platform chemicals and biofuels products. [Note: 5-hydroxymethyl furfural (5-HMF), furan dicarboxylic acid (FDCA), gamma-valerolactone (GVL)] [1].

2.5 Bio-oil Model compounds

It is estimated that bio-oils contain over 400 different organic compounds, which are mostly oxygenates[5]. Hence, the crude bio-oil from pyrolysis of lignocellulosic biomass requires upgrading either by zeolite cracking or catalytic HDO to improve the hydrocarbon fuel fractions, which is necessary for blending with petroleum-based fuels and compatible for use in internal combustion engines [5,6,50]. By catalytic upgrading in the presence of hydrogen, the oxygen is removed from oxygenates in the form water through hydrodeoxygenation (HDO) and hydrogenation, and in the forms of carbon dioxide and carbon monoxide via decarbonylation and decarboxylation reactions [50,56]. In contrast, due to the lack of deoxygenation, emulsification of crude bio-oil with diesel causes internal combustion engines to corrode.

Consequently, just like petroleum bio-version of value-added bioproducts and chemicals can be produced from bio-oil when it serves as a feedstock for an integrated biorefinery. Due to this complexity of bio-oil components, many researchers used its model compounds instead of bio-oils themselves, to investigate the mechanism of catalytic hydrogenation or HDO [6]. Consequently, the possibility of multiple side reactions during bio-oil storage prompted HDO studies at research scale motivated the choice of model compounds rather than bio-oil itself because of the complexity of interactions between organic compounds in the actual bio-oil [57]. HDO studies tend to focus on specific model compounds or mixtures of oxygenates that mimic real bio-oil [58]. The hydrodeoxygenation of major oxygenate compounds in bio-oil can be represented by HDO of phenols and substituted phenols. Thus, the study of HDO of representative phenolic oxygenate compounds can provide insight into their HDO processes during the catalytic upgrading of the actual bio-oil. In addition to simplifying the reactions that are occurring during the HDO process, this approach highlights the structure-reactivity of bio-oil components, the analysis needed, and the pathways leading to the products that are formed.

Furthermore, studies using model compounds have proven useful in the development, evaluation, and performance of different catalysts synthesised, thereby serving as a means to designing and improving catalyst for catalytic upgrading of bio-oil [5,23]. It has been particularly helpful to understand HDO reaction mechanisms and the development of kinetic models that describe these reactions through the approach of model compound studies [56]. However, in comparison to actual bio-oil environments, which involve additional interactions from neighbouring compounds, results from model compounds studies may not necessarily reflect the catalytic upgrading reaction mechanisms and behaviour occurring.

Bio-oil cannot be used in its crude state without further treatment such as upgrading to remove the oxygen and improve compatibility with current petroleum-based fuels and the

combustion engines. Hundreds to thousands of oxygenates (such as phenol, ketones, aldehydes, furans, sugars, and carboxylic acids) are present in biomass pyrolysis bio-oil. The term catalytic upgrading of bio-oil represents a complex network of many reactions, each with its own bond strength and preferred deoxygenation pathway. As a result of the numerous types of C–O bonds in bio-oil, each with different bond energies and deoxygenation pathways that are thermodynamically more favourable are readily promoted [56]. Thus, model compound studies, with their limitations, provide valuable information about effective hydrogenation strategies for selectively hydrogenating the targeted C–O bonds, while minimising bond cleavage. The phenolic compounds reported in the literature include cresols, guaiacol, vanillin, and anisole. As a result of their multiple functional groups, these model compounds are usually studied as a basis for bio-oils HDO. In fact, phenolic compounds (e.g., phenols, anisoles, guaiacols, and syringols) are the main cause of coke formation, which leads to catalyst deactivation during catalytic upgrading actual bio-oil [5]. **Scheme 2.1** shows the structures and major functional groups [i.e., hydroxyl (–OH) and methoxyl (–OCH_3)] present in lignin derived phenolic compounds found in bio-oil. As a result, the catalytic HDO of lignin-derived phenolic monomers has recently received a lot of attention.

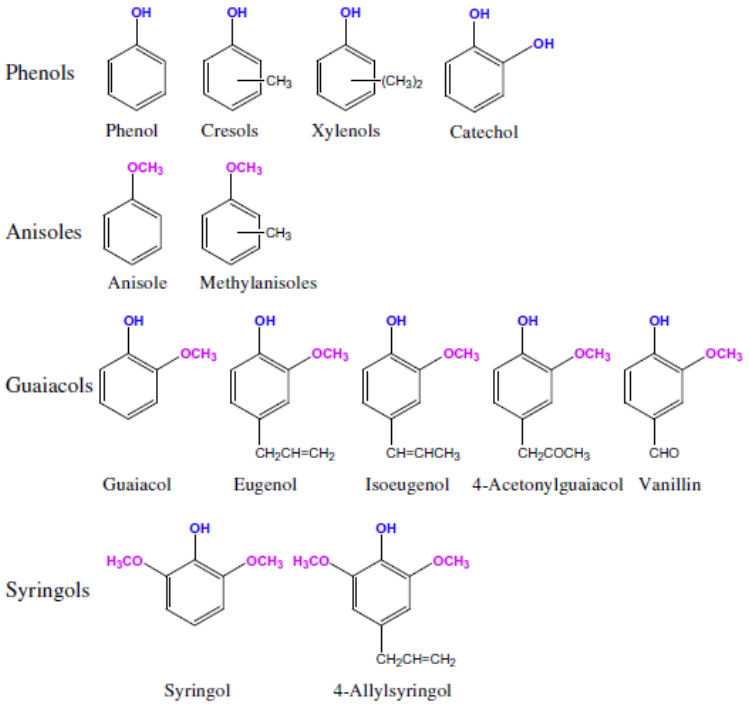

Scheme 2.1. Structure of phenolic compounds commonly present in bio-oil[59]

2.5.1 Anisole

Anisole, also known as methoxybenzene (i.e., methyl phenyl ether), is an oxygenate organic compound found in bio-oil with the molecular formula $CH_3OC_6H_5$. It appears in liquid state at room temperature. Structurally, it comprises of the following functional groups an ether (−O−), a methyl ($-CH_3$) and phenyl ($-C_6H_5$) as shown in **Scheme 2.2**. One of the major functional groups of lignin phenolics, methoxyl, is present in anisole. The HDO of anisole is normally studied as a model compound for providing insight into catalytic upgrading of bio-oil, due to its methoxy−phenyl group (see **Figure 2.2**). This is characteristic of lignin depolymerization fractions present in bio-oils derived from lignocellulosic biomass [57,59,60].

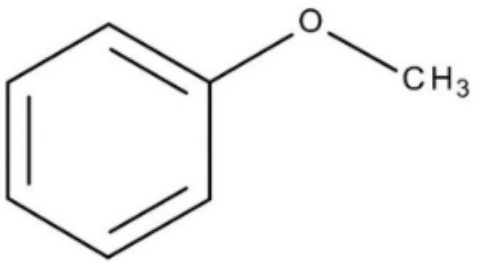

Scheme 2.2. Anisole

2.5.2 Guaiacol

As a result of the pyrolysis of lignocellulosic biomass, guaiacol which is a phenolic organic compound is present in bio-oil which is a precursor for vanillin and eugenol. Guaiacol (2-methoxyphenol) is another common phenolic oxygenate compound found in bio-oil with a methoxy and hydroxyl functional groups as shown in **Scheme 2.3**. The key to bio-oil upgrading is the removal of oxygen from these molecules and the addition of hydrogen. To achieve this, catalyst development is critical.

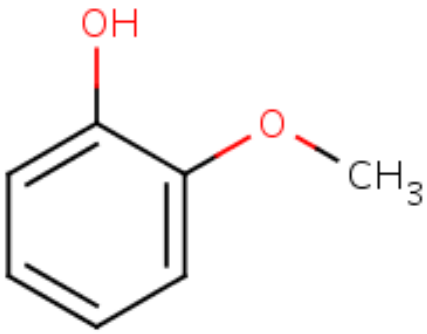

Scheme 2.3. Structure of guaiacol.

Guaiacol is one of the bio-oil model compounds of interest because of the presence of two oxygen-containing functional groups: phenolic (-OH) and methoxy (-OCH_3) provides it with the capability to repolymerize, which is an inherent property of bio-oil under thermal treatments [40]. Guaiacol's structure includes three types of C-O bonds, which are C_{AR}-OH, C_{AR}-OCH_3

and $C_{AR}O\text{-}CH_3$. As a result of catalytic HDO of guaiacol, the following products cyclohexane, phenol, benzene, cyclohexanone, cyclohexanol, 1-methylcyclohexane-1,2-diol, and catechol have been reported. **Scheme 2.4** shows most of the reaction pathways to the products.

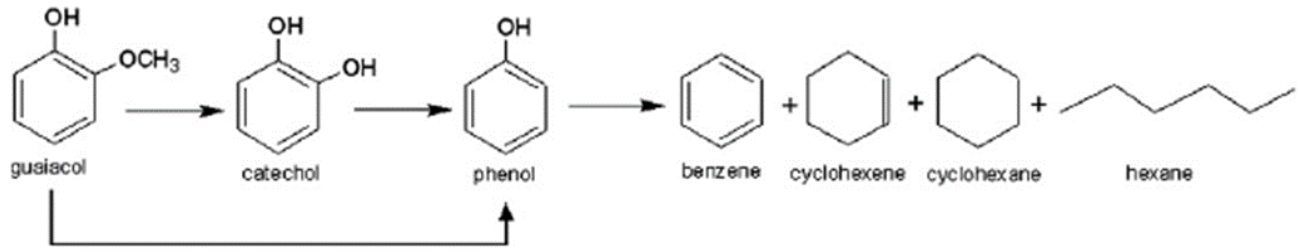

Scheme 2.4. HDO reaction pathways for guaiacol[40].

The catalytic performances of ZrO_2, SiO_2 and ZrO_2-SiO_2-supported Ni and NiCu catalysts were evaluated in the HDO of guaiacol model compound to hydrocarbons. Cyclohexane selectivity of 80.8% and methylcyclohexane selectivity of 12.4% were achieved with complete conversion of guaiacol under 300°C and 5.0 MPa hydrogen pressure [61]. It was also found that the acidity of SiO_2-ZrO_2 complex oxides support is greater and stronger than that of ZrO_2 support. The findings showed that the strong acidic sites on the catalyst surface can promote the production of methyl-substituted compounds during guaiacol HDO.

The HDO of guaiacol has also been studied using a MoS_2 catalyst impregnated on two different activated carbon supports with distinct porosity and oxygen surface functionality [62]. It was found that the dispersion of MoS_2 was correlated with the activity differences on the carbon supports. In the presence of more oxygen on the support (mostly carboxylic, hydroxylgroups), the MoS_2 dispersion and HDO activity were reduced. The catalytic HDO of guaiacol has been reported for bimetallic Ni–Fe nanoparticles supported on carbon nanotubes (CNTs) [48]. Combined Ni and Fe catalysts exhibit high activity and significantly enhanced selectivity to cyclohexane or phenol based on the ratio of Ni/Fe, whereas poor catalytic performance was observed for monometallic Ni and Fe catalysts. Additionally, the size of the

metallic nanoparticles on the surface of the support also influence the catalytic performance [48]. Ni–Fe/CNT catalyst exhibits selectivity-switchable performance due to the synergistic interaction between Ni domains, where hydrogen can be easily activated during HDO reaction, and Fe domains, which are strongly oxophilic.

2.5.3 Vanillin and m-cresol

When thermal processing is applied to cellulose and hemicellulose biomass, relatively small oxygenates are found in the bio-oil produced, but lignin component of biomass breaks down into high concentrations of phenolic molecules (phenol, guaiacol, syringol, and their derivatives) [59]. This suggests that high lignin biomass pyrolysis bio-oil contains a significant number of phenolic compounds. Vanillin (4-hydroxy-3-methoxybenzaldehyde) and m-cresol are oxygenated phenolic compounds also present in biomass pyrolysis bio-oil. Additionally, both vanillin and m-cresol structures are excellent model compounds of oxygenates found in bio-oils due to the three functional groups; aldehyde, ether, and hydroxyl, as shown in **Scheme 2.5**. As models for bio-oil oxygenates, these species are preferred since they represent the primary structure of bio-oil lignin fractions [5]. In addition, both are members of the same group as guaiacol and anisole. The removal of oxygen is normally achieved during HDO of the compounds through hydrogenolysis of C−O bonds, which remove oxygen in the form of water [23].

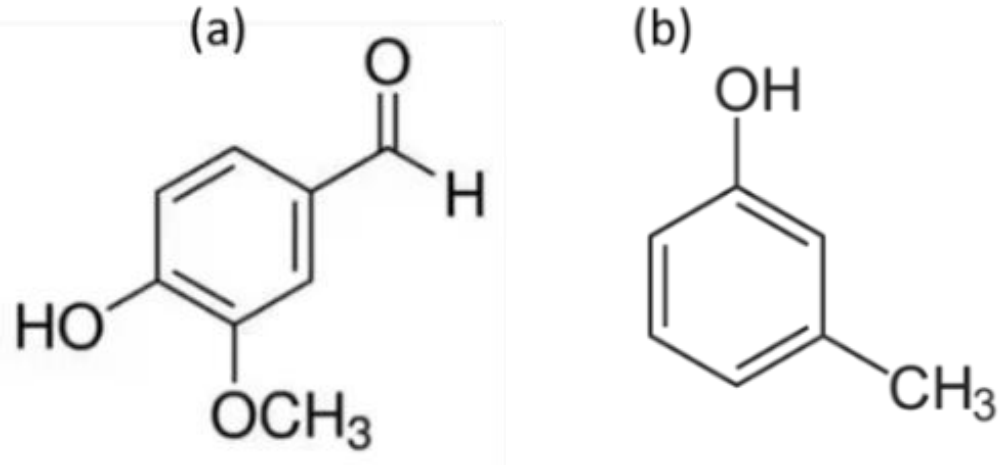

Scheme 2.5. The structure of (a) vanillin and (b) m-cresol.

Fundamentally, an aldehyde group in the phenolic model compound can undergo HDO through one of four routes: (1) hydrogenolysis of the C=O bond directly; (2) hydrogenation of the C=O bond to form alcohol, followed by hydrogenation of the C–O bond; (3) hydrogenation of the C=O bond to form alcohol followed by dehydration and rehydrogenation of the C=C bond; and (4) decarbonylation of the C=O bond to produce CO and alkanes [5]. Specifically, vanillyl alcohol is formed through hydrogenation (HYD) of the aldehyde group in vanillin, while the fuel product, creosol is produced by hydrodeoxygenation (HDO) of vanillyl alcohol in a consecutive reaction pathway [23,24]. Due to the unreactive methyl group in creosol instead of the highly reactive C=O bond in vanillin, cresol is more stable than vanillin.

In the literature, HDO of vanillin, which is a typical phenolic compound of lignin-derived bio-oil is usually converted to p-creosol (2-methoxy-4-methylphenol), which is a promising future biofuel [5,7,23]. **Table 2.3** shows the selected studies on vanillin HDO, the catalyst type, main product and selectivity recorded. It is clear a wide range of catalysts have been designed and tested for HDO of vanillin with varying activity and selectivity. In addition, the following catalysts have been tested for HDO of vanillin: Pd/C,Pd/Al_2O_3, PdRh/Al_2O_3,

Pt/SiO_2, Pt/C and Rh/Al_2O_3, with the bimetallic $PdRh/Al_2O_3$ catalyst showing the highest selectivity (99%) towards creosol with minimal uptake of hydrogen [5,23,24].

Table 2.3. Selected studies on HDO of vanillin: catalyst, main products, and selectivity.

Catalyst	Conditions	Conversion (%)	Main product	Selectivity (%)	Reference
Pd/C, Pt/C, $PdRh/Al_2O_3$, Pd/Al_2O_3, Rh/Al_2O_3, Pt/SiO_2	338K, 1 MPa, 263 mM, 1000 rpm, and 1 h,	21 to 99	Creosol	4 to 99	(Aliu et al., 2021)
Co_XP@POP	300 mg, 2 mmol, catalyst (50 mg), and isopropanol (30 mL), 40 bar, 150°C, 800 rpm and 7 h.	98	2-methoxy-4-methylphenol	83.4	(Shit et al., 2019)
Pt/C, Au/C, Pd/C, Rh/C, and Ru/C	Water, 30 bar, 100°C, 100 mg (vanillin), 50 mg (catalyst), 900 rpm, and 3 h.	98 to 100	p-creosol	10 to 95	(Santos et al., 2018)
Ni/NCB	vanillin (228 mg), Ni/NCB (20 mg), 0.5 MPa, 150 °C, water (10 mL), 2 h.	74.4	2-methoxy-4-methylphenol	64.6	(Nie et al., 2017)

Note: Porous organic polymer (POP), porous nitrogen-doped carbon black (NCB) and layered double hydroxides (LDHs).

Due to its ability to be converted into various high-value-added chemicals (e.g., benzene, toluene, and xylene) and biofuels (e.g., p-creosol), vanillin is considered a promising platform molecule for connecting biomass resources with biochemicals [7]. The HDO of vanillin to p-creosol (2-methoxy-4-methylphenol) is mostly the result of two reaction stages: the first stage involves the hydrogenation of vanillin to vanillyl alcohol (i.e., 4-hydroxymethyl-

2-methoxy phenol), which is specifically an aldehyde (−CHO) being converted into an alcohol (−CH_2OH) and followed by hydrogenolysis of vanillyl alcohol to p-creosol. The cost of noble metal has a significant impact on the overall process' economics; despite the fact that complete vanillin conversion was achieved after 3 hours with about 92% selectivity towards p-creosol, commercialising noble metal catalysts for HDO is challenging due to their high cost [5]. Thus, the catalyst promoted both hydrogenation and hydrogenolysis reactions during the HDO of vanillin. It has been reported that compared to other commonly used heterogeneous Ni-based catalysts, such as Ni/SiO_2, Ni/Activated carbon, Ni/carbon black, Ni/MgO and Ni/ZrO_2, achieve poor hydrogenation or p-creosol selectivity under the same conditions was observed compared to Ni/NCB catalyst [22]. As demonstrated by the nitrogen-doped carbon material, which suggests that in most instances, the functionalization of carbon supports is required to get around this restriction and enhance hydrogenolysis of carbon–oxygen bonds. However, the findings from the study of a Ni-Co-P/HAP (hydroxyapatite) catalyst for HDO of vanillin revealed high catalytic activity, resulting in 93.97% selectivity towards 2-methoxy-4-methylphenol and 97.86% conversion [63].

An investigation of vanillin HDO carried out using catalysts of noble metals (Pd, Au, Ru) supported on biochar that has been chemically activated with $ZnCl_2$ and HNO_3 to enhance its specific surface area and demineralize it has been reported [64]. The maximum selectivity of 92% toward p-creosol was achieved after 3 h of vanillin HDO at 100°C and 30 bar hydrogen pressure with water as solvent using Pd/biochar activated chemically with $ZnCl_2$. It has been reported that phenolic compounds of bio-oils have the most difficult C-O bond to cleave, making them extremely resistant to HDO [2]. The HDO of vanillin can be summarised according to **Scheme 2.6**. These finding highlights biochar's potential as a viable choice for HDO catalyst support.

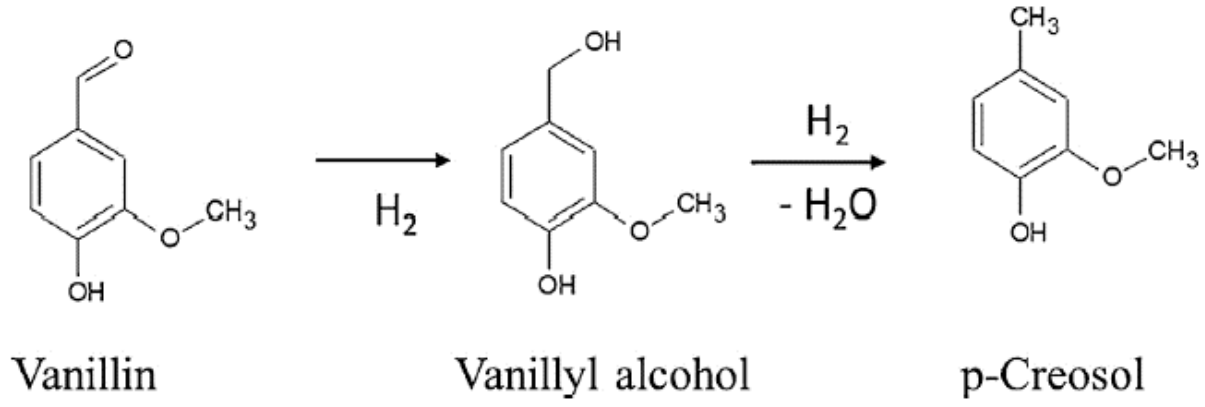

Scheme 2.6. The reaction pathway for vanillin HDO [23].

2.5.4. Furfural

An important component in the conversion of lignocellulosic biomass to biofuels and biochemicals is furfural[41]. This potential platform molecule is a potential source of renewable energy. Chemically, furfural, C_4H_3OCHO, (also known as 2-furancarboxyaldehyde, furaldehyde, and 2-furanaldehyde) is derivative of pentose that is found in hemicellulose portion of lignocellulosic biomass, a raw material that is rich in pentose sugars. Focus has been placed on furfural in recent times, as a possible platform feedstock for the production of biochemicals and biofuels. It contains an aldehyde (C=O) and two olefin groups (C=C-C=C) as the two main functional groups. There is an aldehyde side group attached to the furan ring, making this a heterocyclic and aromatic aldehyde, as shown in **Scheme 2.7**. Basically, a complex process of acid-catalysed hydrolysis is employed to deconstruct lignocellulose biomass into a series of sugars (i.e., $C_5 – C_6$), which can then be rearranged by detaching some of their oxygen atoms to produce various renewable platform compounds like furfural and 5-hydroxymethylfurfural, HMF [41].

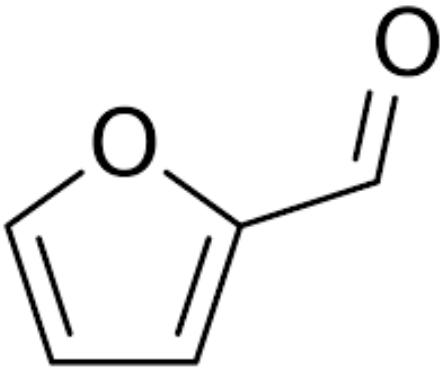

Scheme 2.7. Molecular structure of furfural

The primary method for producing furfural is the hydrolysis and dehydration of xylose, which is found in significant amounts in hemicellulose. Furfural, as a platform chemical, may be utilised as a feedstock for catalytic hydrogenation and decarbonylation processes to produce furfuryl alcohol, tetrahydrofuran (THF), furan, and 2-methylfuran. The catalytic hydrogenation of the C=O link results in the formation of furfuryl alcohol or 2methyl furan. Furfuryl alcohol, 2-methylfuran, furan, tetrahydrofuran, tetahydrofurfurfuryl alcohol, and even ring-opening products like pentanols, pentanediols and levulinic acid can be produced via catalytic hydrogenation of furfural, based on the characteristics of the catalyst applied [65]. A variety of C_4 and C_5 molecules can be derived from furfural through a number of catalytic processes, including selective hydrogenation, oxidation, hydrogenolysis, and decarbonylation. These molecules are crucial building blocks for the creation of liquid hydrocarbon fuels and additives as well as the synthesis of valuable chemicals. This confirms that furfural as a building block provides a viable and diverse platform for lignocellulosic biofuels and value-added chemicals [66]

. Using furfural as a sustainable chemical platform allows the production of value-added chemicals in simplified steps than if fossil feedstocks were used. Its hydrogenation is therefore one of the most flexible processes for converting furanic components to biofuels (e.g., 2-

methylfuran). The reaction pathways leading to the formation of these products is shown in **Scheme 2.8**. Several authors have published a comprehensive review that discusses recent advances in the catalytic hydrogenation of furfural towards furfuryl alcohol, 2-methylfuran, furan and other value-added products in terms of different non-noble metal, noble metal catalytic systems, reaction mechanisms that are related to the different catalytic materials, and reaction conditions [67]. The catalytic hydrogenation of furfural can be carried out in either liquid phase or gas phase.

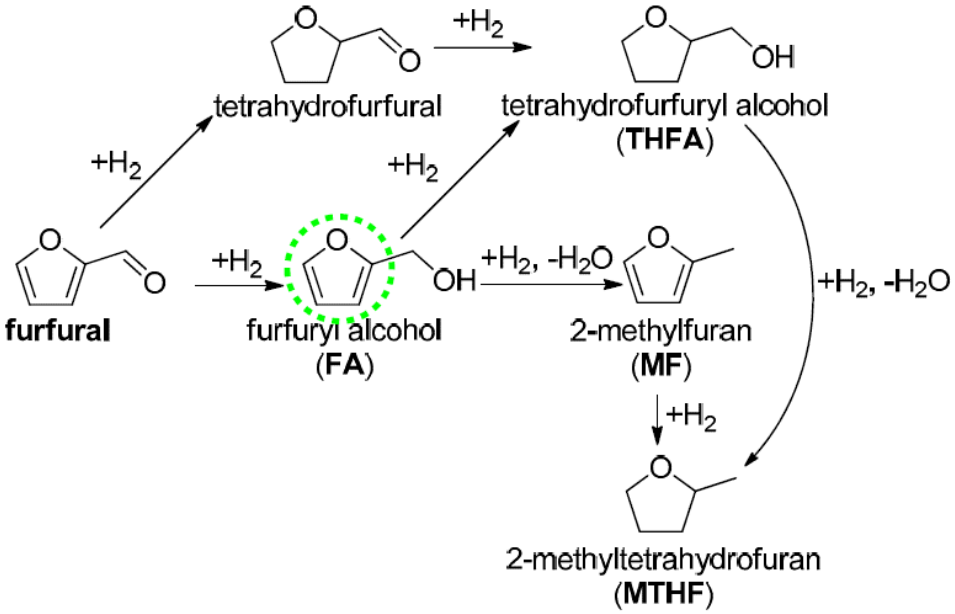

Scheme 2.8. Reaction pathways for catalytic hydrogenation of furfural [67].

Furfural hydrogenation has been extensively studied utilising a variety of non-noble metal catalysts, including Co, Zr , Cu, Ni, , and Mo, as well as noble metals (e.g., Pt, Pd, Ru, Au, Ir, etc.) supported on diverse materials, including carbon, biochar, TiO_2, SiO_2, SBA-15, and Al_2O_3. **Table 2.4** summarises the investigations on selective catalytic hydrogenation of furfural using either liquid or gas phase, including the catalyst type, major product, and selectivity. It has been reported that the use of two metal active sites provided in bimetallic catalysts, one of which promotes hydrogen adsorption, while the second promotes C=O group

adsorption [68]. For instance, in a bimetallic system of Cu-Pd/C catalyst the Cu sites were showed to adsorb and activate furfural at the C=O group and hydrogen dissociated on Pd active sites [69].

Table 2.4. Selected studies on furfural hydrogenation: catalyst, main products, and selectivity.

Catalyst	Conditions	Conversion (%)	Main product	Selectivity (%)	Reference
Cu/SBA-15 silica	5 h, 170°C, 15 wt% Cu catalyst (150 mg), H_2 flow 10 $mlmin^{-1}$, feed flow 2.3 $mmolh^{-1}$, and vapor phase hydrogenation	54	Furfuryl alcohol	95	(Vargas-hernández et al., 2014)
Ru/SiO_2 and Ru/SBA-15	Liquid phase hydrogenation, 100°C, 10 or 25 bar, 900 rpm, 100 mg catalyst, 5 h, and 10.86 mmol reactant in 50 cm^3 toluene.	48	Furfuryl alcohol	91	(Durndell et al., 2019)
NiB, NiCeB, NiCuB, NiFeB, NiCoB, and MoNiB supported on γ-Al_2O_3	Liquid phase hydrogenation, 3 h, 80°C, 5.0 MPa, 2 g catalyst, 10.0 g furfural in 40 mL methanol	7.7 to 91.5	Furfuryl alcohol	87.2 to 100	(Wei et al., 2011)
Pd-TiO_2/C	Aqueous phase hydrogenation, 180°C, 2.1 MPa, 300 psig, 2–5 g (catalyst), 0.06 h, and 0.5–4.0 $mlmin^{-1}$.	82	Furfuryl alcohol (FA), 2-methylfuran (2MF), tetrahydrofur furyl alcohol (THFA), and 5-hydroxy-2-pentanone (5H2P)	30 (FA), 13 (2MF), 5 (THFA) and 21 (5H2P)	(Pirmoradi & Kastner, 2021)
Pd, Cu and bimetallic Pd–Cu supported	Aqueous phase hydrogenation, 110°C, 0.6 MPa, 90 min, 0.60 g	98.5	Furfuryl alcohol	93	(Fulajtárova et al., 2015)

on activated carbon, MgO, and $Mg(OH)_2$	FA in 10 mL H_2O, and 0.10 g (catalyst)				

For selective vapour and liquid phase hydrogenation of furfural, a range of catalysts, including both noble and non-noble metals can be used. Multifunctional catalysts often include two or more active sites, with each active site playing a specific role in the hydrogenation or HDO reaction system. Catalyst screening studies demonstrated that both the metal function and the support were important in directing the selectivity to furfuryl alcohol during catalytic hydrogenation of furfural [69]. Several catalytic processes have been investigated for the conversion of furfural into C_4 and C_5 chemicals, and the review of these studies has been published in the literature [41]. It is important to note, however, that most of these studies are still carried out at the laboratory-scale, owing to the cost and catalyst deactivation issues associated with implementing these heterogeneous catalysts in commercial processes. Therefore, future studies of scalability will be important.

2.6 HDO catalysts

Understanding the structure–function relationships that determine catalytic performance (e.g., activity, selectivity, lifetime) enable advances in heterogeneous catalysis. The development of HDO catalyst for deoxygenating and upgrading biomass pyrolysis bio-oil requires an understanding of the factors that promote cleavage of C–O bonds and the formation of C–C bonds. The development of heterogeneous catalysts for HDO of biomass pyrolysis bio-oil with a particular emphasis on model compounds has been explored using variety of catalyst combinations. Studying catalysts and the reaction networks they promote using model compounds has been the focus of many HDO studies [56]. An overview provides a comparison of the performance of noble metals, transition metals, base or non-precious metals and metal

carbide catalysts, for HDO of typical bio-oil model compounds and consequently bio-oil catalytic upgrading.

It has been reported that the stability of the catalyst and support will be crucial in the presence of steam and a low hydrogen-to-carbon ratio atmosphere [56]. Thus, in an actual bio-oil environment may result in significant deactivation of catalysts that show excellent stability in model compound studies. Both model compounds and bio-oil studies, hydrogenation and deoxygenation take place simultaneously at metal sites, while hydrogenation is primarily promoted by metal sites [60]. Today, despite varying levels of oxygen removal, several monometallic catalysts (such as Pt, Ag, Au, Pd, Ru, Ni, Rh, and Co) have been thoroughly investigated in the HDO process.

Furthermore, the activity and selectivity of bimetallic catalysts with a major hydrogenation metal and an additional oxophilic metal, such as Ni-Cu,Ni-Fe,Co-Cu, Co-Mo ,Co-Fe , Ni-Mo, Pt-M (where, M = Co, Ni,Fe, Cu), and Pd-Fe, are shown to be favourable in catalysing HDO reactions [70]. Thus, majority of HDO catalysts bring together active metals with a variety of supports, including sulfided Mo-based catalysts, Ni-based catalysts, noble metal catalysts supported by Al_2O_3, SiO_2, Al_2O_3-SiO_2, zeolites, activated carbon, carbon nanotubes, and others [5,24]. Acidity (i.e., acid type, strength, and number), network structure (i.e., pore size distribution and surface area), and surface functional groups of a heterogeneous catalyst can all have a substantial impact on catalytic activity and selectivity. The results clearly demonstrated that deoxygenated products could form with stronger binding of oxygen from carbonyl group to metal. It is important to identify the nature of active sites and mechanisms of HDO reactions of model compounds over the catalyst in order to develop efficient catalyst bio-oil conversion systems. It is often the active metal sites that activate hydrogen and hydrogenation reactions, and the support acid sites promote the cleavage of C-O bonds and could also act as spillover for additional hydrogen during HDO [18].

In addition to conventional Ni(Mo), Co(Mo) catalysts, supported noble metal and transition metals catalysts have been extensively studied for catalysing HDO with crude bio-oil and its model compounds [40]. It has been shown that HDO can be achieved with the use of traditional hydrodesulfurisation (HDS) catalysts, such as sulfided CoMo and NiMo supported on Al_2O_3. Although metal sulfides display reasonable catalytic HDO activities, they deactivate rapidly, especially when water is formed as a by-product [48]. It is possible to improve the water resistance of HDO catalysts by modifying their support. Deactivation of the HDO catalyst during upgrading of bio-oil is a major issue, and the processes of deactivation are yet unclear [71]. The process of deactivation can be influenced by water effect (which can alter the phase of the active metals or support), polyaromatic species chemisorption, or poisoning by coke deposition. Compounds containing more than one oxygen atom (e.g., vanillin, guaiacol, furfural, etc.) appear to be more prone to polymerization-induced carbon formation. On the catalytic surface, polymerization and condensation reactions lead to the formation of coke. Also, as the acidity of the catalyst increases, coking increases, whereas acid sites are required for HDO to occur. This implies a trade-off in HDO catalyst design and selection of support.

2.6.1 Noble or Precious Metal Catalysts

Metal sites of catalysts are important in the HDO reaction because hydrogen is first dissociated into H atoms on the catalyst and then adsorbed on the metal sites [18]. Afterwards, hydrogen transfer occurs between the reactants and the adsorbed H. As metal sites produce active hydrogen, their activity directly affects hydrogenation, HDO, and the distribution of products. Pd/C, Pd/Al_2O_3,$PdRh/Al_2O_3$, Pt/SiO_2, Pt/C, and Rh/Al_2O_3 were among the noble metal catalysts that were tested for HDO of vanillin; however, the bimetallic $PdRh/Al_2O_3$ catalyst used the least hydrogen and showed the highest selectivity (99%) towards creosol [5,24].

The results from several studies have demonstrated that the typical sulfided Co-Mo and Ni-Mo catalysts exhibited lower catalytic activity in HDO of bio-oil and its model compounds than the noble-metal catalysts. The exorbitant cost of noble metals catalysts, on the other hand, limits their industrial scale and widespread practical application. However, sulfided transition metal catalysts deactivate fast due to the low sulfur content of the bio-oil, resulting in sulfur removal from the catalysts and coke production [40]. As a result, it is required to develop noble-metal-free catalysts that meet characteristics such as low-cost, non-sulfided, high HDO activity, and good regeneration capacity. For the noble metal catalyst designs, monometallic or bimetallic catalysts developed by impregnation of Rh, Pt, and Pd, on various supports demonstrated equal or superior activity than the traditional $CoMo/Al_2O_3$ catalyst, with less coke deposition [2].

2.6.2. Transition metal catalyst

Non-noble metals, particularly transition metals in their oxides, nitrides, carbides, or phosphides, emerge as an excellent alternative to expensive and limited noble or precious metals because they are sulfur-free, low-cost, abundant, and have an oxophilic nature [72]. The common group of transition metal catalysts normally contain sulfided molybdenum (Mo) on an alumina support promoted with either Cobalt (Co) or Nickel (Ni) metal in a bimetallic system. Transition metal phosphides (Ni_2P, MoP, WP, and Fe_2Psupported on silica) have recently been shown to convert phenolic compounds of bio-oil via HDO with greater stability than conventional $CoMo/Al_2O_3$ catalysts, owing to decreased coke deposition [2]. Examples of transition-metal carbides include Mo_2C, NbC, WC, and NiMo carbide. Dispersed active metal nanoparticles have a greater activity than bulk metal particles, since more active sites are exposed to the catalyst as compared to bulk metal particles [73].

To improve catalytic performance, high metal loadings are frequently used with transition metal like Ni, resulting in bulk metal particles. With microporous support materials, high metal loading is likely to result in bulk metal nano-sized particles blocking the support pores, thereby lowering metal dispersion. To address this challenge, chemical treatment methods such as acidic (using H_2SO_4) or basic (using KOH) treatment would be employed to engineer mesoporous biochar support with high surface area to achieve highly dispersed active metal sites. Typical examples of chemicals commonly used for activation of catalyst support like biochar include H_2SO_4, H_3PO_4, KOH, NaOH, $ZnCl_2$, K_2CO_3, etc. A transition metal catalyst can also be used for selective catalytic hydrogenation, taking advantage of the possible bifunctional systems. Such catalysts firstly need to activate oxy-compounds, which can be achieved with either the valence of an oxide of a transition metal or with an exposed cation, often associated with the catalyst support [6]. Secondly, active sites are present that activate hydrogen and its transfer reactions. Using acid catalysed reactions, zeolites catalysts can convert small oxygenates such as aldehydes and ketones; however, they are found to be limited in deoxygenating phenolic compounds [59].

2.6.3 Base or Non-Precious Metal Catalysts

Although noble metals have exhibited excellent catalytic performance and durability, their high cost and scarce availability aroused the search for new, more economical catalytic active phases [72]. Another attractive group of catalysts for HDO reactions are non-sulfided base metals, which includes Ni, Cu, Mo, Fe, Zn, and their alloys. Due to their advantage over transition metal sulfides and noble metal catalysts, they are regarded as promising substitutes for them. This is because in addition to being relatively cost-effective, base or non-precious metal catalysts also demonstrate excellent catalytic activity.

It has been reported that Ni-based catalysts demonstrated better syringol conversion, selectivity, and yield of oxygen-free products than Fe and NiFe catalysts (primarily alkylbenzenes by transalkylation reactions) in HDO [74]. The maximum syringol conversion of 99.91% was observed when 10 wt% Ni/activated carbon (AC) was used. Studies have shown that the bimetallic Ni-Cu supported catalysts are even more active than Ni, such as Ni-Cu/Al_2O_3, and Ni-Cu/CeO_2 achieved anisole HDO degree of 99.2% [75]. The monometallic counterparts include Ni/Al_2O_3, Ni/ZrO_2, Cu/ZrO_2, Ni/SiO_2, Ni/Cr_2O_3 and others. Hence, the activity of Ni-based catalysts in various catalytic reactions as well as HDO has attracted widespread attention. The properties of base metals make them plausible candidates for HDO catalysts, since they are generally oxophilic, inexpensive, and environmentally benign [76]. An overview of the pros and cons of the various HDO catalysts is shown in **Figure 2.5**.

Figure 2.5. Summary of the pros and cons of the various HDO catalysts[72]

2.6.4 Supports for HDO catalysts.

Catalyst supports are often porous materials responsible for stabilising and dispersing of metal active phase on the catalyst. The support may also provide acid sites, which promote dehydration, hydrolysis, and transalkylation capabilities [18]. The selection of support material is a crucial part of HDO catalyst composition, design, and development. Additionally, the choice of the support material also plays a crucial role in ensuring the catalyst meets the criteria of good resistance to acid and base media, low cost, high dispersion of active metals, and high thermal stability. Although carbon support materials match these requirements and have a

higher resilience to coking than acidic supports [22], they nevertheless have difficulties with oxidative regeneration.

In recent times, it has been found that noble metals (Pt, Pd, and Ru) supported on reducible metal oxide supports (TiO_2, ZrO_2, Nb_2O_5, and CeO_2) have demonstrated superior activity in the deoxygenation of phenolics to hydrocarbons when compared to catalysts based on non-reducible metal oxide supports (e.g., alumina, mesoporous silica, and zeolites) [77]. Apart from the noble metals, the catalyst carriers account for a significant portion of the overall cost of carrying out HDO. A catalyst with high specific surface area can provide more active metal sites accessible to reactant molecules. Thus, the catalyst support should possess adequate pore structure for enhanced diffusion and surface area for dispersion of active metals. It is often found that catalysts with acidic characteristics promote the cleavage of C-O bonds, while metal oxides with oxygen vacancies, such as ZrO_2 and TiO_2, act selectively as adsorbents and activators of reactants [18].

As an example of catalyst support effect, it has been reported that the dispersion of Mo sulfide species was affected by differences in carbon support surface chemistry, especially oxygen surface group functionalities [62]. Thus, when conventional wet impregnation is employed, a pre-treatment of the carbon support is needed to improve the dispersion of the active metal. Several supports such as SiO_2-Al_2O_3, Al_2O_3, CeO_2-ZrO_2, MgO, ZrO_2,TiO_2, SiO_2, activated carbon, etc. have been investigated and reported in the literature for HDO of bio-oil model compounds. Alumina support (Al_2O_3) has been found to be an unsatisfactory support because it will convert to boemite (AlO(OH)) in the presence of higher amounts of water produced during HDO of bio-oil or its high oxygenate model compounds [46,78,79]. There is a strong negative effect of water in the pyrolysis oils on conventional alumina supported catalysts (e.g., NiMo/γ-Al_2O_3), as alumina is converted into hydroxides [78], which causes deactivation over time. Thus, carbon has been discovered to be a more promising support than alumina

because the neutral nature results in lower tendency for coke formation. It has been demonstrated that the concentration of adsorbed phenolic compounds on SiO_2 support (interact via H-bonding) was only 12% that of Al_2O_3 at 400°C, where chemisorption is primary mode of adsorption [80]. This suggests deactivation of active sites due to chemisorbed organic compounds and consequently coke formation could take place more readily on alumina support than silica. It has been discovered that phenate-type species (i.e., salt or ester of phenol) adsorbed on alumina support of CoMo/ γ-Al_2O_3obstruct access to sulfide edge sites [71]. Therefore, HDO catalyst support should be chosen based on two factors, firstly, it should have a low affinity for carbon synthesis, which is related with the support acidity, and secondly, it should activate oxy-compounds to facilitate HDO and adequate activity [6].

2.7 Biochar as a catalyst support

As a result of the thermal degradation of lignocellulosic biomass under oxygen-free environment, biochar is produced, which is a carbon-rich material that can be used for many applications [42]. Biochar can be produced using a variety of techniques, including slow and fast pyrolysis, microwave-assisted pyrolysis, gasification, and hydrothermal carbonization of biomass. The composition of biomass feedstock, the method of production and operating conditions determine the biochar's properties. Biochar is mostly produced by slow pyrolysis and hydrothermal carbonization of biomass. Pyrolysis is widely known for its ability to convert biomass into bio-oil, biochar, and gaseous products [81]. The biochar residue material is useful for a variety of environmental applications, including carbon capture and storage, catalysts and adsorbents, activated carbon production, wastewater treatment, energy storage (e.g., fuel and supercapacitor), and soil amendment [42]. It is a heterogeneous composite material containing both graphite-like microcrystalline aromatic structures and amorphous less-carbonized fractions [42]. The investigation of biochar qualities revealed that it has a relatively high porosity and surface area, as well as a high concentration of minerals such as K, Ca, and P, and

functional groups on the surface [42,54]. Thus, it can be utilised as an adsorbent, catalyst support, and catalyst. Moreover, the biochar produced during the slow pyrolysis of biomass can be used as a catalyst support for HDO and hydrogenation of typical bio-oil model compounds including catalytic upgrading of crude bio-oil itself.

The catalytic performance, activity, and selectivity during a HDO reaction of a model compound is generally influenced by the acid-base property, surface area and pore size distribution of the support. Therefore cost-effective, sustainable, and robust catalyst supports need to be developed, with adequate mesoporosity and surface area to disperse the active metal and promote the hydrogenation and deoxygenation reactions during HDO. It has been shown that metal-mesoporous support catalysts exhibited impressive anisole HDO performance in comparison with metal-microporous support catalysts [60,82]. Mesoporous biochar is of particular interest as a catalyst support for a variety of HDO reactions as a result of its enhanced surface area, porous networks, and improved mass transport.

Internal diffusion limits the performance of conventional microporous zeolites, mesoporous silicas, titania, zirconia, and alumina supports for HDO catalysts for vanillin and furfural hydrogenation. It became clear that these types of catalyst supports were limited for HDO, necessitating the development of a novel catalytic system that satisfied the requirements of cost-effectiveness, stability against coke formation, and acidic effects of bio-oil. Biochar offers the benefit of shape selectivity in terms of structure since the pore structure may be modified or altered by physical or chemical treatment. This research work focuses on designing a robust non-noble metal-based biochar-supported catalyst for HDO of vanillin, hydrogenation of furfural and catalytic upgrading of crude bio-oil. **Figure 2.6** depicts the production of biochar, syngas, and bio-oil by thermo-chemical conversion (e.g., pyrolysis, gasification, and hydrothermal carbonization) of woody biomass [83].

A diagram of biochar porosity that includes many functional groups is shown in **Figure 2.7**. In this study, a novel biochar support was engineered via acidic and alkali treatment methods to prepare biochar-supported Ni catalysts, with aim to enhance mesoporous structure and surface area compared to the original biochar.

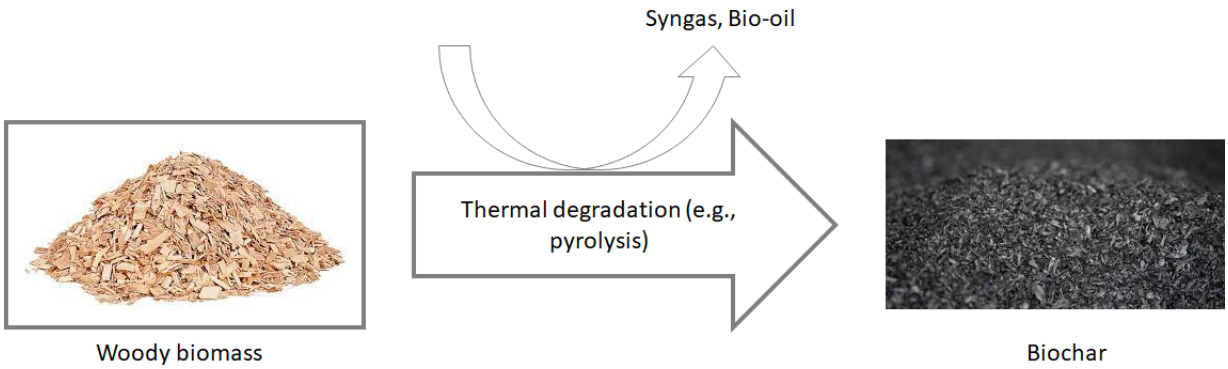

Figure 2.6. Production of biochar via pyrolysis of woody biomass.

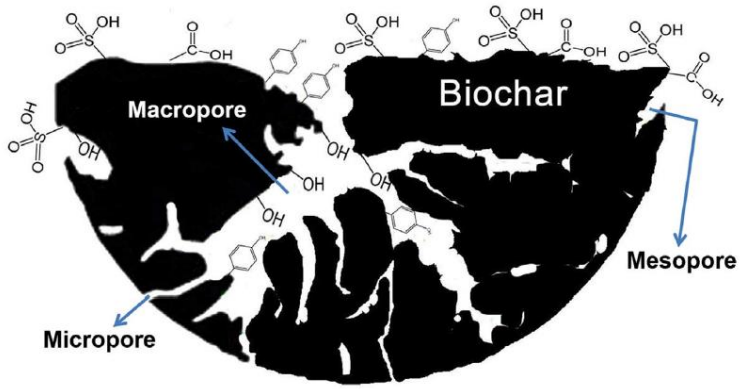

Figure 2.7. A diagram depicting the biochar porosity comprising different functional groups [84].

The improved mesoporosity of the biochar is intended to facilitate improved internal mass transport and desorption of molecules. This characteristic could potentially produce highly dispersed Ni species on the surface of the catalyst and increases the number of Ni sites dispersed in mesopores. The hypothesis is that these sites can catalyse the HDO of vanillin, hydrogenation of furfural and upgrading crude bio-oil and improve catalytic performance and

selectivity. It was hypothesised this is due to better access to Ni sites located in mesopores. It has been reported that more oxophilic (i.e., tendency to form oxides via hydrolysis or abstraction of oxygen) metals such as Ru, Co and Ni are preferable for HDO phenol because they favour direct dehydroxylation (i.e., hydrogen addition to a hydroxyl group) followed by hydrogenolysis [85]. Due to stronger acid sites provided by metal oxides, oxygen-containing functional groups can be adsorbed by the catalyst more easily [18]. Thus, the C=O bond in vanillin would selectively adsorb onto the surface of the Ni/biochar catalyst. Unsaturated C-C bonds can be activated and reduced when nickel active metal, which has a strong hydrogen dissociation capacity, is present [70]. The rational design of active, stable, and selective catalyst systems has been limited by the inability to understand gaps between reaction conditions, underlying mechanisms, and product selectivity [86]. The mechanisms of furfural and vanillin hydrogenation were explored based on kinetic modelling and product selectivity using an engineered biochar supported Ni catalyst in this study. Furfural was selected as a biobased platform molecule and model for aldehyde, and vanillin, a phenolic oxygenate of chemical prevalent in bio-oil.

The ability to design biochar to have tailored features, such high surface area and porosity through physical and chemical alterations, as well as its renewable nature are some of its advantages as a catalyst support for HDO and hydrogenation. A cost-effective, renewable catalyst or catalytic support for upgrading bio-oil can be fabricated from biochar because of its high carbon content and embedded surface functional groups. Its usage as a catalyst or carrier in the upgrading of bio-oil itself, the conversion of syngas, and the transesterification for the production of biodiesel has also been published in the literature [54,87]. By chemically treating biochar with an acid (H_2SO_4) or an alkali (KOH), its sorption capacity can be enhanced, the catalytic activity and selectivity increased. Additionally, using FTIR, it was discovered that the surface of biochar contains functional groups including C-O-C and -COOH. The interaction

of reactants with biochar surfaces during reactions is known to be improved by these surface functional groups [88]. Additionally, functional groups on the surface of biochar could improve the dispersion of active metals by promoting metal-support interactions. Furthermore, integrating the circular economy concept, recycling biochar as a catalyst carrier for the HDO or hydrogenation of bio-oil or its model compounds will improve the overall process economics. The HDO method for upgrading bio-oil becomes more environmentally friendly, sustainable, and economically viable when non-noble metals like nickel are used as active metals and renewable biochar is used as a catalyst carrier. These non-precious metals show strong activity as catalysts for upgrading bio-oil and related model compounds, but they need greater metal loadings than their noble metal counterparts, typically by 10-20% higher to attain equivalent selectivity and activity [89,90]. This metal loading range is quite higher than that used when noble metals are utilised as the active phase in the catalyst. Compared to noble metals, nickel is less expensive and has shown a high hydrogenation activity, so it is commonly used as an active metal catalyst [48]. This shows that the choice of catalytic support and the active metals used both have an impact on catalyst activity.

As a result, the goal of this research is to design and develop a renewable, robust, sustainable, and cost-effective catalyst for HDO of vanillin selectivity into p-creosol, hydrogenation of furfural into 2-methylfuran, and ultimately crude bio-oil upgrading utilising nickel-impregnated biochar produced from biomass via slow pyrolysis of wood chips.

2.8 Mass transport and kinetic models

Usually, reaction rate equations for three-phase solid-liquid-gas catalytic reactions of bio-oil model compounds in batch reactors are described using Langmuir-Hinshelwood-Hougen-Watson (LHHW) kinetic type models assuming a single or dual adsorption sites [23,24,65,91,92]. As a result, external mass transport, inter- and intra-particle diffusion

limitations may have played a major influence in catalytic activity and/or selectivity since the reaction is a three-phase heterogeneous process [92]. Among the advantages of this approach are (1) the process of adsorption of reactants, surface reaction, and desorption of products on the catalyst's surface is considered, and (2) the developed and validated reaction rate equation can be extrapolated to concentrations outside the experimentally measured range [23].

However, to develop true kinetic models, these diffusion resistances (i.e., both external and internal mass transport limitations) must be negligible, thus ensuring that concentration-time data are obtained under the kinetic control regime of the reaction. Generally, the HDO and/or hydrogenation of bio-oil model compounds, the gas phase is practically pure hydrogen, and the gas-liquid interface is considered to be instantly saturated with respect to hydrogen, in which case the gas-phase mass transport limitation may be ignored [92,93]. In the bulk liquid phase, the level of mixing and catalyst loading determines the mass transport limitation for the transfer of dissolved hydrogen to the catalyst surface. Therefore, in most studies the effect of stirring rate (i.e., impeller speed of the batch reactor) is explored to determine the speed under which external transport limitation becomes negligible. Likewise, experiments with diverse ranges of catalyst particle sizes are typically carried out to identify the particle size at which internal transport limitations become negligible in order to demonstrate the lack of pore diffusion restrictions [5,92].

Additionally, the Wiesz-Prater criterion can also be applied to ascertain if the kinetic model data are affected by both internal and external mass transport limitation [23,68,94]. Wiesz-Prater criterion is defined by **equation 2.1** and should have a value less than 0.3 for reaction order of ≤ 2 [93].

2.1

where, r_0 denotes the initial reaction rate, η the effectiveness factor, φ it the Thiele modulus, ω the catalyst loading, and L is the characteristic length of the spherical catalyst particle.

The kinetic of vanillin HDO was studied using batch autoclave reactor (100 mL Parr reactor) by employing two plausible reaction rate equations developed from the dual site of the Pd/C catalyst under the assumption of dissociative chemisorbed hydrogen [23]. The LHHW type kinetic models shown in **equations 2.2 to 2.5** have been used to explore the experimental data of bio-oil model compounds hydrogenation and HDO. Several LHHW type kinetic models of heterogeneous reactions have been outlined in the literature to study the hydrogenation of oxygenate model compounds [91]. For vanillin HDO over Pd/C catalyst it was found that the kinetic model developed with the assumption of competitive adsorption of dissociative hydrogen and vanillin described the experimental data with a correlation coefficient greater than 99% [23]. The kinetic model HDO of vanillin has also been studied in which with conversion and concentration of products, a reaction network approach was used to develop and determine the reaction rates by assuming a pseudo-first order based on experimental data obtained using a batch reactor at 413-573 K, 1.2 MPa of hydrogen, and employing a takovite-derived, reduced $NiAlO_x$ mixed oxide catalyst [95].

On this basis of mass balance, a set of ordinary differential equations (ODEs) were developed for each compound of the reaction network. The validation of the ODEs used to model reaction rates achieved a good fitting between experimental and calculated data.

Model-I: The assumption is based on surface reaction as the rate controlling step, dissociative adsorption of hydrogen, one-site competitive adsorption of substrate (SB) and hydrogen, and total coverage of active sites [91].

2.2

Model-II: Non-competitive adsorption of dissociative $H_2$and substrate (SB) during HDO based on the assumption that hydrogen atoms dominate active site S_1, and vanillin dominates S_2.

2.3

Model-III: the model assumed one type of adsorption site (competitive adsorption) and the rate-determining step as a surface reaction between an adsorbed hydrogen and a partially hydrogenated substrate (SB) species.

2.4

Model-IV: The Eley–Rideal reaction mechanism involving substrate (SB) and product (p).

2.5

Where, C_H denotes dissolved hydrogen concentration in the solvent, C_{SB} concentration of substrate, k_s surface reaction rate constant, k_H hydrogen adsorption constant, k_{SB} substrate adsorption constant, C_P desired product concentration, and r the rate of reaction.

Using 100 mL batch autoclave reactor, Srivastava and co-workers [92] applied Model-I, Model-III (**equation 2.3**), and Model-IV (**equation 2.4**) to study the kinetic of furfural hydrogenation to furfuryl alcohol and 2-methylfuran [92]. The results showed that the most appropriate kinetic model that best matched the experimental data was a dual-site mechanism with dissociative adsorption of hydrogen and surface reaction as the rate-controlling step (Model-III for 2-methylfuran and Model-I for furfuryl alcohol). In another study involving vapour-phase hydrogenation using a pyrex glass reactor, the purposed kinetic models (Models II and III) were used to investigate furfural hydrogenation on copper chromite with the assumption of one/two sorts of adsorption sites and a surface reaction between an adsorbed

hydrogen and a partly hydrogenated furfural as the rate-determining step [65]. The results showed that Modell-II developed assuming surface reaction as the rate-controlling step and a two-site adsorption prove to be satisfactory fits of the experimental data. On the other hand, a packed bed reactor (PBR) was used to study the multi-step aqueous phase hydrogenation kinetics of furfural to furfuryl alcohol, 2-methylfuran, tetrahydrofurfurfuryl alcohol, and 5-hydroxy-2-pentanone over Pd-TiO_2 on an activated carbon catalyst at temperature 180°C and hydrogen pressure 2.1 MPa [68]. Using non-linear regression of experimental data, parameters of the reaction models were obtained for Langmuir-Hinshelwood type kinetic model which assumed two active sites, such as metal site for hydrogenation and acid site for ring opening. There was a good agreement between the kinetic model and experimental data, with a R^2 of 0.93–0.96 and typical residuals of less than 5%. Thus, one of the objectives of this study is to develop a kinetic model for furfural hydrogenation to 2-methylfuran based on LHHW approach and power law method.

2.9 Conclusion

The multi-component nature provided insights into the complexity of bio-oil, leading to the focus on model compounds as a basis for the development of robust catalysts and elucidation of reaction mechanisms. The chemistry of bio-oils model compounds from pyrolysis has been reviewed in detail including phenolic compounds such as guaiacol, vanillin, anisole, and platform molecule furfural. In addition to the properties and composition of bio-oil, the method of production and catalytic upgrading was discussed in detail. For the purpose of designing and developing efficient HDO catalyst, studies focus on bio-oil model compounds. In this respect, phenolic compounds such as vanillin and guaiacol are mostly studied. Three functional groups are present in vanillin, including carbonyl, hydroxyl, and ether bonds, making it a good representation of oxygenates in bio-oils. Results from HDO of model compounds studies may not necessarily represent how compounds will behave in bio-oil environments

during catalytic upgrading, which contain additional interactions with neighbouring compounds. Moreover, metal-based catalysts may rapidly deactivate at high temperatures during the HDO reaction of either model compound or actual bio-oil due to metal leaching and structural changes resulting from the exposure to water. Thus, the design and choice of catalyst support is critical to the success of the HDO process. As a result of its excellent hydrogenation capacity, nickel-based catalysts have great potential for HDO of lignin derivatives, phenolic model compounds and bio-oils. Furthermore, catalyst performance is also influenced by the structure of the catalyst, which affects how the active sites are dispersed. In this work, chemical activation method will be applied to enhance the biochar specific surface and mesoporous structure to improve both the dispersion of Ni nanoparticles and mass transport of molecules during HDO. On the other hand, functional groups containing oxygen on the surface of the biochar can act as active sites, chemisorbing the reactant molecules and forming intermediates during HDO reaction.

Chapter Three

Materials and Methods

3.1 Introduction

This chapter describes the materials such as vanillin, solvents, catalysts, and gases used in this study. Also included is information about the suppliers and purity of the chemicals and gases used. This is presented and discussed in **Section 3.2**. In addition, the experimental procedure and analytical methods used for characterising products and materials after experiments are also described. In the following **Section 3.3**, the method for preparing the catalyst used in this study is described. The catalyst support used in this research work is biochar from thermochemical reforming (TCR) of sewage sludge and was obtained from the Hohenburg plant in Germany. This chapter also explains how applied acid and alkali treatments modified biochar to improve its physicochemical properties such as surface area, pore size distribution, and pore volume. A major objective of this modification is to evaluate the effectiveness of enhanced catalyst physicochemical properties in improving the conversion, hydrogenation and hydrodeoxygenation of vanillin. The modified biochar support is compared to the unmodified biochar support to determine if it is more effective. The equipment used for catalyst preparation and procedure for hydrogenation of selected bio-oil model compounds are well described in this Chapter. The experimental setup and reactor description is presented in **Section 3.5**. Additionally, a description of analytical methods for identifying and quantifying the reactant and products was also provided. Also explained are the instrumental methods used to characterize the prepared catalysts and the modified biochar support before and after reaction. This chapter also covers experimental design using response surface methodology (RSM) using Minitab statistical software to optimize the reaction conditions for vanillin conversion and p-creosol yield.

3.2 Materials

Information on the purity and suppliers of chemical reagents and gases used in conducting this research work are presented in **Table 3.1**. Note that all analytical grade chemicals were used in the experiment as they were purchased without any prior purification.

Table 3.1: Chemicals and gases, their suppliers and percentage purity.

Materials	**Supplier**	**Specification**
Chemical reagents		
Vanillin (4-Hydroxy-3-methoxybenzaldehyde, 4-(HO)C_6H_3-3-(OCH_3)CHO)	Alfa Aesar, UK	99%
Vanillyl alcohol (4-Hydroxy-3-methoxybenzyl alcohol, $HOC_6H_3(OCH_3)CH_2OH$)	Sigma Aldrich, UK	98%
P-creosol (2-Methoxy-4-methylphenol, $CH_3OC_6H_3(CH_3)OH$)	Sigma Aldrich, UK	≥ 98%
2-propanol $(CH_3)_2CHOH$	Sigma Aldrich, UK	99.99%
Nickel (II) nitrate hexahydrate $(Ni(NO_3)_2 \cdot 6 H_2O$,	Sigma Aldrich, UK	99.99%
Furfural	Sigma Aldrich, UK	99%
2-methyl furan	Sigma Aldrich, UK	99%
Furfuryl alcohol	Sigma Aldrich, UK	98%
Furan	Sigma Aldrich, UK	99%
Tetrahydrofuran	Sigma Aldrich, UK	≥99%
Tetralin	Thermoscientific, UK	>98%
Potassium hydroxide (KOH)	Sigma Aldrich, UK	90%
Sulfuric acid (H_2SO4)	Fisher scientific	95%
Dimethyl disulfide	Sigma Aldrich, UK	≥99.0%
Dichloromethane	Sigma Aldrich, UK	≥99.9%
Gases		
Hydrogen (H_2)	BOC gases	-
Nitrogen (N_2)	BOC gases	-
5% Hydrogen-nitrogen mix (5% H_2/N_2)	BOC gases	-
Helium (He)	BOC gases	-
Compressed air	BOC gases	-
Others		
Biochar	Thermo-catalytic conversion of sewage sludge	-
Bio-oil	Thermo-catalytic conversion of sewage sludge	-

3.3 Catalyst preparation

The bio-oil and biochar used for this research work were generated at Hohenburg plant in Germany, by pyrolysis of dried sewage sludge wastes as explained in 3.3.1. This biochar was further modified via chemical treatment to improve its physicochemical properties. This is described in the following sections. Consequently, the as-received biochar and the chemically modified biochars were used as a support to prepare different catalysts with varying surface areas, pore size distribution and pore volume.

3.3.1 Thermochemical reforming (TCR) of dried sewage sludge

The biochar and bio-oil were produced for supply to this study (not produced in this study) by Hohenburg plant in Germany using a 500 kgh^{-1} TCR reactor at intermediate pyrolysis of dried sewage sludge at atmospheric pressure using an augur screw reactor at 450°C under nitrogen atmosphere.

i) 500 kgh^{-1} sewage sludge of dried matter was introduced into a TCR reactor.

ii) The residue was then subjected to pyrolysis at 450°C to yield a dark amorphous solid liquid.

iii) Both the produced biochar and vapours from the pyrolysis were post-reformed in a fixed bed reactor.

iv) The post-reforming reactor works at 700°C, which ensures further decomposition of volatile components,

v) Counterflows between vapours and biochar to increase the contact area and thus the efficiency of catalytic cracking.

vi) The average solid residence time allowable in the auger screw reactor was 20 minutes, which was enough for pyrolysis to take place.

vii) The average residence time allowable for the biochar and vapors in the post-reformer was 1 hour, which was enough for the decomposition of the two elements. The temperature of the cracked vapours was rapidly reduced by using a shell and tube water cooled heat exchanger. It condenses the vapour into liquid form during this process.

viii) Gravity settling of the condensed liquids to allow for phase separation was done after 24 hours. Natural separation occurs with differences in densities between the oil phase and water phase.

ix) After 24 hours, the separate collection of the oil phase is made. This oil phase makes the bio-oil product.

x) The biochar thus obtained from the above process of pyrolysis was used as a support for the catalyst in the present work.

xi) Further, it was also used to upgrade the bio-oil model compounds, the bio-oil obtained in the following process.

3.3.2 Chemical activation of biochar

i) 7M KOH (aq) was mixed with biochar in the ratio 3:1 (KOH (aq) : Biochar) by weight.

ii) The obtained mixture was stirred at a temperature of 120°C for up to 3 hours.

iii) The mixture obtained was filtered by vacuum in order to separate the chemically impregnated biochar from the 7M KOH (aq).

iv) Washing steps with deionize water were carried out a couple of times for the removal of excess KOH from the biochar at every step of washing**; the filtrate was tested with the litmus paper after every washing step until a neutral pH is obtained** [96]. The KOH activated biochar was labelled as thus: biochar (KOH).

3.3.3 Acidification of Biochar

i) About 300 ml of concentrated sulphuric acid (95%-98%) was added into 50 ml round bottom flask containing 20g of biochar, then fitted with a reflux condenser.

ii) The mixture was then heated on a hot plate at 120°C for 3 hours, monitoring the temperature using a heating mantle and thermocouple.

iii) After heating, the mixture was cooled down to ambient temperature.

iv) The slowly cooled mixture was added to 300ml of de-ionized water (2/3 ice) so that the mixture may cool to room temperature.

v) The reaction was then stirred to allow it to completely be quenched.

vi) The mixture obtained was diluted and filtered by vacuum filter.

vii) The precipitate was repeatedly washed with hot distilled water until the later is free from sulfate ions, as proved by the testing if the pH. [96]. The solid material produced was denoted as biochar (H_2SO_4).

3.3.4 Preparation of Ni/biochar, Ni/biochar (KOH), Ni/biochar (H_2SO_4)

i) Nickel (ii) nitrate hexahydrate (17.82 g) was added to 50 ml deionised water to give aqueous solution.

ii) Biochar (20 g) was slowly added to the aqueous solution produced in i) above and the resulting mixture was stirred using magnetic stirrer at 800 rpm, at 70°C leaving behind a wet solid.

iii) The wet solid was transferred to an oven, dried overnight at 80°C.

iv) The dried catalyst was calcined at 500°C for 5.5 hours under nitrogen atmosphere in a turbular furnace to produce the Ni/biochar catalyst., it is worth notting that all catalysts used in this study, Ni/biochar, Ni/biochar (KOH), Ni/biochar (H_2SO_4) were prepared according to the same methodology described above.

3.4 Catalyst Characterization

Catalyst characterization is a critical aspect of catalyst design and development and chemical reaction optimization. It provides useful information about the catalyst surface chemistry necessary for structural modification or optimization needed for improved activity and selectivity. This section outlines different catalyst characterization techniques used to study the properties of biochar support and the synthesized catalysts used in this research work.

3.4.1 Transmission Electron Microscopy (TEM)

Particle size distribution of the prepared catalysts was studied using TEM. Prior to TEM analysis, the sample is prepared by dissolving the sample in ethanol by stirring, embedding in a TEM grid and dried to evaporate the ethanol to form electron dense and less dense regions on the grid.

i. An electron beam from mostly tungsten source accelerated by a high voltage of electron beam of about 20KV was focused on the sample through the condenser lens.
ii. The electron dense regions absorb more electrons and less are transmitted while the electron less-dense regions absorb fewer electrons and transmit more electrons [97].
iii. The transmitted electron beams pass through the objective lense to the detector.
iv. The detector envisions the sample to give a level of resolution and magnification based on the differences in the transmitted electrons.

A diagram illustrating this can be seen in **Figure 3.1**.

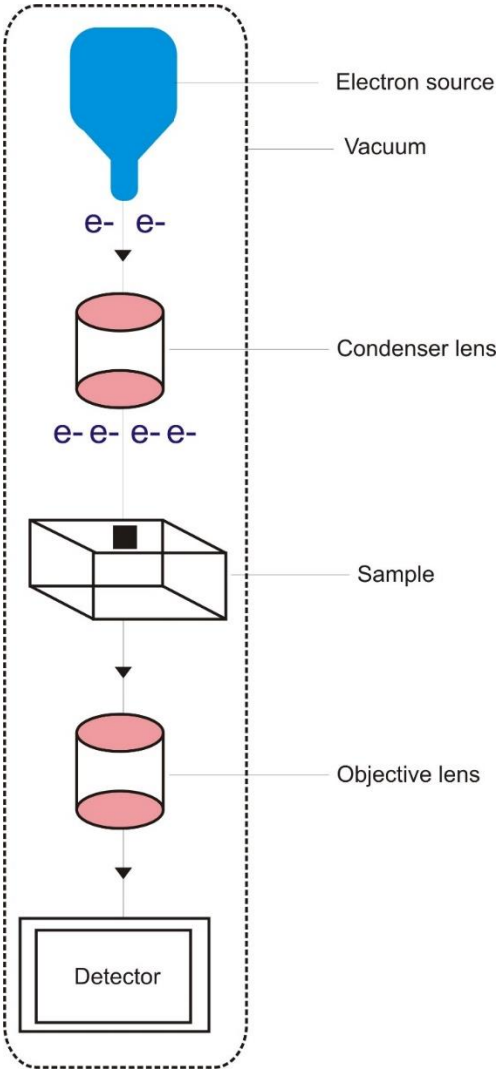

Figure 3.1: Schematic diagram for Transmission Electron Microscopy analysis.

3.4.2 Scanning Electron Microscopy (SEM)

A Hitachi TM3030 Scanning electron microscopy (SEM) was used to analyse the surface morphology and textural properties of the catalyst by placing a gold coated sample onto the microscope stub and exposed to high energy beam.

The principle of SEM is based on emitting a high energy beam of electrons from an electron gun which serves as the cathode. Prior to the analysis, the sample was coated with a thin layer of gold using a sputter coater.

i. The sample (coated with gold) was mounted onto the sample stub.

ii. The SEM chamber was pumped up to a level of achievable low vacuum for imaging.

iii. The following SEM chamber parameters were set; beam voltage, beam current, working distance, and magnification and the sample stub was aligned with in the SEM chamber for proper orientation and focusing of the electron beam on the sample surface.

iv. In the scanning mode, initial scan of the sample with very low magnification to locate regions of interest was performed.

v. This was done in order to make images as clear and sharp as possible, paying attention to the focus and working distance.

vi. Imaging parameters like beam current, acceleration voltage, and aperture size have been adjusted to optimize image quality and resolution.

vii. The high-resolution images from the sample surface were captured using the digital imaging system of the SEM.

viii. The SEM images were analysed to understand the texture, composition, morphology and elemental distribution of the sample surface.

ix. Interpretation of the SEM data was made to draw conclusion with regards to the characteristic properties of the sample. **[98,99]. The SEM is equipped with Energy Dispersive X-ray spectroscopy (EDX) which is used to analyse the elements present** in the sample. EDX uses X-rays to eject the inner electrons of the atoms, causing the outer electrons to drop from higher to lower energy levels based on Moseley's law. This explains the relationship between the atomic number and characteristic frequency of light released by the atoms [98].

Figure 3 demonstrates a pictorial representation of the principle of EDX.

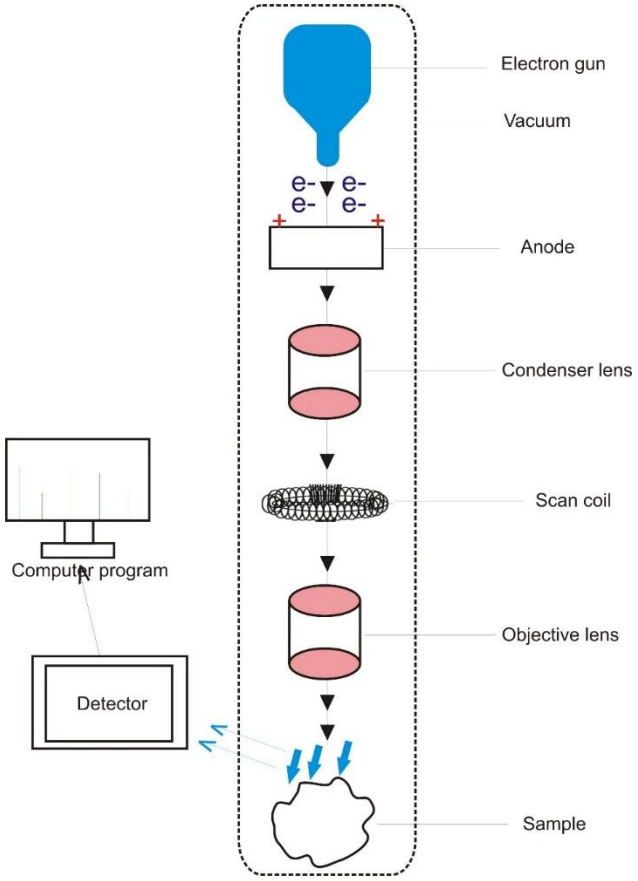

Figure 3.2: Schematic diagram for scanning electron microscopy analysis.

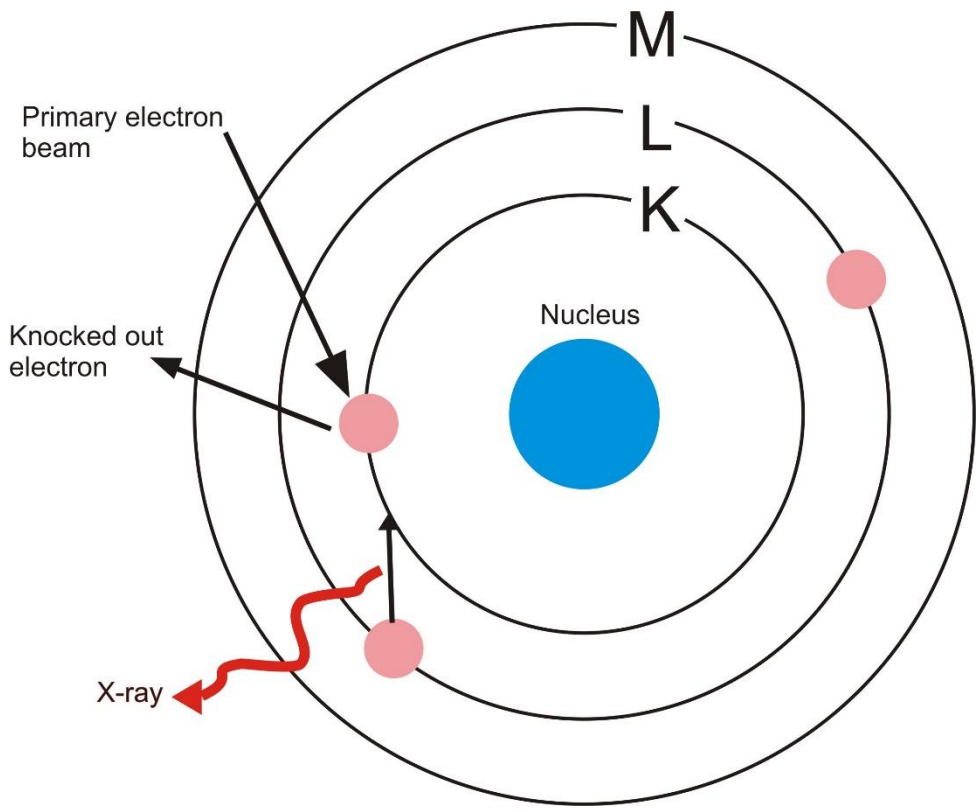

Figure 3.3: Schematic diagram for Energy-Dispersive X-ray spectroscopy analysis.

3.4.3 Thermogravimetric Analyses (TGA)

Thermogravimetric analysis is an analytical technique in which weight loss of the sample is measured with respect to time or temperature. In this study, it was used to examine the thermal stability of the biochar support catalysts. **Figure 3.4** shows a schematic diagram of a typical TGA equipment. A PerkinElmer TGA 800 equipment was used to carry out thermogravimetric analyses of the samples.

i) A zeroed sample plan was placed in the sample collection tray, where the prepared catalyst (17.5 mg) was placed on it.

ii) To create an inert atmosphere within the thermogravimetric analysis (T.G.A) chamber, the equipment was switched on for nitrogen flow.

iii) The sample pan loaded with catalyst was placed in the furnace in the TGA chamber.

iv) The thermogravimetric analysis of the sample catalyst was operated in a nitrogen atmosphere.

v) The temperature was ramped up from 25℃ to 800℃ at 10℃/min using the TGA furnace.

vi) The changes in sample weight were continuously recorded against the temperature from (25℃-800℃) during which the gaseous products are removed during heating.

vii) The thermobalance essentially included a microbalance for sample weighing, a computer program for setting and controlling experimental conditions, and a furnace for heating and cooling, was used for the collection and following of experimental data simultaneously in the course of experiments.

viii) TGA data was analysed after that to find the thermal stability, decomposition temperature and weight loss or gain characteristics of the catalyst.

xii) The results obtained from Thermogravimetric analysis were interpreted to understand the thermal behavior of the catalyst under consideration.

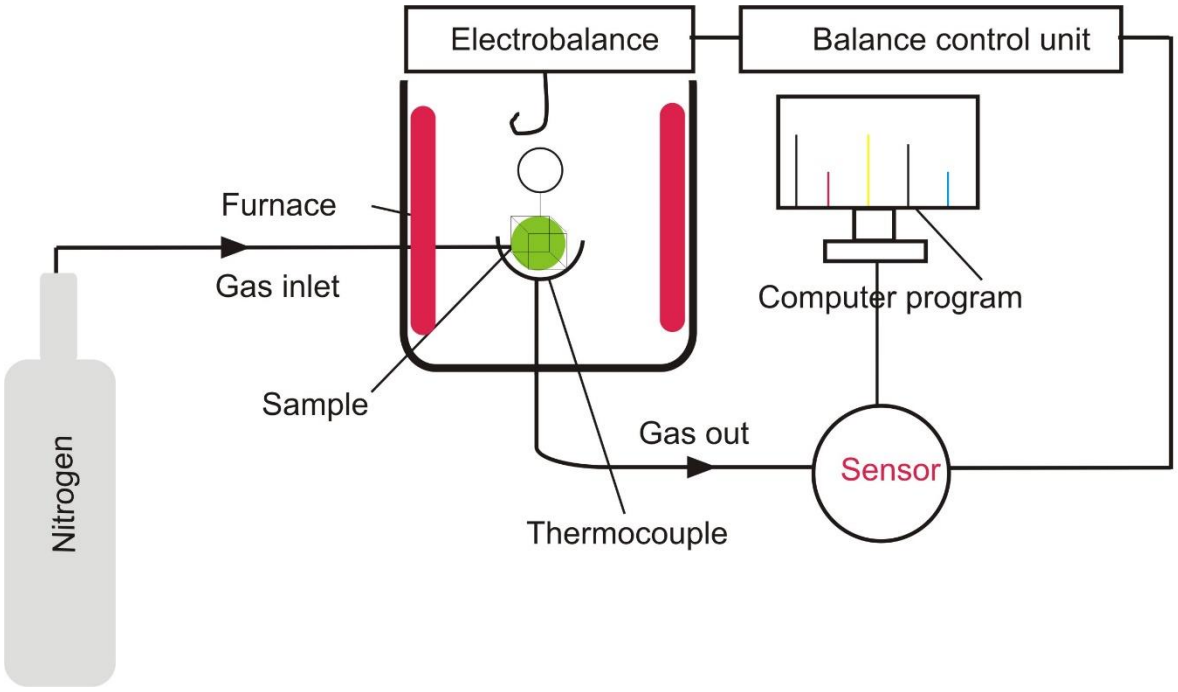

Figure 3.4: Schematic diagram for Thermogravimetric analysis Set-up.

3.4.4 Fourier-transform infrared spectroscopy (FT-IR)

A Perkin Elmer FTIR analyser was utilized to study the functional groups present in the prepared catalysts and biochar supports. After setting the program, about 100 mg of the sample was introduced into the sample crystal. The analysis was carried out under nitrogen to prevent overeating of the sample.

i) The catalyst loaded sample holder was placed into the FT-IR spectrometer and was irradiated with a beam of I.R light over a range of wavelengths (4000-750 cm^{-1}) to obtain an infrared (IR) spectrum.

ii) The FT-IR spectrum was obtained in terms of intensities versus the wavelength at which the reflection or transmission of the infra-red light occurs.

iii) The FT-IR spectrum obtained from ii) was analysed to identify the functional groups present the catalyst sample [100].

The basic principle of FT-IR analyses is based on Beer-Lambert law which established the linear relationship between concentration (C) and absorbance (A_{bs}) of a sample [101].

Figure 3.5 shows the schematic diagram of a typical FTIR working principle. In this study, with a resolution of 0.4 cm^{-1} and a scanning rate of 100 scans per second, FTIR spectra are collected using a LiTaO3, KBr window detector.

The basic principle of FTIR analyses is based on Beer Lambert law which established the linear relationship between concentration (C) and absorbance (A_{bs}) of a sample. The absorbance is thus calculated as follows:

3.1

Where A_{bs}= Absorbance, ε= Molar extinction coefficient ($M^{-1}cm^{-1}$) and b = Length of light path (cm) and c = Molar concentration (M),

The molar extinction coefficient measures the amount of light a substance absorbs at a specific wavelength. The concentration is the amount of analyte in solution and the path length of light is the width of the cuvette for measuring absorbance and is typically 1 cm.

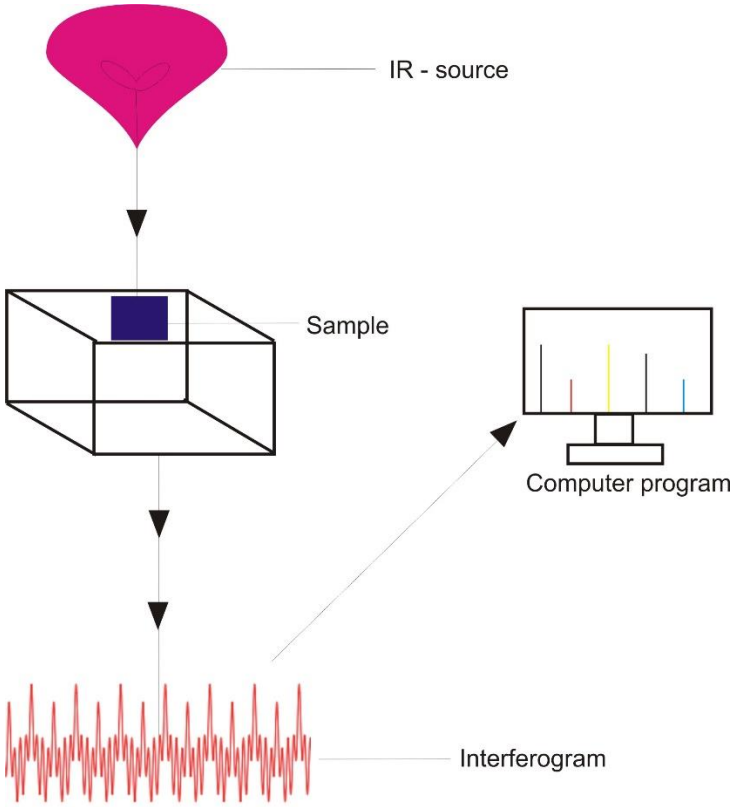

Figure 3.5: Schematic diagram for Fourier transform infra-red spectroscopy analysis.

3.4.5 Brunauer-Emmett-Teller (BET) and Barrett-Joyner-Halenda model (BJH)

A Micrometrics Analytical Instrument 3Flex equipment was used to determine the catalyst and biochar support material specific surface area, pore-size distribution, and pore-volume through the nitrogen adsorption-desorption method according to the following procedure:

i) The catalyst sample was vacuum-degassed at a high temperature (200°C- 300°C) to ensure complete removal of adsorbed moisture and volatile impurities.

ii) The degassed catalyst sample was loaded to the sample cell of the Bet analyzer where the temperature was sustained and later on nitrogen (N2) gas passed into the sample cell at low pressure (77k).

iii) The amount of gas adsorbed on the catalyst sample was measured by using the BET analyzer on the various pressure point.

iv) The specific surface area of the catalyst sample was determined from the graph of the relative pressure (p/po) versus the amount of gas adsorbed.

v) The pore size distribution was subjected to more analysis with the help of the Barret-Joyner-Halenda (BJH) method.

v. Based on Brunauer-Emmett-Teller (BET) and Barrett-Joyner-Halenda (BJH) model equations, the surface area and pore size distributions were respectively calculated.

The BET equation is given as:

3.2

where V is the quantity of gas adsorbed, P_0 is the saturated pressure of adsorbate, P is equilibrium pressure of adsorbate and C is the BET constant. A plot of the group $P/V(P_0-P)$ against relative pressure (P/P_0) is relative pressure, derived from the BET adsorption isotherm in **equation 3.2** [102,103] and used to determine the volume of gas required to form a monolayer, V_m and the BET constant, C.

The BET surface area was calculated from **equation 3.3** [103]:

3.3

where V_m represent the molar quantity of gas adsorbed (cm^3), N_A is the Avogadro's number ($6.02 \times 10^{23}\ mol^{-1}$), S is area of adsorbed N_2-gas molecules, M_v is molar volume of gas adsorbed (cm^3).

The catalyst porosity was calculated using the BJH model by the principle of capillary condensation of N_2 gas described by Kelvin equation shown in **equation 3.4**.

At the boiling point of nitrogen, kelvin equation may be represented as;

(nm) 3.4

where r_k is the radius of curvature of the adsorptive condensed in the pore, $P_0$is the N_2 saturation vapor pressure at liquid nitrogen temperature, $P_{eq}$is the equilibrium pressure of adsorptive nitrogen. In order to accommodate condensation that occurs after the formation of adsorbed layer on the pore walls e.g. in a cylindrical pores:

3.5

Where r_p is the cylindrical radius andt_a is thickness of adsorbed film.

3.4.6 X-Ray Powder Diffraction (XRD)

With the aid of the XRD technique, it is possible to determine the crystallinity of the prepared catalyst, the crystal phase, and the elemental composition of the materials. XRD is a non-destructive analytical method used to characterise the crystallographic nature of a sample. The basic principle is centered on diffraction of filtered x-rays from a cathode resulting to the constructive interference of the crystalline and monochromatic x-rays [104] material in accordance with Bragg's law ($n\lambda = 2dsin\theta$) which explains the relationship between the diffraction angle (2θ), lattice spacing (d) and the wavelength (λ) of a crystalline sample [105]. The diffraction angle patterns obtained are compared with standard database [106].

i) The powdered catalyst sample was mounted on the XRD instrument of the XRD and scanned from 2θ values of 5 to 70.

ii) The scanning process was initiated to permit x-rays to interact with the catalyst sample as the 2θ values were swept.

iii) The instrument detected the amount of interaction of the sample with monochromatic x-rays and then processed to peak intensities.

iv) The peak intensities are converted into count rate which represents the intensities of x-ray diffraction.

v) The count rate data was further processed as computer output.

vi) The xrd results was interpreted in terms of catalyst composition, structure and properties.

3.4.7 Hydrogen Temperature-Programmed Reduction (H_2-TPR)

H_2-TPR is a technique that could be used to study the reducible nature of a catalyst. Hydrogen is used in hydrogen temperature programmed reduction because it is a strong reducing agent that can react with metal oxide materials [107-110]. By monitoring the amount of hydrogen that is consumed by the sample as it is heated, information can be gained about the strength and number of reducible sites on the surface [107,108].

H_2-TPR provides useful basic information on the catalyst reduction temperature, metal phase or any other reducible metal present in the catalyst or catalyst support. It also provides the optimal activation conditions such as heating rate, and hydrogen consumption. H_2-TPR analyses depend on metal particle size and active catalyst loading [111].

In this research work, H_2-TPR analysis was done at Harwell research complex in collaboration with the UK Catalysis Hub using Chem-BET Pulsar TPR-TPD chemisorption analyser. [112].

i. The sample (0.1 g) was placed into the reactor and pretreated in a continuous flow of helium at 30 ml min^{-1} and 400°C for 2.5 hours to purge volatile matter and impurities.

ii. The reactor was then cooled to room temperature following pre-treatment and heated in a continuous flow of hydrogen gas (50-80°C) at 10°C min^{-1} flow rate.

iii. The changing concentration of the hydrogen was measured as the sample was heated through a Thermal Conductivity Detector (TCD).

iv. Data was collected through thermal conductivity detector and analysed to determine the reduction profile of the sample.

v. It is worth notting that hydrogen was used to reduce gas.

3.4.8 Carbon dioxide Temperature-Programmed Desorption (CO_2-TPD)

Carbon dioxide temperature programmed desorption (CO_2-TPD) is an analytical technique employed to characterise the surface basic properties of a catalyst or sample [113]. CO_2 is used in temperature programmed desorption because it is a weakly adsorbed molecule that is sensitive to the presence of acid sites on the surface of a material. By monitoring the amount of CO_2 that is released from the surface as it is heated, information could be gained about the strength and number of acid sites.

The catalyst could be classified as having weak, moderate or strong basic sites based on the basic strength [114]. The CO_2-TPD analyses were done at Harwell in collaboration with the UK Catalysis Hub using a Chem-BET Pulsar TPR/TPD chemisorption analyser.

i. About 0.1 g of the catalyst was firstly treated in a constant flow of Helium (He) with a flow rate of 30 ml min^{-1} at 300°C for 60 minutes.

ii. Subsequently, the sample was allowed to cool to about 120°C and subjected to CO_2 for 1 hour,

iii. The physiosorbed CO_2 was then removed by sweeping with

3.5 Catalytic Tests

The Parr reactor 45\98 system used in this study consists of a 100 mL cylindrical reactor vessel, a thermocouple for temperature sensor, a stirrer to aid mixing, a heating jacket to heat up the reactants, and a pressure indicator. It also contains a liquid sampling valve and gas venting valve for sample collection and gas purging respectively. As a result of these components, all the HDO experiments in this study could be conducted. The schematic diagram of the reactor system and setup is shown in **Figure 3.6**. The reactor is designed to operate at a maximum pressure of 138 bar at 500℃.

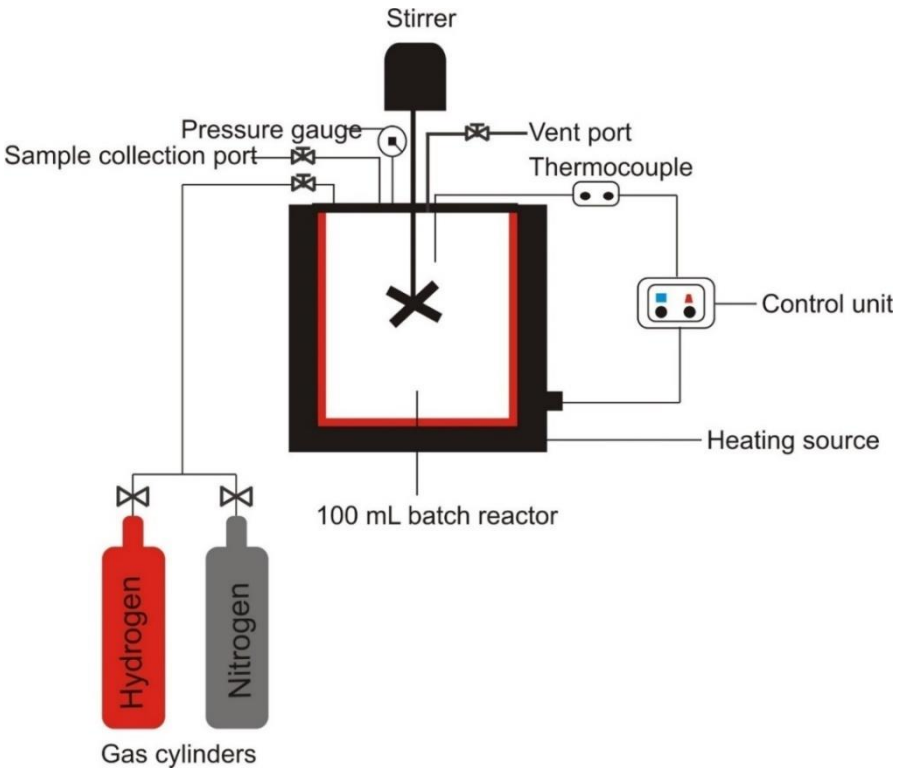

Figure 3.6: Schematic Diagram of the Experimental Set-up

3.5.1 Experimental Procedure

As shown in **Figure3.6**, a 100 mL Parr reactor was used to conduct the hydrodeoxygenation (HDO) reaction experiments. The experiments involve the HDO of

vanillin and furfural, which are common oxygenate model compounds in bio-oil. Prior to the reaction, the catalyst was activated (ex-situ) in a Carbolite Geo TF1200 tubular furnace under a constant flow of H_2/N_2 at 500°C for 5 hours. A desired amount of the catalyst (0.4-0.8 g) and reactant solution 50 mgL^{-1} of solvent (2-propanol or 1,2,3,4- tetrahydronaphthalene) were fed into the reactor, sealed, and purged three times with nitrogen. It was then heated under ambient pressure until the experimental temperature is reached. To pressurize the Parr reactor to the desired experimental pressure, hydrogen gas was injected into it as a reactant and stirred until the desired revolutions per minute were reached after the reactor reached the required temperature. At the moment hydrogen was introduced into the reactor, the reaction start time was set. For complete or uninterrupted reactions, the samples were collected at the end of the experimental run-time while samples are collected at regular intervals of reaction time for kinetic studies. Firstly, 2-propanol solvent was chosen based on results reported in the previous study which showed 100% conversion and selectivity (p-creosol) when using this solvent [24]. Secondly, based on GC analysis of the product mixture, the solvent peak remains unchanged, indicating that 2-propanol solvent has not been hydrodeoxygenated during HDO of vanillin and can be confirmed as not participating itself in the reaction. The reaction was performed at the set-point within 100°C to 150°C temperature range, hydrogen (H_2) pressures of 30 to 50 bar and 1000rpm stirring rate based on the experimental design shown in **Table A1**. The sample collection followed a similar technique reported in the literature, where the sample collected was fixed (in microliters) to minimise pressure loss [115].

3.5.2 HDO of bio-oil from dried sewage sludge

A Parr 4848 reactor was used to perform the HDO of bio-oil. Prior to the reaction, about 4g of the Ni/acidified biochar catalyst was reduced in-situ under hydrogen in the reactor vessel. For the sulfided catalyst, the Ni/acidified biochar catalyst was mixed with Dimethyl disulfide in the ratio 1:1 before reduction. The catalyst reduction was carried out under43 bar of hydrogen, heated from 20°C to 370°C, the pressure was increased to 95 bar at 370°C and left for 3 hours. After cooling, about 21g of the bio-oil was fed into the reactor, sealed and purged 3 times under hydrogen. It was then heated to 370°C at 45 bar and then pressurized to 95 bar of hydrogen. The product was collected after cooling by loosening the autoclave and poured into a beaker.

3.6 Product Analysis

For every experiment, about 2 mL of liquid samples were collected periodically and analysed using a gas chromatograph (GC-Agilent 6890N) equipped with an FID detector and column (30 m × 0.320 mm × 0.25 μm). The GC was operated at an inlet pressure of 4.1 psi with helium as the carrier gas. The inlet and detector temperatures were set at 320℃ and 330℃, respectively. The oven temperature was programmed at 60℃ and subsequently ramped to 300℃ at a heating rate of 24℃min^{-1}. Then, 1 μL of the collected sample was injected into the column using a split ratio of 20:1 for each analysis. Despite the fact that the reaction pathway indicates the formation of water molecules, the GC-FID could not detect peaks for water. As a result, the yield was calculated using the moles of the reactant and products, and the selectivity was also calculated with those moles. The following equations (**Equations 3.5 to 3.7**) were used to quantify reactant conversion, yields of products, as well as their selectivity.

3.5

3.6.1 Mass Balance

Decarboxylation of furfural to form furan resulted in the formation of carbon monoxide as a gaseous product. The mass balance was calculated as the difference between the total mass of products (liquid and gas) and mass of reactant mixture fed into the batch reactor. The mass balance of the liquid and gaseous products from the reaction were calculated from **equations 3.8 and 3.9**.

$$Liquid\ product(wt.\%) = m_p/m_r \times 100 \quad (3.8)$$

$$Wt.\%\ of\ gaseous\ products = 100 - liquid\ product\ yield \quad (3.9)$$

where m_p is mass of liquid product and m_r is the mass of reactant.

3.7 Reaction optimization

For optimization, response surface methodology (RSM) makes it easy to evaluate independent reaction variables and their interactions, thereby saving money and time. The reaction parameters: temperature (100 – 150°C), H_2 pressure (30 - 50 bar), and catalyst loading (0.4-0.8g) were studied using response surface methodology (RSM) in 3-level Box-Behnken design (Minitab 19 statistical software) for hydrodeoxygenation of vanillin over Ni/biochar. **Table 3.1** shows the experimental conditions used in the optimization study. 15 sets of experimental conditions were randomly generated from RSM as shown in **Table 3.2** using reactions factors and levels in **Table 3.2**. The 15 sets of experiments were conducted in duplicate to ensure variability of data. The data obtained from the experiments was fitted using

a regression equation to model vanillin conversion from HDO of vanillin. It is worth noting that the catalyst loading as used in this research work refers the weight in grams of catalyst per reaction solvent volume (mL).

Table 3.2. Reaction factors and levels.

Factors	Lower level	Higher level
Temperature (°C)	100	150
H_2-Pressure (bar)	30	50
Catalyst loading (g)	0.4	0.8

Table 3.3. Design of experiment.

StdOrder	RunOrder	PtType	Blocks	Temperature (°C)	Pressure (Bar)	Catalyst loading (g)
1	8	2	1	100	30	0.6
2	11	2	1	150	30	0.6
3	12	2	1	100	50	0.6
4	7	2	1	150	50	0.6
5	5	2	1	100	40	0.4
6	10	2	1	150	40	0.4
7	15	2	1	100	40	0.8
8	3	2	1	150	40	0.8
9	14	2	1	125	30	0.4
10	13	2	1	125	50	0.4
11	9	2	1	125	30	0.8
12	6	2	1	125	50	0.8
13	2	0	1	125	40	0.6
14	4	0	1	125	40	0.6
15	1	0	1	125	40	0.6

A renewable Ni/biochar, Ni/biochar (KOH) and Ni/biochar (H_2SO_4) were also used to test the effect of chemical (KOH and H_2SO_4) modification of the biochar support on vanillin deoxygenation and the best catalyst was used for HDO of furfural, binary mixture of vanillin and furfural and TCR bio-oil.

3.7 Analysis of Variance (Annova)

Annova is a statistical tool employed to analyse the variations in response variables studied under different combination of reaction conditions [116]. The relative contribution of reaction variables (temperature, pressure and catalyst loading) on vanillin deoxygenation was determined using Annova at 95% confidence level at α =0.05. The significant terms were obtained by comparison of their p-values with the α values of 0.05.

Results from Annova were used to assess the effect of linear, square and 2-way interactions of the reaction variables. The results obtained from the procedures described in this chapter are presented in **chapters 4 and 5**.

Result from analysis of variance was used to generate a polynomial model that could be used to predict the degree of vanillin conversion within the studied range of temperature, pressure and catalysed loading as shown in **Table 5.4**.

CHAPTER FOUR

Catalyst characterisation

4.1. Introduction

There is a close relationship between the microstructures of heterogeneous catalysts and their catalytic properties and performance. A discussion of the results of the characterization of the prepared catalyst and the modification of the biochar will be presented and discussed in this chapter. In order to develop, design, and optimize novel catalysts, characterization is essential. Therefore, using characterisation techniques, the effect of modifying the biochar support with potassium hydroxide and sulfuric acid on its physicochemical properties such as pore volume, pore diameter and surface area will be assessed. This chapter presents the catalytic properties of biochar, Ni/biochar, Ni/biochar (KOH) and Ni/biochar (H_2SO_4) and improvements in some desirable catalytic properties resulting from chemical modification of the biochar support. Characterisation techniques will help quantify the differences between the catalysts for HDO of vanillin and bio-oil upgrading generally. The superior catalytic properties of hierarchically porous materials containing micro-, meso-, and macro-pores have attracted significant attention compared to single-mode pores[117]. In this study, a hierarchically porous, renewable and novel catalyst was developed by chemically modifying the pore structure.

A comprehensive understanding of how microstructures relate to catalytic properties requires structural information. This is critical for the design of new catalyst as well as the study of reaction mechanism. The results obtained using the following characterisation techniques are also presented here and discussed. Hydrogen Temperature Programmed Reduction (H_2-TPR) and carbon dioxide Temperature Programmed Desorption (CO_2-TPD) were used to determine the reduction temperature and basic strength of the synthesized catalysts. The results are presented and discussed in **Sections 4.7 and 4.8**, respectively. The

changes in the catalyst pore size distribution and surface area were quantified through nitrogen adsorption and desorption measurement technique. The BET equation was applied to determine the surface area of the catalysts prepared using the original biochar and those modified through alkali and acid treatment. While BJH model was used to describe their pore size distribution. However, an analysis of the thermal stability of the catalysts was conducted by thermogravimetric analysis (TGA). The actual active metal content of the synthesized catalyst was confirmed using inductively coupled plasma-optical emission spectroscopy (ICP-OES) analysis. The catalyst morphology and elemental composition of biochar were determined using the SEM-EDX and the results reported in **Section 4.3**. On the other hand, the particle size distribution of the impregnated nanoparticles of Ni metal was analysed using TEM and the results are presented and discussed in **Section 4.4**. In **Section 4.5**, the impact of chemical modification on the crystallinity of the catalysts was examined using XRD technique. The characterized catalyst was tested in the HDO of vanillin, furfural and bio-oil from the thermo-catalytic conversion of sewage sludge. It will be possible to quantify the impact of the differences in catalysts based on the characterisation differences observed on HDO of vanillin and bio-oil upgrading generally. With the knowledge from the characterisation, a better understanding of the effect of catalyst surface chemistry, active metal phase, strength of active sites, functional groups, and the distribution of nanoparticles of Ni on HDO will be obtained.

4.2 Physicochemical Properties of the Prepared Catalysts

Heterogeneous catalysts have close connections between their structural features and their catalytic activity. Two of the fundamental characteristics of heterogeneous catalysts include total catalyst surface area and porosity (i.e., pore size distribution and pore volume). The pore size of biochar can be tuned to improve catalyst activity and product selectivity, which is accomplished in this study through chemical treatment. **Table 4.1** shows the surface area of the synthesized catalysts calculated using the BET equation and the pore volume estimated using BJH equation for both the pristine and chemically

activated biochars and their corresponding prepared Ni/biochar, Ni/biochar (KOH) and Ni/biochar (H_2SO_4) catalysts, while their nitrogen-sorption isotherms and pore size distributions are shown in **Figure 4.1**. The porous structure of heterogeneous catalysts can greatly influence the accessibility of reactant molecules to active sites, the reaction mechanism, and the selectivity of desirable products [117]. The International Union of Pure and Applied Chemistry (IUPAC) categorizes pores into three sizes: micropores (<2 nm), mesopores (2–50 nm), and macropores (>50 nm). In this study, the hysteresis loop as a result of nitrogen adsorption-desorption pathways indicates Type IV isotherms (**Figure 4.1**), which is consistent with the presence of mesoporous structures that have pores ranging from 2 to 50 nm in size. The results demonstrate that both and KOH and H_2SO_4 chemically activated biochar has a greater specific surface area than the Ni impregnated biochar. Similarly, once impregnated with Ni nanoparticles, a little reduction in the pore volume is seen for all the catalysts (Table 4.1). This suggests that chemical treatment created more mesoporous structures in the biochar, resulting in an increase in the volume of gas uptake as a function of relative pressure (P/P_0), as shown in **Figure 4.1a**. As can be seen from **Figure 4.1b**, the pore size distribution plot confirms this conclusion. The pore size distribution of a heterogeneous catalyst can have a significant impact on the diffusion properties of reactive species during HDO conversion of vanillin to creosol.

However, the hysteresis loops were similar in shape but occurred at different positions in terms of relative pressure, size, and volume due to the increase in the pore size of the biochar caused by the chemical treatment. Consequently, the H3 hysteresis loops are thought to be associated with aggregates of plate-like particles that form slit-like pores [118]. It can be observed that both the surface area and the pore volume of the catalyst increased significantly for the chemically treated biochar support in relation to the untreated biochar (**Table 4.1**). For the chemical activation of biochar with KOH, the surface area and pore volume increased by 64.8% and 65.3%, respectively, compared to that of Ni/biochar (74.84 m^2g^{-1} and 0.095 cm^3g^{-1}). Meanwhile, acid treatment with H_2SO_4 resulted in a 372.3% increase in surface area and a 256.8% increase in pore volume relative to Ni/biochar. Due to improved specific surface area

from KOH and H_2SO_4 treatment, surface active sites can be readily accessible to reactant molecules. However, in **Figure 4.1b**, it can be observed that the mesopores of the chemically treated biochar improved compared to the Ni/biochar. The Ni/biochar (H_2SO_4) developed narrower mesopores compared to those found in Ni/biochar (KOH). A similar observation was reported by Zhang et al. [119] where it was also showed that KOH activated wood pellet biochar significantly increased surface area. This suggests that chemical treatment has the potential to create mesopores (i.e., pores with sizes of 2 to 50 nm) within the biochar as a result of leaching, dehydration and oxidation [120,121].

In addition to offering accessible active sites and efficient mass transport effects, engineered porous biochar materials also provide ample area for the incorporation of catalytically active phases, in this case Ni nanoparticles. The main way KOH and H_2SO_4 improve the porous structure and pore volume of the biochar is through reaction with active O-containing species, which results in a large amount of gaseous products thereby creating pores within the biochar [122]. As a result, the blocked pores in the biochar are also opened, and the size of the small pores is enlarged. This enhanced mesoporous structure of the biochar following chemical treatment and explains the increases in surface area and pore volume, with surface area and pore volume decreasing in the following order: Ni/biochar (H_2SO_4) > Ni/biochar (KOH) > Ni/biochar. This is also consistent with findings reported in the literature regarding chemical activation [96,123]. ICP-OES analyses revealed that the actual Ni metal content in the prepared catalysts ranges from 14.7 to 15.3 wt.%.

However, some of the mesopores that were produced as a result of the KOH treatment may have been blocked by the Ni nanoparticles due to impregnation, especially those with pore sizes between 3 and 4 nm, as seen in **Figure 4.1c,d**.The pore size distribution curve before and

after Ni impregnation of H_2SO_4 activated biochar is identical (**Figure 4.1c,d**), unlike that of the KOH counterpart, corroborating the results presented in Table 4.1.

Table 4.1. Surface area and pore volume of Ni/biochar, Ni/activated biochar, and Ni/acidified biochar.

Catalyst	Surface Area (m^2g^{-1})	Pore Volume (cm^3g^{-1})	Ni Content (%)
Biochar	**94.64**	**0.12**	**-**
Ni/biochar	74.8	0.1	15.1
Biochar (KOH)	**135**	**0.23**	-
Ni/biochar (KOH)	123.3	0.2	15.3
Biochar (H_2SO_4)	**383.4**	**0.34**	-
Ni/biochar (H_2SO_4)	353.3	0.3	14.7

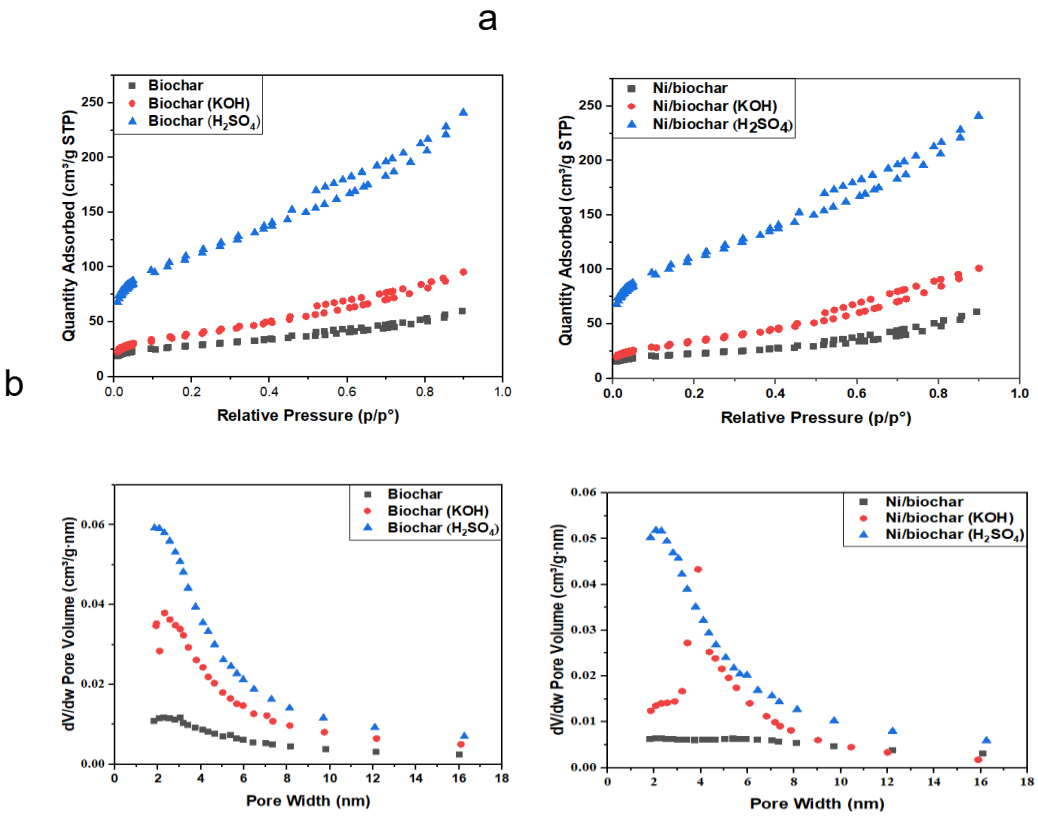

Figure 4.1. The (**a**) N_2 adsorption–desorption isotherm and (**b**) pore size distribution of the prepared catalysts.

The pore size distribution of the catalysts further confirms that they are mesoporous materials, with a pore size distribution found mostly in the range between 2 nm and 16.24 nm (mesopore range 2 to 50 nm). Bio-oil model compounds are molecularly complex, and so, it is often essential to ensure that reactants and products are transported efficiently to and from the active surface by considering the pore size distribution. It is therefore evident that alkali and acid treatment of biochar can enhance its transport and active sites accessibility properties. In comparison with modified biochar, the limitations of mass transport make unmodified biochar unsuitable as a catalyst support. It is most likely that the active sites in unmodified biochar would be confined by its pore sizes, making it more difficult for molecules to interact them. This is due to the limited available surface area. It is believed that porosity-enhanced biochar as a catalyst support can improve its performance.

1. Larger pores lead to faster rates of diffusion and less hinderance of transport.

Generally, in a given material, larger pores allow for easier and faster movements of molecules through them. This is because larger pores offer less resistance to diffusion. In contrast, smaller pores can create a barrier to diffusion, limiting the movement of molecules, thereby slowing down the rate of transport [124-126].

However, it is important to note that the relationship between pore size and diffusion rate can be influenced by other factors, such as the nature of the molecules being transported, the temperature and pressure of the system, and the presence of other substances that may interact with the material. So, while larger pores generally lead to faster rate of diffusion, it's not always a simple or straightforward relationship [124,126,127].

2. A higher surface area leads to more availability of active sites.

Higher surface area generally leads to more availability of active sites. A higher surface area provides more opportunity for molecules or particles to interact with the material, leading to more active sites and greater availability for reactions to occur [128]. However, it's important

to note that simply having a high surface area is not always enough to ensure good reactivity or selectivity [128]. The nature and properties of surface sites, as well as the specific conditions of the system, can also play important roles in determining the overall performance of the catalyst material [128].

3. **The active sites of the modified biochar could be more stable as a result of chemical treatment.**

Chemical treatments, such as acid or alkaline washing, can modify the chemical composition and surface properties of biochar, leading to the creation of new or more stable active sites [129]. Alkaline treatment, on the other hand, can increase the basicity of the biochar surface, which can improve its stability in acidic environment [130]. Overall, chemical treatment can modify the surface chemistry and properties of biochar, leading to the creation of more stable and/or reactive active sites to enhance the performance of biochar. This can enhance the performance of biochar in various applications, such as catalysis, water treatment or soil remediation [131].

The results shown in **Table 4.1** suggest that chemically modified biochar catalysts will exhibit more efficient transport of reactants and products to and from the active surface than unmodified biochar catalysts, owing to their larger surface area and pore volume. As a consequence, by chemically treating biochar, its porosity can be tuned, which represents a potential strategy for developing novel catalysts for HDO and hydrogenation of bio-oil model compounds. An overview was published in 2018 in which Sajjadi et al. [9] examined the effects of chemical activation on biochar's physicochemical properties, functionalities, and applications, including the use of H_2SO_4 and KOH [132].

4.3 Catalyst Morphology, Textural Properties and Metal Distribution

Catalytic properties are closely related to the microstructure of heterogeneous catalysts. The SEM photomicrograph of the biochar is shown in **Figure 4.2a**. The surface topology and

morphology reveal that the raw biochar is composed of agglomerated particles with irregular shapes and sizes and rough surfaces (**Figure 4.2a**). In spite of the surface roughness, no cracks or fissures are apparent on the surface of the biochar. In order to identify the elemental composition of biochar, Energy Dispersive X-ray (EDX) technique was used. The elemental composition of biochar is influenced by the chemical structure of the biomass feedstock from which it was derived by pyrolysis processing. Based on the EDX elemental analysis result, it is clear the raw biochar contains the following elements: Al, Si, Fe, K, Ca, Mg, Ti, S, and P, which may have originated from the biomass (**Figure 4.2b-l**).

Furthermore, elemental mapping by EDX indicated that the biochar was composed of uniformly distributed oxygen (42.6%) and carbon (38.8%), occurring as a result of charring caused by the pyrolysis of the biomass. The O/C ratio is approximately 1.1 which indicates that there are more oxygen atoms than carbon atoms in the biochar material [133]. This is typically associated with biochars produced from feedstocks with high lignin or cellulose content, or biochars that were pyrolyzed at low temperatures or for shorter durations [133].

It is important to note that the O/C ratio is just one of many parameters that should be considered when evaluating the properties of biochar [134]. Other important factors include surface area, pore size distribution, pH, and nutrient content. Additionally, the specific application of the biochar will influence which properties are most important to consider [133,134] This suggests that more O-containing functional groups were reserved on the surfaces, making the biochar more hydrophilic in nature [135].

Typically, biochars have O/C ratios between 0.2 and 0.6, those with O/C ratios approaching 0.6 being the least stable [136]. Although EDX can provide useful elemental composition information, it is not the most suitable technique for precise measurement of O/C ratio in biochar. Employing techniques such as elemental analysis, XPS, or solid -state NMR

spectroscopy will yield more reliable results for determining the O/C ratio in biochar [137,138]. This is because EDX cannot distinguish O in biochar and those due to the presence of alkali and alkaline earth metals, such as K, Ca, and Mg. Hence, the high oxygen content can be a combination of both organic and inorganic components. It has been reported in the literature that some of the oxygen atoms in biochar belong to existing functional groups or are part of functional groups arising from the pyrolysis bio-oil originating from the source biomass [139]. This also confirms that biochar is not a structurally homogeneous material, rather it is a mixture of different chemical structures and features a heterogeneous combination of elements.

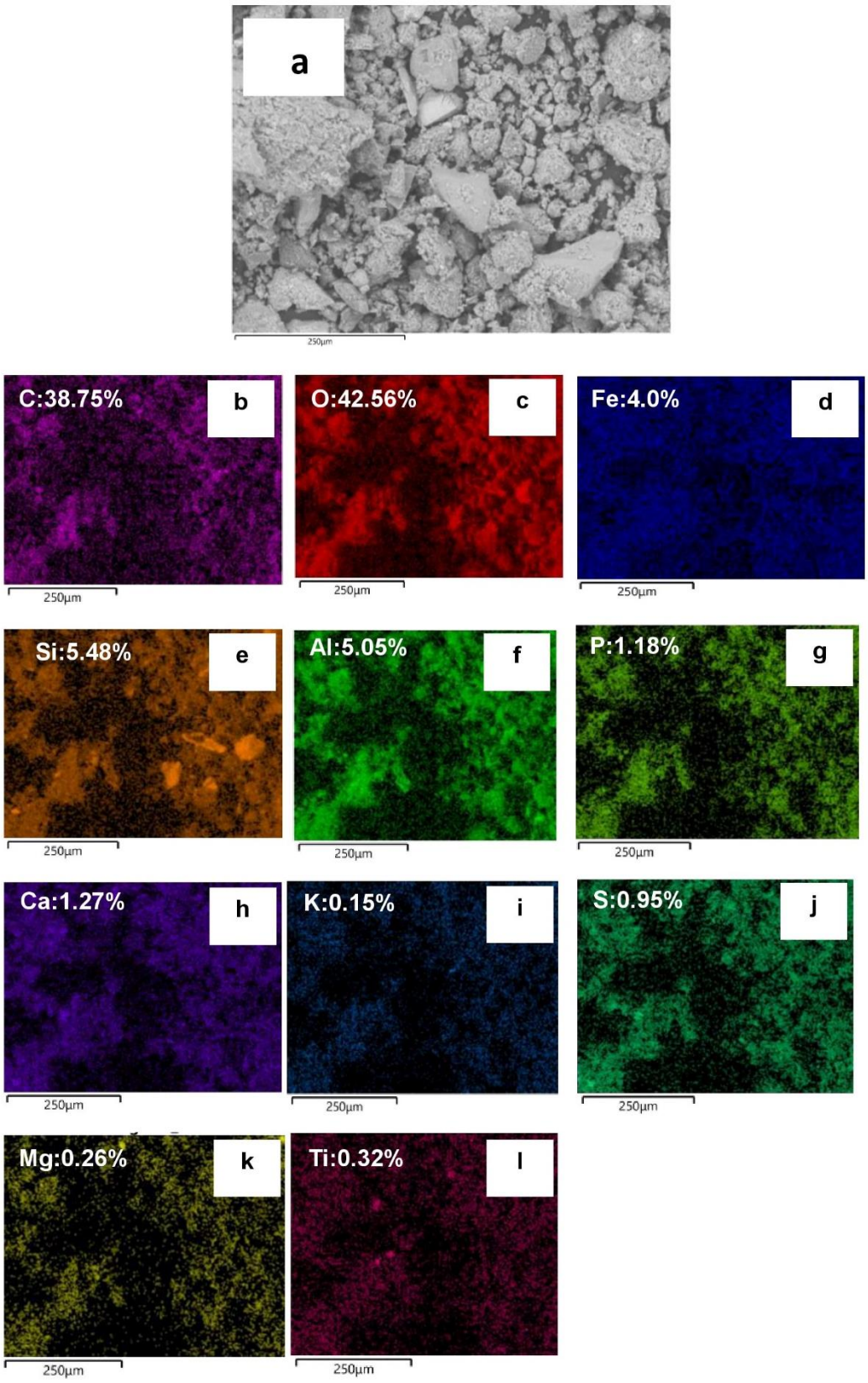

Figure 4.2. SEM-EDX analysis of biochar. (**a**)SEM micrograph; (**b-l**)EDX elemental mapping.

Based on its high oxygen content of approximately 43%, the biochar contains abundant oxygen functional groups. Thermal decomposition of biomass hemicellulose, cellulose and lignin creates the oxygen functional groups of biochar in its solid matrix.

4.4 Catalyst Dispersion and Particle Size Distribution

Catalysts can be characterized at the atomic level using TEM and related microanalysis techniques. Based on the structural information available through TEM, metal support interactions and its dispersion on the carrier surface can be explored close to the atomic level. The TEM images and grain size distribution of the Ni nanoparticles (NPs) are shown in **Figure 4.3**. It is worth noting that the area covered with the shadows of particles over a light background corresponds to clusters of Ni nanoparticles dispersed on the biochar surface. Due to the porous structure of biochar, it can be observed that Ni NPs are well dispersed on its surface, potentially enhancing its effectiveness as a catalyst. Catalytic activities are contributed by both dispersed Ni nanoparticles and biochar support. The grain size of Ni nanoparticles on the Ni/biochar, determined based on the image analysis performed using image J software, is mostly between 6 and 11 nm, whereas that of Ni/biochar (KOH) is between 4 and 12 nm and that of Ni/biochar (H_2SO_4) is between 4 and 10 nm. Overall, the average Ni grain sizes on the surfaces of the catalysts are 7.5 nm (Ni/biochar), 9.5 nm (Ni/biochar (KOH)) and 8.5 nm (Ni/biochar (H_2SO_4)). The Ni metal nanoparticles are aggregated (**Figure4.3**). While chemically treating biochar with KOH and H_2SO_4 increases its mesoporosity and surface area, there was no significant enhancement in the dispersion of active Ni metal relative to Ni/biochar. In spite of this, Ni NPs impregnation may not exert a significant effect on the pores in the biochar and may not reduce the active surface area of the biochar.

Figure 4.1 and **Table 4.1** show the surface area and distribution of pore size, confirming that Ni NPs impregnation exerted minimal impact, particularly for the chemically modified biochar.

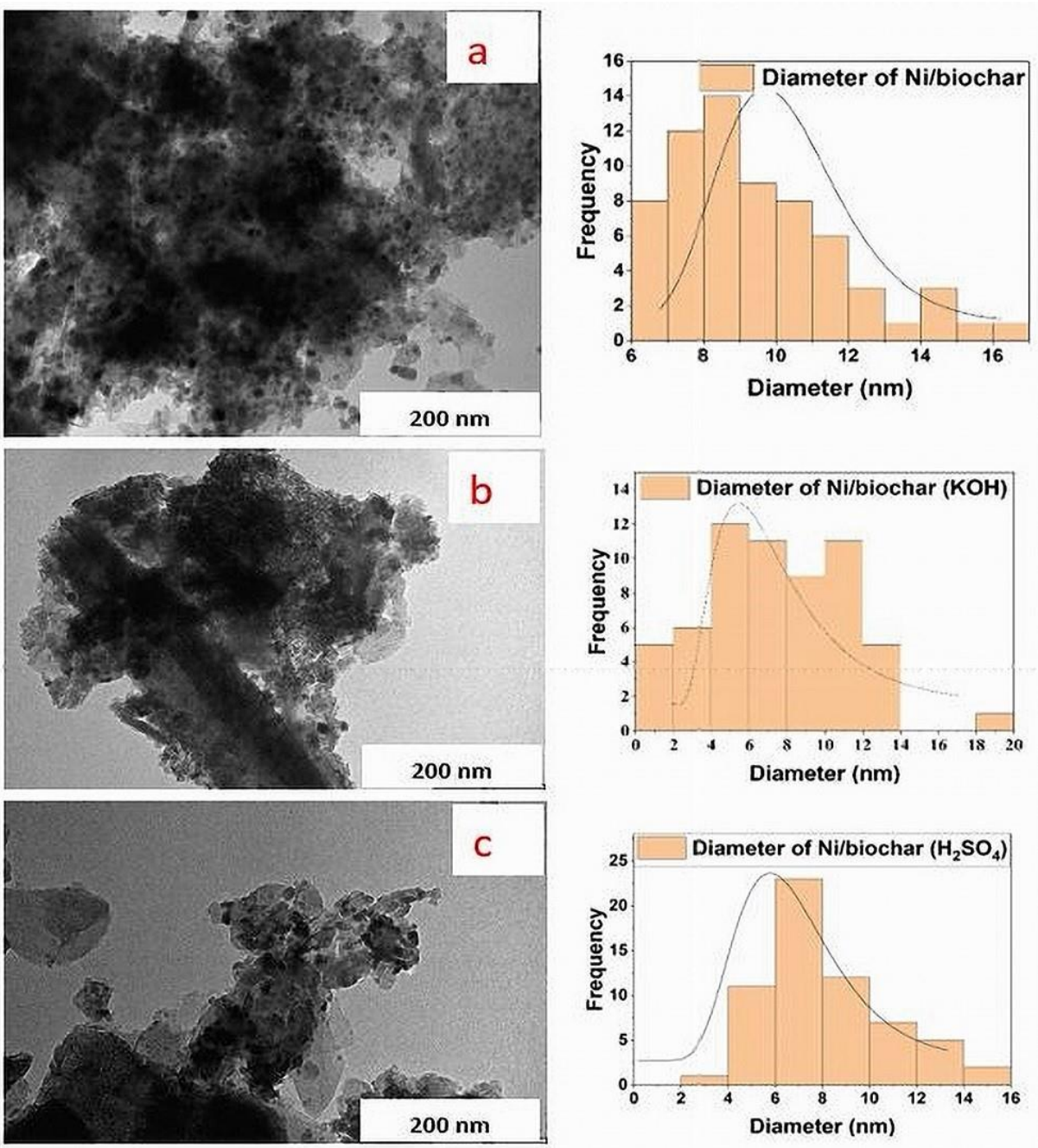

Figure 4.3. TEM analysis and histograms of the Ni metal nanoparticle sizes of (**a**) Ni/biochar, (**b**) Ni/biochar (KOH), and (**c**) Ni/biochar (H_2SO_4).

Metals are mostly present in their oxide form, which is confirmed by the XRD analysis of the biochar (**Section 4.5**). Notably, the following trace elements were detected: Si (5.48%), Al (5.05%), Fe (4.0%), Ca (1.27%), and P (1.18%), along with others (K, S, Mg, and Ti) with concentrations lower than 1%, which were well distributed on the surface of the biochar (**Figure 4.2b–l**). This demonstrates the heterogeneous nature of the biochar surface.

Interestingly, it has been reported in the literature that oxides of Ti, Al, and Si provide excellent catalytic support to Ni and Cu for HDO reactions [123,140-142]; thus, despite their minor occurrence on the surface of the biochar, they could contribute to the performance of the prepared Ni/biochar catalysts. The dispersion of these elements on the surface of the biochar can be found in **Figure 4.3a-c**.

4.5 X-Ray Diffraction (XRD) Analyses

The crystalline nature and the structural changes from chemical modification and Ni-metal impregnation of the biochar samples and their corresponding catalysts were studied using XRD. Catalyst properties such as crystal structure, crystallite size, and phases are characterized by XRD patterns.

Figure 4.4 shows the XRD patterns of the fresh and used catalysts. The sharpness of most of the peaks in the XRD patterns indicates that the biochar samples and their corresponding catalysts possess good crystallinity. It can be seen that the XRD pattern of biochar supports both unmodified and modified have prominent cellulosic peaks at 2θ = 6 (101) (**Figure 4.4a**) [143]. As the crystallite sizes of cellulose and hemicellulose decrease, this broadening occurs. As a result of the impregnation and calcination of Ni metal active material, the cellulosic peaks of the biochar catalysts become more broad and less intense in appearance (**Figure 4.4b**). The broad diffraction peak at $2\theta = 25.7°$ indicates the presence of graphite (002), which is an amorphous carbon with irregular structure [139].

XRD analysis of biochar reveals that it primarily contains amorphous compounds as a result of cellulose's decomposition, indicating an amorphous carbon structure. A sharp crystalline peak at 2θ equals 27° and 46° of **Figure 4.4** indicates the presence of quartz (SiO_2) and calcite ($CaCO_3$), respectively. Compared to raw biochar and biochar (KOH), the acid-treated biochar (biochar (H_2SO_4)) exhibited an amplified intensity in some peaks, such as

$CaCO_3$, CaO and Al_2O_3 (**Figure 4a**). Aside from calcite, quartz, and graphite, biochar samples also contain associated mineral crystals, such as CaO, Al_2O_3 and $Ca(OH)_2$. These are indicated by the following peaks that can be identified in the XRD patterns include SiO_2, occurring at 2θ = 21.33° and 27.07° [140], and CaO, $CaCO_3$, Ca $(OH)_2$ and Al_2O_3, appearing at 2θ = 38.92°, 46.13°, 50.54° and 68.61°, respectively [141,142].

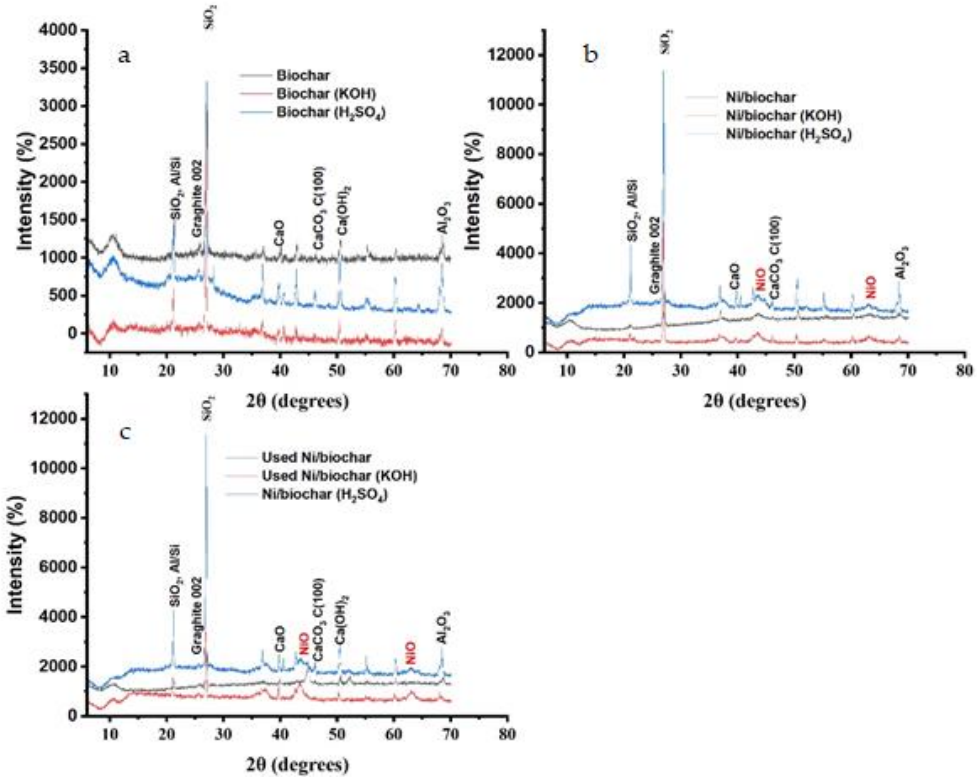

Figure 4.4. XRD diffraction patterns of (**a**) biochar supports, (**b**) fresh Ni/biochar catalysts, and (c) fresh vs. used Ni/biochar catalysts.

In addition to the peaks of the biochar supports, both fresh and used catalysts exhibited the characteristic peaks of NiO at 2θ values of 37°, 44.5° and 64.5° (**Figure 4b,c**) [144]. The presence of oxidized NiO nanoparticles on the surface of the biochar indicates that the impregnated nickel (II) nitrate hexahydrate decomposed during calcination. Interestingly, in the XRD patterns before and after the reaction experiments, the peak positions and intensities

of the catalysts did not change (**Figure 4b,c**). This indicates that no phase transformation or deactivation occurred as a result of the HDO of vanillin over the course of the reaction time.

4.6 Fourier Transform Infrared Spectroscopy (FT-IR)

When carbonaceous feedstock is subjected to a thermochemical conversion in an oxygen-deficient environment, biochar materials are produced. The pyrolysis process produces aromatic carbon, and a wide range of volatile organic compounds that partially condense on surface and pores of biochar. Hence, biochar is a polycondensed carbon material that is heterogeneous in composition. On its surface, biochar has an abundance and diversity of functional groups. A certain amount of surface functional groups is present in unmodified biochar, such as C–O, C═O, and –OH [145]. In the process of impregnation of Ni active metal, the functional groups on the surface of biochar play an integral role by providing adsorption sites. Biochar and its prepared catalyst were studied by FT-IR spectroscopy in order to determine their molecular structure, individual molecules, and molecular mixture composition. The impact of treating the biochar chemically to enhance mesoporosity and surface area on the surface functional groups was also explored. Organic and inorganic compounds in the catalysts are identified by FT-IR analyses illustrate the changes in surface functionalities of the Ni/biochar catalysts resulting from the chemical modification of biochar support.

Figure 4.5shows the FT-IR spectra of the prepared Ni catalysts supported on biochar, biochar (KOH), and biochar (H_2SO_4). On the surface of the biochar samples, there are abundant oxygen-containing and carbon-based functional groups. The results reveal the presence of several matching functional groups, such as a phenolic OH-group at 3400 cm^{-1} [146], carboxylic acids, -COOH, at 2330 cm^{-1}[147], -C-O stretching in cellulose at 1030 cm^{-1}[148], and C=C vibration for aromatic groups at 1580 cm^{-1} [146]. A decrease in the intensity of the –OH functional group peak and a slight decrease in the C=C vibration peak for aromatic groups can

be observed in the spectrum of Ni/biochar (KOH) and Ni/biochar (H_2SO_4). This indicates that some of the surface functionalities of the biochar support may have been lost as a result of acidic and basic treatments. In addition to the inorganic O- components (**Figure 4.2**), it is well known that the O-atom occurs in biomass feedstock as part of the following functional groups, such as hydroxyls, phenols, ethers, carbonyls, and carboxyls, while the H-atom occurs on surfaces of aromatic (i.e., C-H) and aliphatic compounds as shown by FT-IR analyses in **Figure 4.5**.H and O are primarily lost as H_2O during pyrolysis of biomass, whereas C is converted into aromatic structures [136]. Thus, chemically treating the biochars exposed a greater proportion of the surface functional groups. **Figure 4.5** confirms this by comparing the peak sizes of chemically modified and unmodified biochar catalysts. Hence, the catalytic performance of chemically treated biochar is more likely to be enhanced because more exposed sites can provide more surface-active sites for reactants.

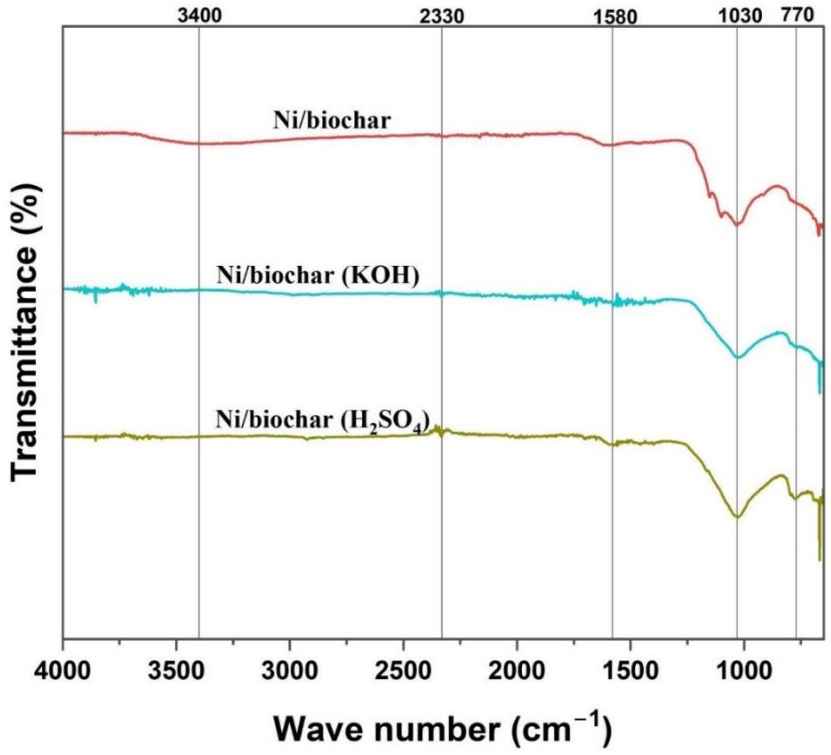

Figure 4.5. FT-IR spectra of biochar, biochar (KOH), biochar (H_2SO_4), and their corresponding Ni catalysts.

According to the results presented in **Table 4.1**, chemical treatment (i.e., KOH and H_2SO_4) of biochar could increase its surface area but did not lead to the formation of new functional groups due to their reaction with O-containing components. The combination of a larger surface area and exposed functional groups should result in enhanced Ni nanoparticle uptake by impregnation on the biochar after chemical treatment. It has been demonstrated in many studies that these functional groups on the surface of biochar are important for reactant adsorption [145]. Identifying the type and nature of functional groups in biochar determines the strength of acid-base surfaces. Basicity-acidity is a vital feature of biochars that can significantly determine their catalytic activity and selectivity in HDO and hydrogenation of bio-oil model compounds. Hence, there are three critical properties of biochar which affect its performance as a catalyst: its pore size distribution, surface functional groups, and chemical composition.

4.7 Hydrogen Temperature Programmed Reduction (H_2-TPR)

A study of the surface chemistry of the prepared catalyst was performed, particularly the reduction of the impregnated Ni metal and its oxides (NiO) in the catalyst. Temperature-programmed reduction (TPR) was carried out using hydrogen gas as a reducing agent, while CO_2-TPD was also performed. **Figure 4.6** shows the H_2-TPR profiles of the raw biochar support and the Ni/biochar, Ni/biochar (KOH) and Ni/biochar (H_2SO_4) catalysts. No reduction peak can be observed in the raw biochar, confirming that the metal oxides found in the biochar as revealed by EDX and XRD remained in their oxide states even at high temperatures under constant hydrogen flow; thus, they were able to contribute to the reaction as catalysts. However, a reduction peak can be observed for the Ni-supported catalysts Ni/biochar, Ni/biochar (KOH), and Ni/biochar (H_2SO_4) at temperatures between 300°C and 450°C.

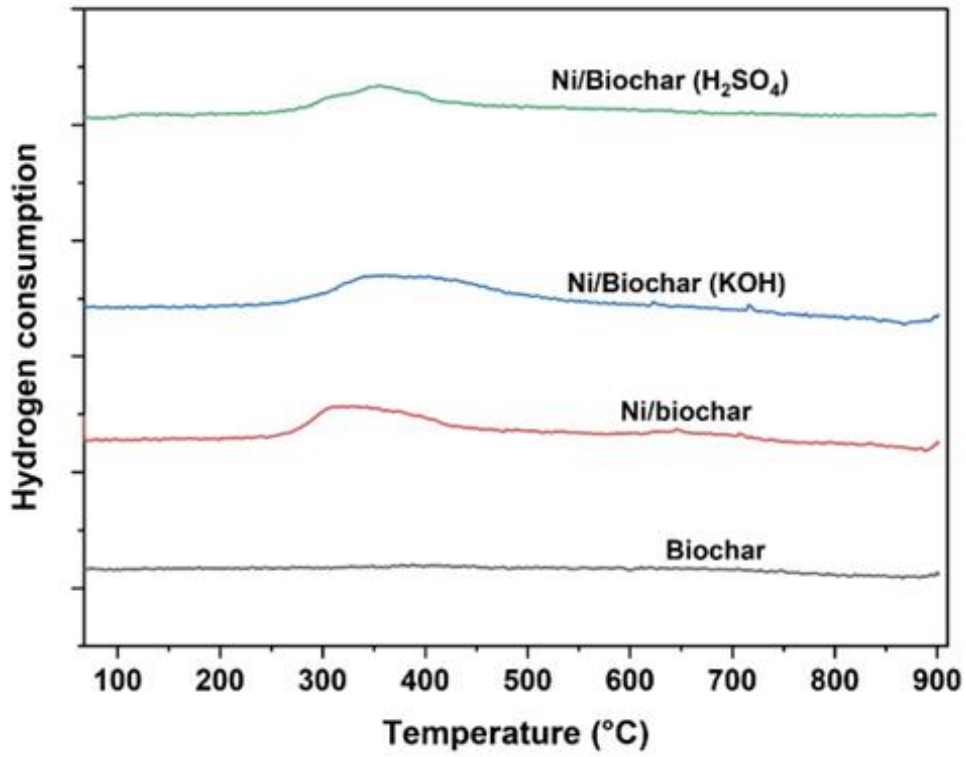

Figure 4.6. H_2-TPR profiles of raw biochar, Ni/biochar, Ni/biochar (KOH), and Ni/biochar (H_2SO_4) catalysts.

The reduction peaks occurred at 350°C for both Ni/biochar and Ni/biochar (H_2SO_4), and at 400°C for Ni/biochar (KOH). Previous studies have reported that nickel oxide (NiO) can be reduced to metallic nickel in hydrogen at 400°C to ensure the conversion of all nickel oxides to the metallic nickel [149-151]. The reduction temperatures were recorded as follows: Ni/biochar (350°C), Ni/biochar(KOH) (410°C), and Ni/biochar(H_2SO_4) (405°C). On the Ni/biochar catalyst, NiO nanoparticles reduce at a lower temperature than on the catalyst produced with chemically modified biochar. The exposed functional groups in the chemically modified biochar provided adsorptive sites for the NiO nanoparticles, thereby increasing the reduction temperature. The results of this study show, however, that total reduction of nickel oxide precursors takes place slightly beyond 400°C for all precursors. The 350 to 400°C reduction temperature observed in the prepared catalyst represents weak to moderate Ni–support interaction. These reduction temperatures represent a reduction in NiO, which is not

present in the raw biochar itself. Consequently, the Ni–support interaction is stronger for Ni/biochar (KOH) than for Ni/biochar or Ni/biochar (H_2SO_4).

4.8 Carbon Dioxide Temperature Programmed Desorption (CO_2-TPD)

The surface interactions between the adsorbed molecules and the biochar surface can be determined using the TPD method. Biochar's acid-base properties may play a critical role during vanillin HDO, since they activate oxygenated compounds on the surface of the support. Additionally, adsorption of reactants is fundamentally affected by the acidity or basicity of the biochar surface [132]. The CO_2-TPD profiles of the biochar and the prepared catalysts are shown in **Figure 4.7**. In the TPD profile, two active sites can be observed for unmodified biochar support and Ni/biochar catalyst, whereas a single active site is seen for catalysts prepared using chemically modified biochar. As indicated by two similar peaks appearing at different temperatures, unmodified biochar and Ni/biochar catalysts exhibit two basic sites. There appears to have been no chemical reaction during the impregnation process since the TCD signals for unmodified biochar and its catalyst counterpart (Ni/biochar) are almost identical. In comparison to unmodified biochar, the surface energy was more uniformly distributed after chemical treatment with KOH and H_2SO_4. The first broad peak occurred at about 675°C, representing moderately basic sites, while the second peak at 790°C is assigned to the strong basic sites of the biochar support itself. Upon impregnation with Ni to produce the Ni/biochar catalyst, a shift can be observed, with the first peak appearing at 700°C and the second peak at 800°C. Meanwhile, the chemically treated biochar catalysts possess only a single peak, with the peak for the Ni/biochar (KOH) appearing at 675°C, and that for the Ni/biochar (H_2SO_4) appearing at 575°C. The results suggest that the surface interaction with the components can be summarized as follows: Ni/biochar > biochar > Ni/biochar (KOH) > Ni/biochar (H_2SO_4). The basic sites are a result of the interaction between O^- and CO_2 [152]. **Figure 4.7** shows a significant increase in the basic sites in Ni/activated biochar and

Ni/acidified biochar when compared to those in the biochar. The increase in basic sites contributes to the high reactivity observed in Ni/biochar (KOH) and Ni/biochar (H_2SO_4).

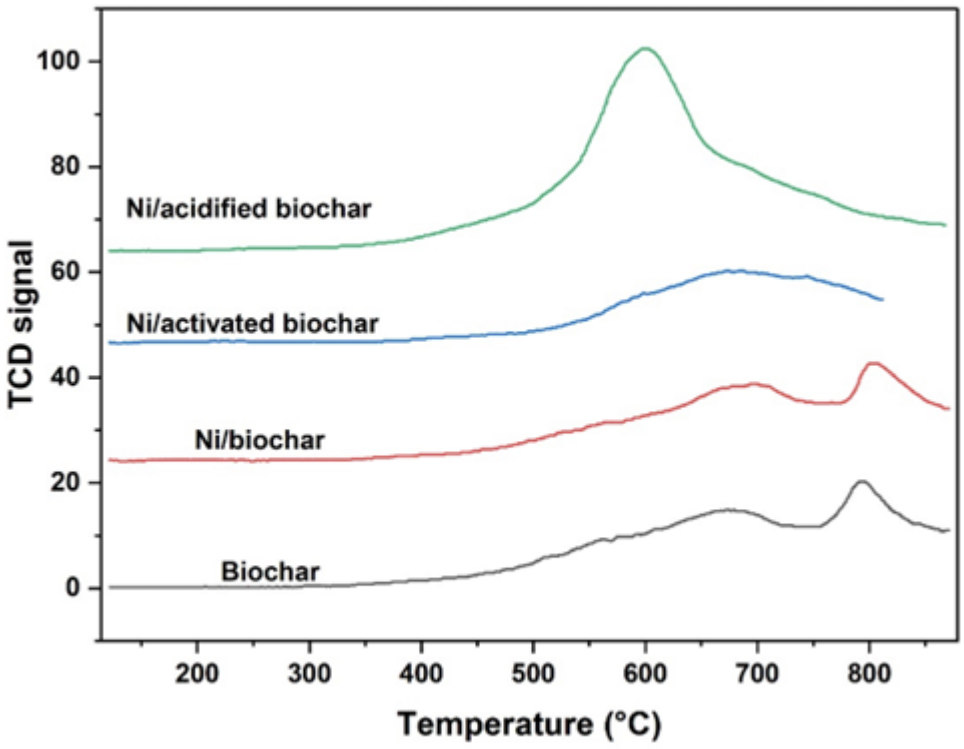

Figure 4.7. CO_2-TPD profile of raw biochar, Ni/biochar, Ni/biochar (KOH), and Ni/biochar (H_2SO_4) catalysts.

4.9 Thermogravimetric Analyses (TGA)

The thermal stability of the prepared catalysts was studied with the aid of TGA. It involves heating biochar supported catalysts at a constant rate of increasing temperatures and monitoring the weight change over time. The response of the catalysts to temperature can be seen in the TGA results displayed in **Figure 4.8**. The first thermal peak occurred at around 100°C, with initial weight losses of about 2.5% (Ni/biochar (KOH) and 5% (Ni/biochar and Ni/biochar (H_2SO_4) being observed in the temperature range of 25°C to 200°C. This may be attributable to moisture loss, some light volatile compounds, and bound solvent evaporation [153]. Biochar contains many condensed organic compounds, and as temperature increases, so

does the weight loss of volatile compounds. This includes phenolic OH-groups and carboxylic acids, -COOH, as identified in the FT-IR analysis shown in **Figure 4.5**.

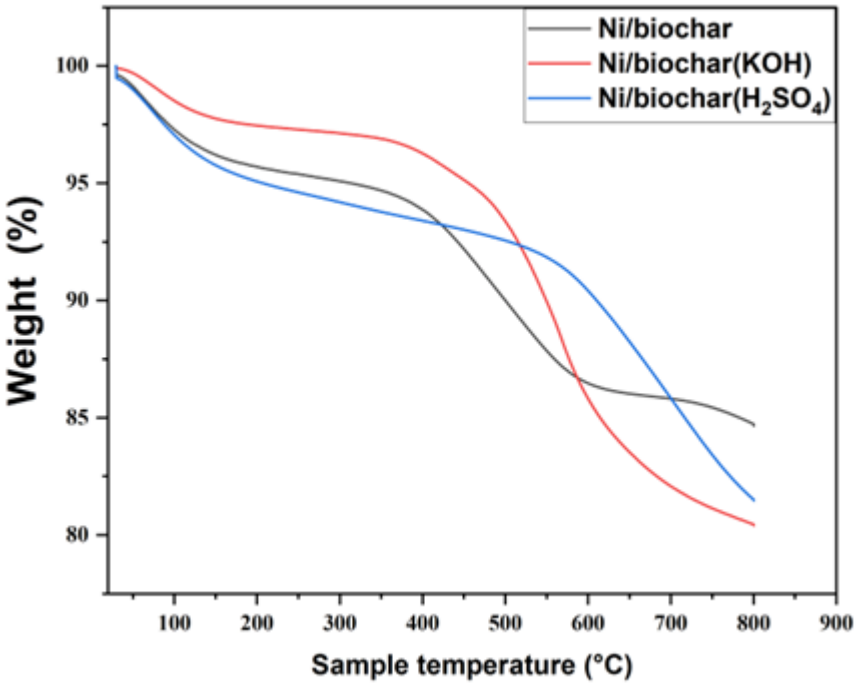

Figure 4.8. TGA thermogram of Ni/biochar, Ni/biochar (KOH) and Ni/biocharH_2SO_4 catalysts.

For the Ni/biochar, significant weight loss of about 12% occurred between 200°C and 650°C, due to the decomposition of hemicellulose and cellulose, and from 650°C to 800°C, weight loss occurred as a result of the thermal decomposition of lignin [135]. The presence of cellulose on the biochar surface could be observed from the FT-IR analysis, and the decomposition from 200°C to 650°C is consistent with this observation. Compared to Ni/biochar, the weight loss of the chemically treated counterpart during the second stage occurred in the temperature range between 200°C and 800°C, indicating that the occurrence of thermal peaks had shifted to a higher temperature. This could be attributed to the thermal decomposition of lignin, cellulose, and hemicellulose compounds on the biochar [153]. Within the studied temperature range of 25°C to 800°C, the total weight loss values corresponded to 15% (Ni/biochar), 18% (Ni/biocharH_2SO_4) and 20% (Ni/biochar (KOH), which is in the same order as their thermal

stability. The additional drop in weight loss can be attributed to the enhanced mesoporosity of the chemically treated biochar, which allows the diffusion of gas in the interior of the biochar during the TGA test. Therefore, due to its excellent proven thermal stability, low cost, and good resistance to acidic and basic media, biochar offers many advantages as a support material for HDO catalysts.

4.10 Conclusion

The results of the characterisation of the prepared catalysts with N_2-adsorption-desorption isotherm technique, CO_2-TPD, SEM coupled with EDX, XRD, and FT-IR have been reported here. It was found that chemical treatment with alkali and acid enhanced the mesoporosity of the biochar support. When the biochar was treated with KOH, the Ni/biochar (KOH) catalyst pore sizes were found to be dominated by mesopores, with a surface area increase of 64.7% and a pore volume increase of 65.3%, while Ni/biochar(H_2SO_4) was mostly microporous and mesoporous, with an area increase of 372.3% and a pore volume increase of 256.8% in comparison to Ni/biochar (74.84 $m^2\ g^{-1}$ and 0.095 $cm^3\ g^{-1}$).

This shows that alkali and acid treatment of biochar can potentially improve its mesoporosity, pore volume and specific surface area. As determined by TGA, the catalysts made with original and modified biochar supports are thermally stable.

However, due to evaporation of volatile compounds, evaporation of bound solvents, and decomposition of hemicellulose and cellulose, the catalysts lose 15% to 23 % of their weight (25 to 800°C) depending modified or unmodified biochar support. Observable on the TPD profile are two basic sites for unmodified biochar support and Ni/biochar catalyst, while the catalysts prepared using chemically treated biochar (i.e., modified biochar) has a single basic site. On the other hand, this study found that the total reduction of nickel oxide on the surface of the catalyst prepared with unmodified biochar supports occur below 400°C. The

reduction temperature as follows: Ni/biochar (350°C), Ni/biochar(KOH) (410°C), and Ni/biochar(H_2SO_4) (405°C). It was discovered that several matching functional groups were present on the catalyst, including phenolic (i.e., -OH) groups and carboxylic acids (i.e., -COOH). NiO nanoparticles were observed on surface of Ni/biochar, which suggests that nickel (ii) nitrate hexahydrate impregnated into the biochar supports decomposed during calcination. Next, these catalysts will be used to catalyse HDO of vanillin to produced p-creosol; the results will be presented and discussed in the following Chapter.

Chapter Five

Effect of Catalyst Modification on HDO of Vanillin and Optimisation

5.1 Introduction

The novel and renewable catalysts developed in this study through chemical engineering of the biochar support, as reported in **Chapter four**, was tested for hydrodeoxygenation (HDO) of vanillin. These tests were conducted to determine the effectiveness of biomass-derived (i.e., biochar) catalyst support for HDO of vanillin to p-creosol. In contrast to previous studies that used either activated carbon or alumina as catalyst support and noble metals or bimetallic catalysts, this study utilizes by-product biochar and inexpensive nickel metal to potentially improve the economic value of the HDO process. It is not the target of this study to remove all three oxygen atoms from vanillin through HDO reaction, but rather to produce p-creosol, which may serve as a fuel source.

The HDO process is a promising method for upgrading bio-oil, but the challenge is designing and developing an efficient catalyst that is low-cost. Catalyst supports also influence catalyst cost and activity significantly. In comparison to unmodified biochar support, the effect of chemically activating biochar with sulfuric acid (H_2SO_4) and potassium hydroxide (KOH) was assessed for HDO of vanillin. It is believed that an increased surface area and internal pores in the biochar are expected to improve mass transport and Ni metal dispersion, thereby improving catalytic performance. Through the use of nickel impregnated biochar derived from biomass pyrolysis, robust and low-cost catalysts were developed for HDO of vanillin into p-creosol. The present chapter shows and discusses the effect of reaction temperature, stability of catalyst and hydrogen pressure on the batch HDO of vanillin to p-creosol over a Ni/biochar catalyst. Furthermore, the effect of external and internal mass transport limitation was studied and reported in **Section 5.2**.

Additionally, the role of both the Ni nanoparticles and biochar support was investigated and discussed in the same **Section 5.2**. A response surface methodology (RSM) implemented in Minitab 19 statistical software was used to study the effects of temperature, pressure, and catalyst loading on HDO of vanillin. Thus, to perform fewer number of experimental conditions, Design of Experiments (DOEs) software was utilized. A true optimization parametric study was conducted using an RSM-based statistical experimental design method and a central composite design, which produced a statistically significant simulation model. This is presented and discussed in **Section 5.3**. Also, covered in this chapter is the catalyst stability through reusability test (**Section 5.4**) as well as the contribution of engineered pore structure through KOH and H_2SO_4 treatments on catalytic performance (**Section 5.5**).

5.2. Catalyst Activity

The results of preliminary experiments for blank (no catalyst), biochar only and Ni/biochar catalyst is shown in **Table 5.1**. Without catalyst, negligible vanillin conversion was achieved, while for experiments conducted with biochar support only produced 1.67% vanillin conversion and negligible products, compared to 93.6% conversion achieved when Ni/biochar was used. It can be seen from **Table 5.1** that the HDO reaction of vanillin cannot proceed with the biochar support alone without impregnated Ni nanoparticles (NPs) added. The activity of the catalyst was significantly improved with Ni NPs impregnated biochar as the catalyst.

Table 5.1. Results for blank, biochar and Ni/biochar catalyst experiment at 50 g L^{-1}, reaction temperature 150°C, stirring speed 1000 rpm, hydrogen pressure 50 bar and 0.6 g catalyst/biochar.

Experimental condition	Vanillin conversion (%)
No catalyst	0.28 ± 0.07
Biochar	1.67 ± 0.27
Ni/biochar	93.6 ± 3.06

The aforementioned results demonstrate that Ni active metal is the major component in the activity of the catalyst. This is consistent with the observation of Aliu et al. [23] also reported on HDO of vanillin, where it was shown that activated carbon does not participate. As a result, biochar provides surface area for the dispersed Ni nanoparticles, and also functions and facilitates the transfer of hydrogen for HDO reaction. Accordingly, Ni nanoparticles act as hydrogenating metals, producing hydrogen radicals (H•), which lower the hydrogenation energy barrier through hydrogen adsorption and dissociation [154]. Based on this observation, it can be concluded that without a catalyst with a suitable active metal(s), no HDO of vanillin will occur and no significant conversion or products will be achieved.

5.2.1. Preliminary experiments

After determining the role of Ni active metal in the HDO of vanillin, some preliminary experiments were performed to select the process variable range to be studied. Thus, a preliminary investigation was conducted for HDO vanillin, investigating conversion and p-creosol yield under the following reaction conditions: starting substrate concentration 0.33 M,

30 bar agitation speed 1000 rpm, temperature 80 to 150°C, and catalyst loading 0.2 to 0.8 g at 0.2 interval. The findings of these studies are summarised in **Figure 5.1**.At all the catalyst loading investigated, the vanillin conversion and p-creosol yield increased, as the reaction temperature increases.

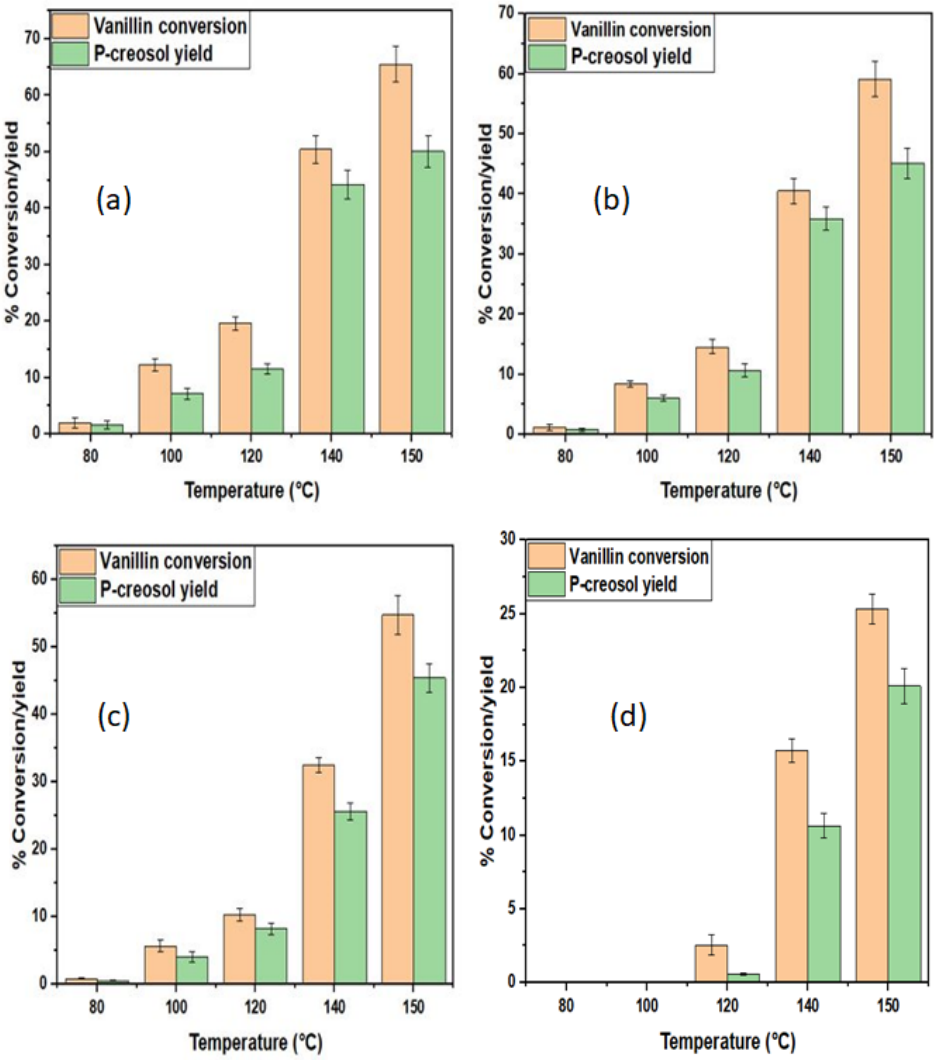

Figure 5.1. Preliminary experimental results: showing vanillin conversion and p-creosol yield; a) 0.8 g catalyst loading b) 0.6 g catalyst loading c) 0.4 g catalyst loading and d) 0.2g catalyst loading at reaction conditions: initial substrate concentration 0.33 M, 30 barinitial hydrogen pressure, agitation speed 1000 rpm.

The results show that catalyst loading, and reaction temperature are important factors in the conversion of vanillin and p-creosol yields. Even with a high catalyst loading of 0.8 g, the yield of p-creosol and conversion of vanillin are negligible at 80°C.In actuality, the experiment is conducted between 100 and 150 °C based on the noteworthy yield and conversion attained. According to early findings, the starting hydrogen pressure studied, which ranged from 30 to 50 bar, had a significant impact on yield and conversion (see Appendix C). This screening experiments established the range of experimental factors used in this research study, which are initial hydrogen pressure 30 – 50 bar, reaction temperature 100 – 150 °C, and catalyst loading 0.4 – 0.8 g, respectively.

On the other hand, there are six stages involved in the HDO reaction of vanillin, which is a three-phase heterogeneous reaction (i.e., gas-solid-liquid). The stages include: (1) H_2 will be transported from the bulk gas phase to the gas−liquid interface, (2) transfer of H_2 gas through the gas−liquid interface into the bulk liquid, (3) transport of H_2 to the catalyst external surface, (4) transport of vanillin in the liquid phase to the catalyst external surface, (5) intraparticle transport of vanillin and H_2 through the pores of the catalyst to the Ni metal active sites for chemical reaction, and (6) transport of the products out of the catalyst pores to the external surface [155]. All reactions must, however, be conducted in a kinetically controlled regime in order to achieve the objectives of this research. As a result, kinetic data can be collected accurately in this regime based on stirring speed that eliminates external transfer limitations.

Additionally, the catalyst particle size must also eliminate restrictions resulting from intraparticle diffusion. Experimentally, the effect of external and internal diffusion restrictions studied and eliminated by varying the stirring speed of the batch reactor from 400 rpm to 1200 rpm, as well as separating catalyst particle size between less than or equal to 102 μm and greater than or equal to 212 μm.

As a result, the Ni/biochar catalyst particle was sieved in order to separate it into the following particle size ranges $d_p \leq 102$ µm, $102 < d_p \leq 150$ µm, $150 < d_p \leq 212$ µm and $d_p \geq 212$ µm. **Figure 5.2** shows the effect of the catalyst particle size on vanillin conversion. As the catalyst particle size decreases, the conversion of vanillin by HDO reaction increases.

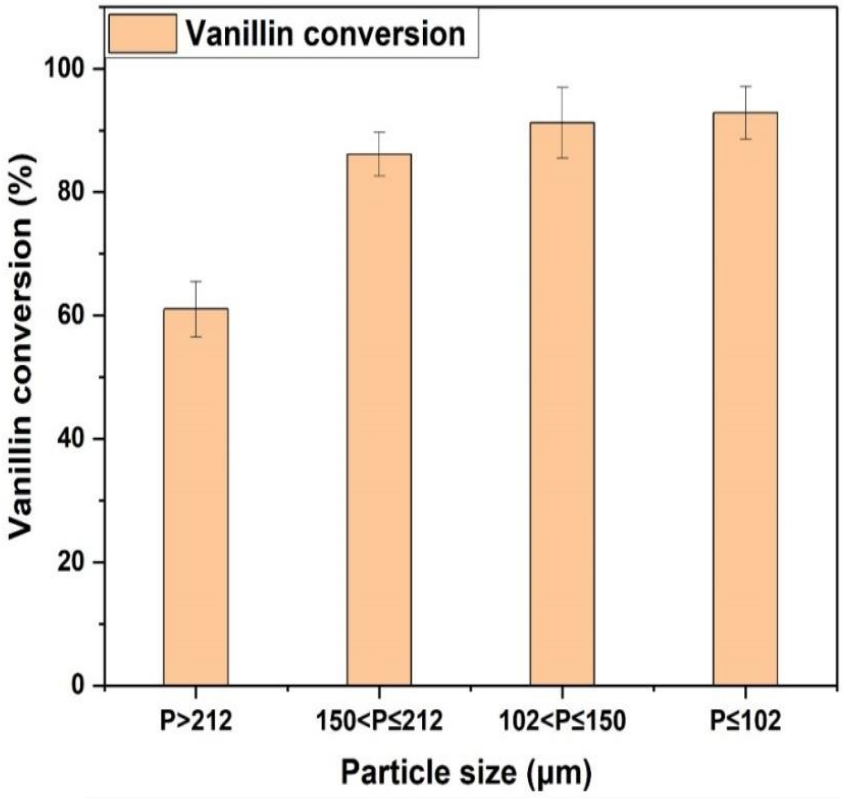

Figure 5.2. Effect of catalyst particle size on vanillin conversion at 50 gL^{-1}, reaction temperature 150°C, stirring speed 1000 rpm, hydrogen pressure 40 bar and 0.6 g Ni/biochar catalyst.

Catalyst with particle sizes greater than or equal to 212 µm have the least conversion of about 60%, while less than or equal 102 µm exhibited the highest conversion of approximately 80%. This implies that the intraparticle mass transport resistance decreases as the catalyst particle decreases. This result suggests that intraparticle mass transport limitation is negligible for catalyst particle sizes less than 102 µm. Hence, most of the experiments reported hereafter

were performed using catalyst particle sizes less than or equal to 102 μm to eliminate internal mass transport limitations.

The result of experiments carried out to investigate influence of batch reactor stirring speed on vanillin conversion is shown in **Figure 5.3**. This is critical in evaluating and eliminating external mass transport limitation on the HDO reaction. The results showed that vanillin conversion increased from 61% to 82% as the stirring speed increased from 400 rpm to 1200 rpm.

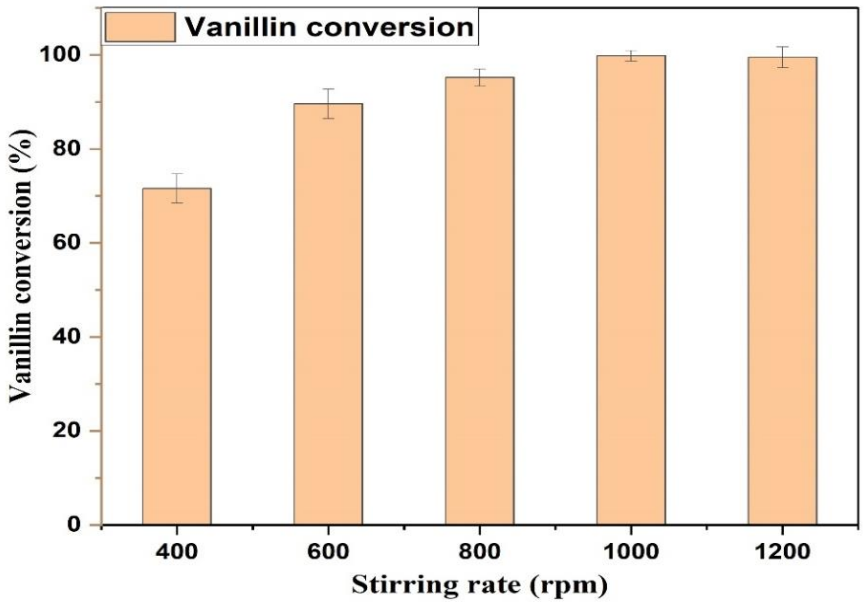

Figure 5.3. Effect of batch reactor stirring speed on vanillin conversion at 50 gL^{-1}, reaction temperature 150°C, hydrogen pressure 50 bar and 0.8 g Ni/biochar catalyst.

The observed increase is because of improved mixing with increasing stirring speed. However, further increase in the batch reactor stirring speed from 1000 to 1200 rpm showed no change in conversion. This result also suggests that external mass transport limitation becomes negligible at a stirring speed of 1000 rpm. Hence, the experiments hereafter were carried out

at 1000 rpm to eliminate the influence of external mass transfer on the HDO reaction and to ensure the reaction is performed under the kinetic regime.

5.2.1. Conversion of Vanillin

The HDO reaction of m-cresol as a bio-oil model compound was reported to produce toluene and methylcyclohexane, as well as other non-HDO products, using a Ni/C catalyst [156]. Comparatively, in previous work, commercial active carbon had already demonstrated to support Ni nanoparticles in HDO of vanillin. It confirms the potential of the developed novel and cost-effective Ni/biochar supported catalyst for HDO reactions.

However, in this study, the HDO of vanillin can result in two products, vanillyl alcohol and p-creosol. It is possible to achieve catalytic HDO via successive transformations of organic compounds containing oxygen. In contrast to HDO's goal of eliminating oxygenates, HDO of vanillin in this research aims to produce p-creosol, which is a potential fuel. Hence, the novel catalyst activity and performance will be evaluated on the basis of selectivity toward p-creosol. In this case, the conversion of vanillin into p-creosol during HDO can be achieved through: (a) intermediate hydrogenation to vanillyl alcohol and additional hydrogenolysis; and/or (b) straight hydrogenolysis of the C=O bond [157,158]. There have been a variety of reaction pathways reported in the literature for vanillin HDO over different catalysts in the past [21,64,159,160].

This study identified p-creosol as the final product of the HDO of vanillin over Ni/biochar catalysts in 2-propanol solvents. P-creosol is formed in a two-step reaction first involving the hydrogenation of vanillin to vanillyl alcohol, and then the further hydrodeoxygenation of this intermediate, as shown in reaction **Scheme 1**. **Figure 5.4** shows the conversion and yields of vanillyl alcohol and p-creosol as a function of reaction time. With HDO approaching completion at 10 h, it is evident that vanillin conversion increases to 100%,

p-creosol yields increase as well, and vanillyl alcohol yields decline negligibly. At 10 h, the hydrogenolysis of vanillyl alcohol, including the cleavage of the C-O bond and the formation of a new C-H bond, had resulted in an almost total conversion to p-creosol. This observation clearly confirms that vanillyl alcohol was the intermediate product and p-creosol was the final product (Scheme 1). The Ni metal facilitates the hydrogenation of C=C and C=O bonds, and the basic sites promote the cleavage of the C–O bond to form deoxygenated product.

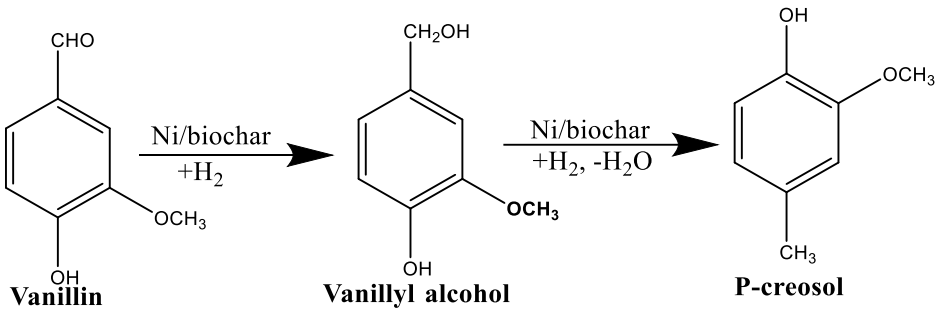

Scheme 1. Reaction pathway for vanillin HDO over Ni/biochar catalyst.

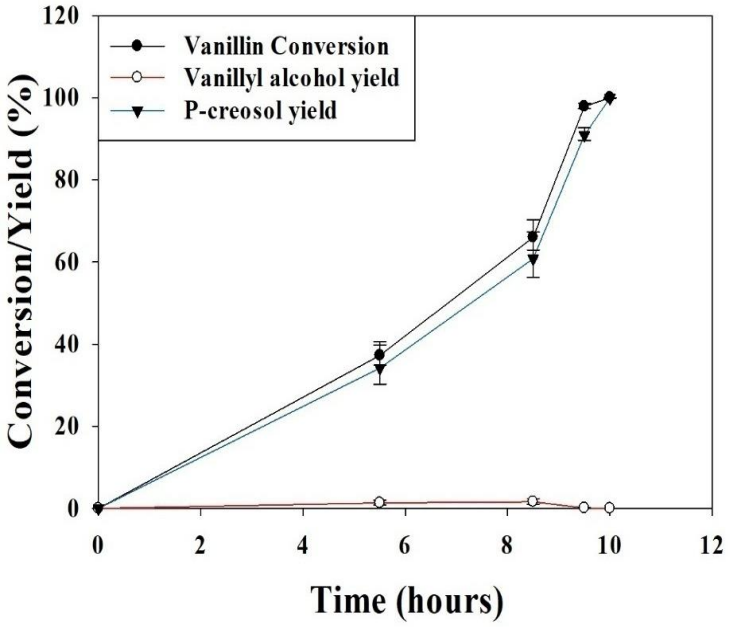

Figure 5.4. Conversion and product yield from vanillin HDO over Ni/biochar catalyst

(reaction conditions: initial substrate concentration 0.33 M; agitation speed 1000 rpm; temperature 150°C; H_2 pressure 50 bar; catalyst 0.8 g; reaction time 10 h).

5.2.2. Effect of Temperature on the HDO of Vanillin

The effect of reaction temperature in the range of 100 to 150°C was studied over Ni/biochar catalyst. The effect of reaction temperature on the HDO of vanillin is shown in **Figure 5.5**. With increasing reaction temperature, vanillin conversion as well as the selectivity of p-creosol and vanillyl alcohol change significantly. With an increase in reaction temperature from 100°C to 150°C, vanillin conversion increases from 26% to 95%, while p-creosol yield increases from 15% to 90%, and vanillyl alcohol yield decreases from 8% to 2%. It is evident that increased reaction temperature favors p-creosol selectivity, while simultaneously diminishing the selectivity toward vanillyl alcohol. This suggests that the HDO of vanillin is endothermic in nature [23,161], with the reaction rate generally increasing as the temperature rises [161]. Based on these results, p-creosol yield increases with an increase in temperature from 100 to 150°C, while vanillyl alcohol yield decreases, showing that vanillyl alcohol is the intermediate product, and is converted via hydrogenolysis to p-creosol.

Similarly, Ru/CNT catalysts for HDO of vanillin showed similar trends in selectivity for p-creosol and vanillyl alcohol when changing the temperature from 50 to 150°C [162]. In other words, the hydrogenolysis of vanillyl alcohol advanced very rapidly at longer reaction times and high temperature [158]. Reactions at higher temperatures were found to exhibit p-creosol selectivity of up to 96%. As a consequence, at 150°C, vanillin conversion was greater than 95% after 9.5 h, with a 99% p-creosol yield.

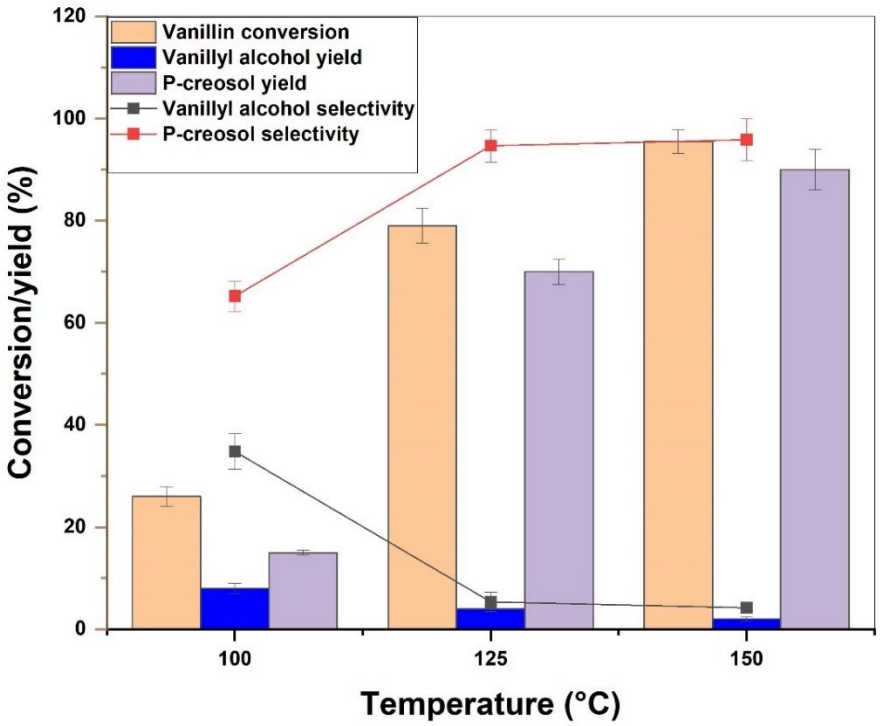

Figure 5.5. Effect of temperature on HDO of vanillin (reaction conditions: initial concentration 0.33 M; catalyst 0.4 g; agitation speed 1000 rpm; H_2 pressure 50 bar; reaction time 9.5 h).

A significant change in selectivity of products occurs with increasing reaction temperature from 100°C to 125°C. On the other hand, the selectivity of p-creosol increased as the HDO reaction temperature increased from 100°C to 150°C, while that of vanillyl alcohol decreased at the same time. Based on the mirror opposites of the selectivity for both p-creosol and vanillyl alcohol products, the results indicate that the selectivity toward p-creosol increases linearly with increasing vanillyl alcohol conversion.

However, comparing the selectivity of p-creosol at 125°C and 150°C, considering energy cost at 150°C and the marginal increase in p-creosol selectivity, the optimum reaction temperature based on selectivity toward the target product which in this case is p-creosol is 125°C. It has been shown that Ni/biochar catalysts are able to hydrodeoxygenate vanillin even under mild reaction conditions (125°C). But the yield of p-creosol at 125°C and 150°C differs significantly from the selectivity toward p-creosol.

5.2.3. Effect of Pressure on the HDO of Vanillin

The effect of H_2 pressure on the HDO of vanillin was studied from 30 bar to 50 bar at a constant temperature of 150ºC. As shown in **Figure 5.6**, an increase in pressure from 30 bar to 50 bar tends to increase vanillin conversion and p-creosol yield. Notably, at 50 bar, the yield of vanillyl alcohol is negligible compared to that obtained at pressures of 30 and 40 bar. Due to the increase in hydrogen pressure, the catalyst surface is exposed to more H_2, allowing hydrogenolysis of vanillyl alcohol to occur more easily [24].

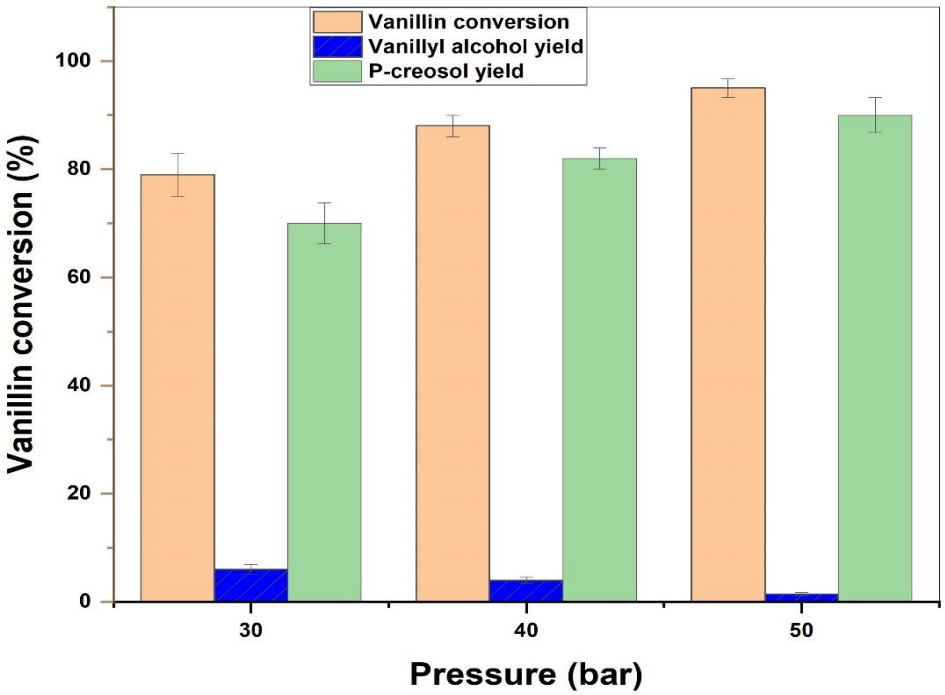

Figure 5.6. Effect of pressure on the HDO of vanillin (reaction conditions: initial concentration 0.33 M; catalyst 0.6 g; agitation speed 1000 rpm; reaction temperature 150°C; reaction time 9.5 h).

It appears that at higher hydrogen pressures, vanillyl alcohol hydrogenolysis is promoted, resulting in a slightly decreased vanillyl alcohol yield. Meanwhile, p-creosol production increases progressively as the reaction pressure increases. Hence, hydrodeoxygenation activity increased with increasing reaction temperature and hydrogen pressure. Specifically, the high

activity of the catalyst with increase in hydrogen pressure can be explained by the small grain size and good dispersion of Ni nanoparticles on the surface of the biochar, as shown in **Figure 4.3** (**Chapter Four and Section 4.4**). In other words, the higher the hydrogen in solution, the more dissociative (H•) on the surface of the Ni NPs, thereby promoting hydrogenation of C=O group in the vanillin structure (Scheme 1) to produce vanillyl alcohol and consequently hydrogenolysis of the C-O group to obtain p-creosol.

5.3. Effect of Reaction Parameters

The effects of three factors—temperature, pressure, and catalyst loading—on the HDO of vanillin were studied using the response surface methodology (RSM), implemented in Minitab 19 statistical software. In RSM, experiments are designed statistically, mathematical models are developed, and response prediction models are validated for accuracy. This Design of Experiments (DOEs) software package was used to assist in achieving optimization using the minimum number of experimental conditions. Response surface methodology in Minitab software was also used to analyse the experimental response data.

Furthermore, the software was used to identify parametric statistical significance, to model regressions and to optimize the analyses. For the modelling and optimization of the HDO of vanillin, a tri-oxygenate model compound of bio-oil was implemented using the RSM approach. By using the RSM, it is possible to determine the combined effect of process factors as well as their high order, enabling the objective assessment of the relationship between different combinations of reaction factors and yield, as opposed to the traditional optimization approach [163,164]. The results obtained, as presented in the appendix (**Table A1**), indicate that the highest vanillin conversion of 97%, with 91.17% p-creosol yield, was obtained at a temperature of 150°C, 50 bar H_2 pressure, and a catalyst loading of 0.6 g. Analysis of variance for the experimental results was used based on a set of 15 replicated experiments (**Table 5.2**) to fit the polynomial

model used **(Equation (1))** in order to determine the effect of linear, square, and interactive reaction variables. Temperature, pressure, catalyst loading, square of temperature, pressure and the combined interaction of temperature and pressure were identified as statistically significant factors for improved vanillin conversion, as shown in **Table 5.2**. On the basis of the effect of variations in the reaction parameters or factors studied, a second-order polynomial empirical model, as shown in **Equation (1),** was able to fit the experimental data obtained. Thus, it can be used to predict the conversion of vanillin as a response. The values of the determination coefficients (R^2) and adjusted coefficient (R^2 adj.) were found to be 99.66% and 99.40%, respectively, which indicates that the model was able to adequately fit the experimental data, with a good predictive power (Rsq. Pred.) of 98.65% (**Table 5.3**).

Table 5.2. Results of analysis of variance for hydrodeoxygenation of vanillin.

Source	**DF**	**Adj ss**	**Adj MS**	**F-Value**	**P-Value Significance**	
del	9	106,44.7	1182.74	355.07	0.000	S
ear	3	9927.7	3309.23	993.46	0.000	S
Temperature (°C)	1	9058.6	9058.58	2719.47	0.000	S
Pressure (Bar)	1	791.2	791.22	237.53	0.000	S
Catalyst Loading (g)	1	77.9	77.88	23.38	0.005	S
Square	3	676.1	225.36	67.65	0.000	S
Temp. (°C) × Temp. (°C)	1	595.6	595.61	178.81	0.000	S
Pressure (Bar) × Pressure (Bar)	1	48.1	48.10	14.44	0.013	S
C Cat. Loading (g) × Cat. Loading(g)	1	7.7	7.67	2.30	0.190	NS
2-Way Interaction	3	40.9	13.64	4.09	0.082	NS
Temp. (°C) × Pressure (Bar)	1	28.6	28.62	8.59	33	S

Temp. (°C) × Catalyst Loading (g)	1	4.6	4.62	1.39	0.292	NS
Pressure (Bar) × Cat.Loading (g)	1	7.7	7.67	2.30	0.190	NS
or	5	16.7	3.33			

Df: Degree of freedom, Adj ss: Adjusted sum of squares, Add ms: Adjusted mean squares, P-value: Probability value, F-value: Fisher value; Temp: temperature; Cat loading: catalyst loading regression equation in uncoded units;

Vanillin Conversion =134.9 − 4.118 T + 2.63 P + 15.60 C + 0.02014 T^2 − 0.0372 P^2 + 0.01070 TP; where T: temperature (°C); P: pressure (bar); and C: catalyst loading.

Temperature and pressure both significantly affected the selectivity for p-creosol linearly and quadratically. This is consistent with the findings of Kristensen et al., where it was reported that both temperature and pressure have statistically significant linear and quadratic effects on the selectivity for cresol using RSM and Ni-Mo/δ-Al_2O_3 catalyst HDO of vanillin [165].

Table 5.3. Model summary.

S	**R^2**	**R^2 (adj.)**	**R^2 (pred.)**
2.14	99.66	99.40	98.65

Three sets of experiments with different combinations of reaction conditions at temperature 120 °C–140 °C, pressure 30–50 bar, and catalyst loading 0.4–0.8 g was conducted in triplicate to assess the predictive power of the empirical model within the lower and higher limits of the experimental conditions studied in **Table 1**. The results obtained from the experiments and the empirical model (**Equation (1)**) predictions are shown in **Table 5.4**. Based on the results, vanillin conversion could be predicted to within an error range of 5.02 to 9.95% with the use of this empirical model. Consequently, RSM can be used to develop an empirical model that

accounts for the interactive effects of reaction variables such as temperature and pressure on the yield of p-creosol obtained from the HDO of vanillin. There are several advantages to using the RSM technique, including the fact that it generates a significant amount of data from fewer experiments, thereby saving time and resources. It can also be used to determine the effect of the interaction between independent and dependent reaction variables [166]. Experimental results from the design of experiments show that experimental conditions that give the best vanillin conversion (91%) and p-creosol yield (97%), were temperature of 150°C, hydrogen pressure of 50 bar and a catalyst loading of 0.6g.

Table 5.4. Validation of the regression model.

Temperature (°C)	**Pressure (bar)**	**Catal0yst (g)**	**Calculated vanillin conversion (%)**	**Experimental vanillin conversion (%)**
120	40	0.4	34.04	44.01
135	30	0.6	45.14	54.48
140	50	0.8	79	84.02

5.4. Catalyst Reusability

An investigation of Ni/biochar stability was carried out for fresh and used catalysts by reusing the catalyst recovered from the first, second, and third experimental cycles. The vanillin conversion, p-creosol and vanillyl alcohol yields and their selectivity after each cycle are shown in **Figure 5.7**.

Vanillin conversion and p-creosol yields showed similar patterns from the first cycle through to the third cycle, with an increase in vanillyl alcohol yield and selectivity in the second, third and fourth cycles. It is clear from **Figure 5.7** that the conversion of vanillin and the yield of the p-creosol product did not significantly change for either the first or the second cycles. However, while both the conversion of vanillin and the yield of p-creosol decreased from the

third to the fourth cycle, the yield of vanillyl alcohol increased. This indicates a decrease in the hydrogenolysis of vanillyl alcohol to p-creosol between the successive experiments. The stability of the catalyst can be attributed to the thermal stability of the prepared catalyst, as indicated by the TGA analysis presented in **Figure 4.8** (**Chapter Four**). This can be explained by the weak Ni-biochar support interaction observed in the H_2-TPR analyses in **Figure 4.6** (**Chapter Four**), resulting in a reduction in the overall vanillin conversion and p-creosol yield in the third and fourth cycles. With a reaction temperature of 150°C, C-C cleavage is not likely to occur; therefore, coke will not form during the HDO of vanillin.

Furthermore, the only products observed in this study were p-creosol and vanillyl alcohol, both of which were produced by hydrogenation and hydrogenolysis. In light of this, it can be inferred that no coke was formed. As a result, the decreases in the conversion of vanillin, p-creosol yield, and selectivity cannot be ascribed to catalyst deactivation resulting from coke on the Ni. It has also been hypothesized that organic species adsorbed onto the surface of the Ni/biochar during the first and second cycles may be responsible for the decline in the catalytic activity of the catalyst in subsequent reaction cycles [167].

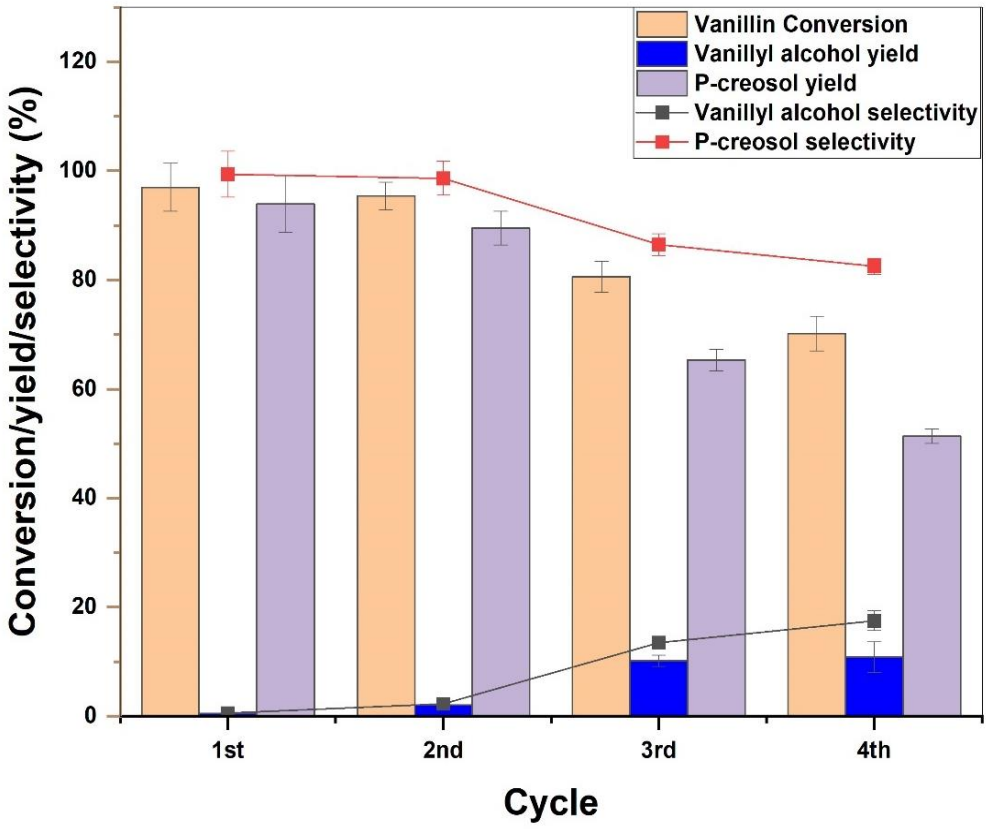

Figure 5.7. Catalyst stability study, showing product yield and selectivity over 4 cycles of reuse (reaction conditions: initial substrate concentration 0.33 M, agitation speed 1000 rpm, temperature 150 °C, H_2 pressure 50 bar, catalyst 0.8 g, reaction time 9.5 h).

5.5. Effect of Chemical Treatment on Catalytic Performance

The novelty of the present work lies in the design of a robust and low-cost catalyst for the HDO of vanillin. Moreover, by supporting Ni nanoparticles on the biochar carrier in which the mesoporous structure of the catalyst is enhanced, specific surface area is increased. The results of catalyst characterization reported in **Chapter Four** confirm that chemically treated biochar will offer the aforementioned advantages. For the purpose of investigating the catalytic performance of catalysts, the HDO reaction of vanillin was chosen as a model reaction. The effect of the chemical activation of biochar on the activity of Ni/biocharin vanillin HDO was studied using Ni/biochar, Ni/ biochar (KOH) and Ni/biochar (H_2SO_4). **Figure 5.8**

demonstrates the impact of the chemical treatment of the biochar on the catalytic performance of the HDO of vanillin. Notably, the catalyst prepared using the KOH- and H_2SO_4-treated biochar clearly outperformed that prepared with raw biochar. As a result of their mesoporous structure, large surface areas, and porosity, chemically modified biochar carriers outperform unmodified biochar in these aspects. This suggests that these attributes of the chemically modified biochar improved mass transport during HDO of vanillin.

As a consequence of the chemical treatment of the biochar support, the catalytic performance improved as follows: Ni/biochar(H2SO4) > Ni/biochar(KOH) > Ni/biochar.

There was a moderate improvement in the catalytic performance of the modified catalysts, especially the H_2SO_4 treated biochar, which showed a high yield of p-creosol and a negligible vanillyl alcohol yield. It is expected that the improved mesoporous structure seen in the particle size distribution from the BET analyses (**Chapter Four** and **Figure 4.1**) of the biochar following chemical treatment would provide a large surface area for Ni metal dispersion and pore size, minimizing the mass transport of vanillin and hydrogen, and thereby increasing catalytic activity. A 23% increase in vanillin conversion was observed with the Ni/biochar (KOH) catalyst, and an increase of 35% over Ni/biochar(H_2SO_4). Despite the biochar's excellent physicochemical properties after KOH and H_2SO_4 treatments as a catalyst support, the active metal, in this case Ni, is the major determinant of catalytic performance as can be seen in **Table 5.1**. This can be plausibly attributed to the reduced basic strength of chemically treated biochar catalysts relative to Ni/biochar (**Figure 4.7**, **Chapter Four**). It could also possibly be attributed to the nature and distribution of the Ni nanoparticles on the surface of the biochar (**Figure 4.3**, **Chapter Four**). Due to the increased surface area of biochar following chemical treatment, the nanoparticles of Ni metal are dispersed more widely.

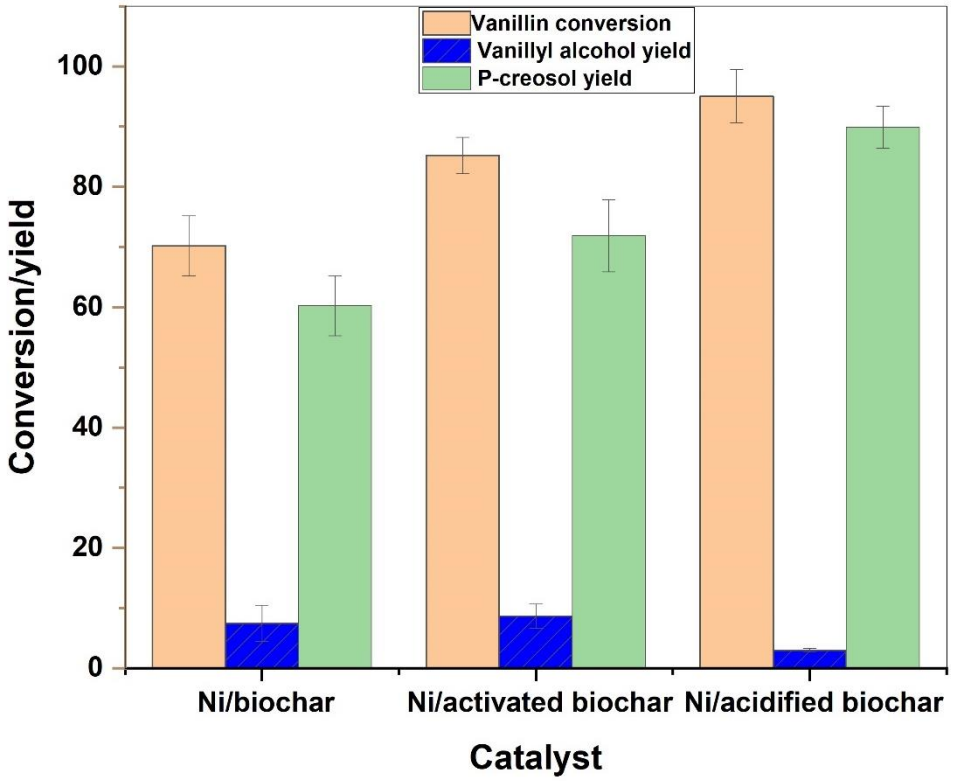

Figure 5.8. The effect of chemical treatment of biochar on catalytic performance (reaction conditions: initial substrate concentration 0.33 M, agitation speed 1000 rpm, temperature 150 °C, H_2 pressure 50 bar, catalyst 0.8 g, reaction time 7.5 h).

Considering the fact HDO reaction is dependent on the Ni metal, the more widely distributed the active Ni nanoparticles are on the surface of the biochar, the less effective the chemically treated biochar support catalyst will be. It is also possible that the Ni loading might not be adequate for the chemically treated biochar to achieve good surface coverage, considering the significant increase in surface area relative to the raw biochar. The Ni/biochar catalyst demonstrated excellent catalytic activity in the HDO of vanillin; however, it has a small specific surface area (**Figure 4.1**, **Chapter Four**) and is prone to the agglomeration of Ni nanoparticles, as can be observed in **Figure 4.3** (**Chapter Four**).

5.6. Conclusion

Biochar obtained from the pyrolysis of wood is used in this work as a support for a nickel catalyst. The conversion of vanillin, an oxygenated phenolic compound found in bio-oil, into p-creosol, a future fuel, was carried out using the developed novel and renewable Ni/biochar catalysts. The biochar support was engineered chemically using KOH and H_2SO_4 to improve its surface area and mesoporous structure before It was also observed that the chemical treatment of the biochar support improved its physicochemical properties, leading to improved catalytic performance in terms of vanillin conversion and p-creosol yield in the order Ni/biochar(H_2SO_4) > Ni/biochar(KOH) > Ni/biochar. The optimization of vanillin HDO using the response surface methodology (RSM) showed that 150°C, 50 bar, 0.6 g catalyst loading, and 1000 rpm were the optimal conditions for vanillin hydrodeoxygenation to p-creosol over a duration of 10 h. P-creosol selectivity was found to be affected by temperature and pressure in both linear and quadratic ways. Ni/biochar catalyst converted vanillin to p-creosol up to 97% with 91.17% selectivity, additionally, the catalyst was stable after four cycles and still highly selective toward the target product.

However, the KOH and H_2SO_4 treatments of the biochar only moderately increased catalyst performance when compared to the observed enhancement in physicochemical properties such as surface area, pore volume and pore size distribution.

Chapter Six

Furfural Hydrogenation and Kinetic Studies, Dual Model Compounds and Catalytic Upgrading of Bio-oil

6.1 Introduction

Another bio-oil oxygenate model compound of interest is furfural. Furfural has been widely researched in this context as a bio-based, cost-effective source that may be converted into a range of valuable products, including biofuels, additives, and other practical value-added chemicals [168,169]. It is selected for study as a model compound here to benchmark and compare the performance of modified biochar catalysts with other industrial catalysts. Also, as a second component for the study of the upgrading of binary mixtures of model compounds, with vanillin. The kinetics of liquid-phase furfural hydrogenation reactions were studied and reported in this Chapter. It is possible to obtain multiple products from furfural hydrogenation, depending on the catalyst used, which includes furfuryl alcohol, 2-methylfuran, furan, tetrahydrofuran, tetahydrofurfuryl alcohol, and even products derived from ring decomposition, such as pentanols and pentanediols [65]. Furfural hydrodeoxygenation products, taking 2-methylfuran as example, are useful chemical feedstocks for producing furan compounds, such as pentanediol, an intermediate in pharmaceuticals and also a fuel additive [170].

Due to the requirement of vaporising furfural, hydrogenation of furfural in gas phase would produce more by-products than hydrogenation of furfural in liquid phase and require more energy [171].

Furfural may be transformed to several compounds in the laboratory using different catalysts. This is typically performed as a slurry reaction involving solid-liquid-gas, can be complex and is influenced by factors such as active metal specificity, metal-support

interactions, and side reactions as well as reaction parameters like temperature, hydrogen pressure and catalyst loading [93]. In addition to being efficient, the developed Ni/biochar (H_2SO_4) catalysts can be economically useful in the production of target products from furfural hydrogenation. In this catalyst, the active metal (i.e., Ni nanoparticle) is immobilised on a porous biochar support as a carrier. Also, the biochar support material has been fine-tuned through acid treatment modification to enhance the catalyst textural properties such as surface area, mesoporosity, and pore volume (see **Chapter Four**), which could potentially improve catalytic performance. The performance of Ni/biochar in the aforementioned reaction will be reported in this Chapter. It is noted that nickel was selected based both on its ability to complete the desired hydrogenation and HDO reactions and suppress unwanted side reactions. Through selective hydrodeoxygenation of furfural, 2-methylfuran is expected to be formed by selectively removing oxygen from the formyl group, suppressing the competitive ring hydrogenation [172].

The first step in creating a kinetic model for the solid-liquid-gas phase of the liquid-phase hydrogenation of furfural is to identify the circumstances that render both internal and external mass transport effects negligible.

Experiments to ensure the reaction is under kinetic control are investigated and reported in **Section 6.1**. While the evaluation of power law kinetic model and Langmuir-Hinshelwood kinetic type model studies are reported in the subsequent Section. The stability of the catalyst based on reusability test for four cycles experiments in terms of furfural conversion and yields of products are presented and discussed in this chapter. It has been shown in **Chapter Four**, that sulfuric acid treatment of biochar significantly improved its properties and the resulting catalyst performance in HDO of vanillin (**Chapter Five**), owing to increased surface area, enhanced pore volume and mesoporosity. In this chapter the effect of sulfuric acid treatment

time on the resulting catalyst performance is investigated in terms of furfural conversion and yields of products. This is presented and discussed in this Section.

Nonetheless, it is anticipated that, compared to a system with just one model compound, the competitive reactions among the different classes of model compounds in a multi-component system and their adsorption upon the catalyst active sites would have a considerable impact on the reaction rate. Thus, the results of an investigation for a binary system containing both vanillin and furfural model compounds are discussed in Section. Finally, the preliminary results of typical bio-oil upgrading are presented and discussed in Section.

6.2 External and intraparticle mass transport effects

The kinetics of the liquid-phase furfural hydrogenation process can be significantly impacted by mass transport effects. The elimination of the transport restrictions is a crucial step in the process validating quantitative kinetic models [93]. These resistances can include external and internal heat and mass transfer as well as the rate of hydrogen transfer from the gas phase to the liquid phase. The diffusion of the reactants from the bulk fluid through the pores structure of the biochar to the active sites are illustrated in **Figure 6.1**. Since in the reactor vessel there are heterogeneous catalyst particles (solid), furfural dissolved in a solvent (liquid) and pressurised hydrogen (gas), it is clear that the hydrogenation of furfural or hydrodeoxygenation (HDO) of vanillin are representative of three-phase reactions [173]. Slurry reactions involve mass transfer between different phases, namely, gas, liquid and solid. The mass transfer resistances in a three-phase reaction system are displayed in **Figure 6.2** at the interfaces between the liquid and gas and the catalyst. Consequently, it is necessary to take into account pore diffusion (internal mass transfer resistance) and gas-liquid and liquid-solid mass transfer (external mass transfer resistance) in the development of appropriate reaction kinetic models. The stages involved are as follows: (1) absorption of hydrogen gas from the bulk gas phase in

to the liquid, (2) diffusion of hydrogen across a boundary layer at the gas-liquid interface, (3) diffusion of dissolved hydrogen through the bulk liquid, (4) diffusion of hydrogen and furfural across a boundary at the external surface of the catalyst particle, (5) internal diffusion of dissolved hydrogen and furfural into the catalyst pores, (6) chemical reaction of hydrogen and furfural at the porous catalyst active sites. Henry's law describes the dissolution of hydrogen gas at the gas-liquid interface.

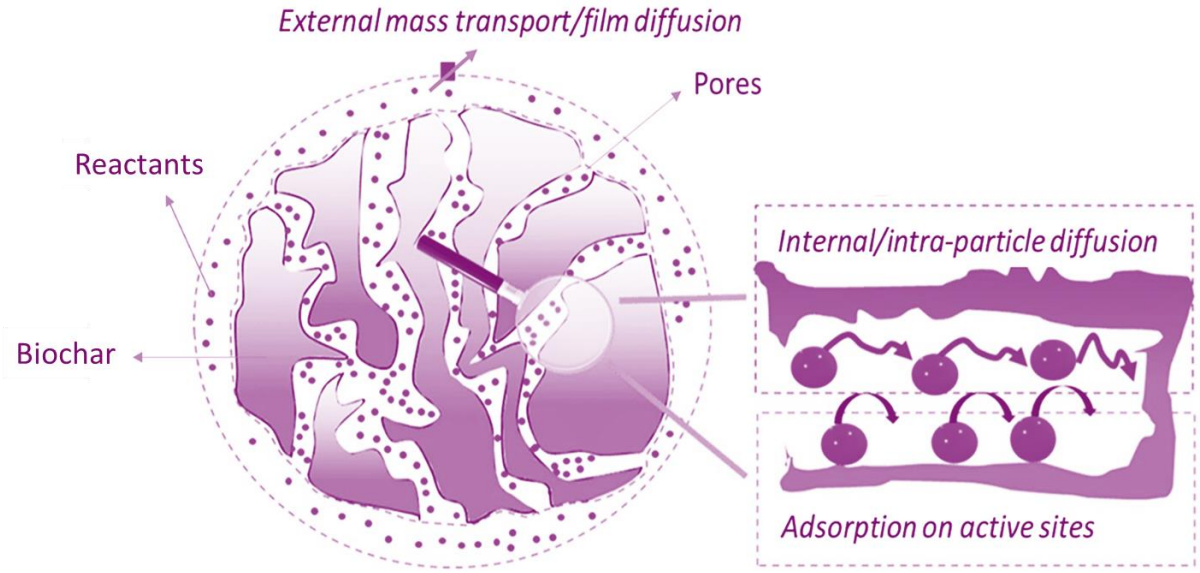

Figure 6.1. Illustration of diffusion steps of reactants from liquid to solid catalyst adsorption on active sites and reaction.

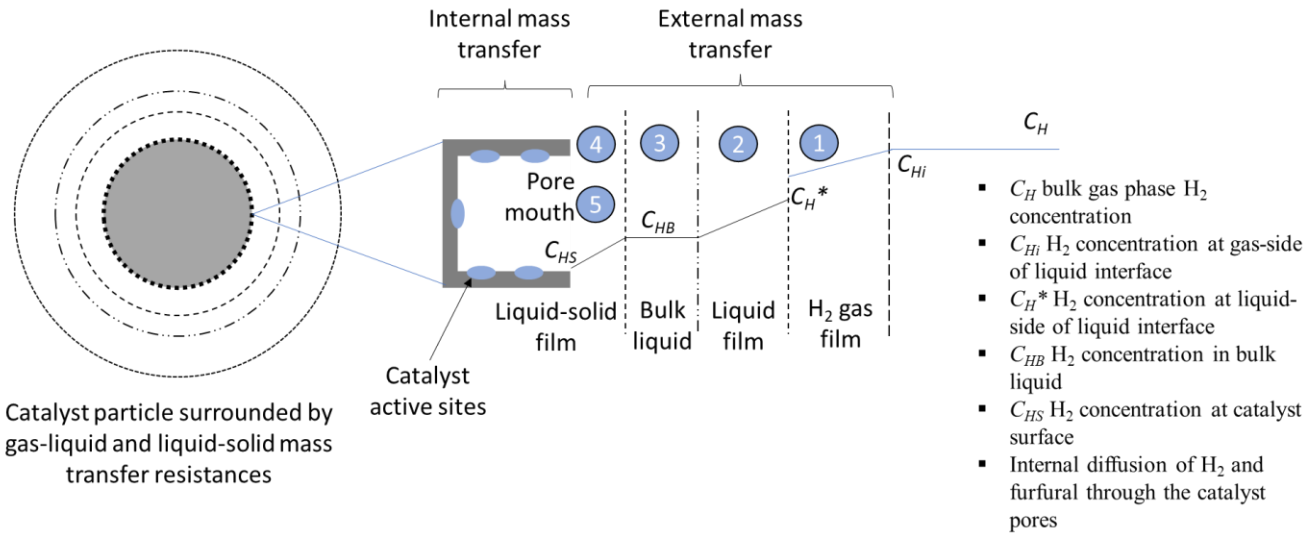

Figure 6.2. Mass transfer resistances at the gas-liquid and liquid-catalyst interfaces in a three-phase reaction system.

It follows that three rate controlling regimes are [174-177]: firstly, the mass transfer resistances at gas-liquid and liquid-catalyst interfaces which involve external mass transport of hydrogen from bulk gas through the gas-liquid interface into the liquid, and then, the diffusion of dissolved hydrogen at the liquid-catalyst through the bulk liquid (Figure 6.2). Thus, the reactants which are furfural and dissolved hydrogen from the bulk fluid diffuse through the boundary layer to the surface of the catalyst via the liquid-solid interface.

Secondly, the intraparticle diffusion which accounts for the internal mass transfer resistance involves the internal diffusion of dissolved hydrogen and furfural into the catalyst pores. In other words, furfural and hydrogen reactants diffuse from the external surface of the catalyst through the liquid-catalyst interface into pores of the catalyst particles. The reactants hydrogen and furfural get adsorbed at the porous catalyst active sites before undergoing surface reaction. It is required that both the external and internal mass transfer resistance is negligible to ensure that the experiment is carried out at intrinsic reaction kinetic control regime. At this state, mass transfer resistances are eliminated only the kinetics data dominate the system. At

the end of chemical reaction, the products desorb from the catalyst surface and diffuse through the pores to the exterior of the catalyst. Consequently, using a batch system for liquid-phase hydrogenation ensure excellent mixing maintaining uniform temperature distribution within the reaction medium, thereby eliminating heat transfer limitations. Thus, temperature gradients appearing from heat transfer limitations are not as prevalent under perfect mixing in a batch reactor liquid-phase system [178,179].

6.2.1 External mass transport study

Studies of external transport resistances are necessary to ensure these are eliminated for kinetic model development. Also, depending on the catalyst concentration and average particle size, it might be challenging to mix and homogeneously distribute the catalyst within the solvent due to its tendency to settle [180]. A sufficient amount of agitation is essential for maintaining an even concentration and temperature throughout the reactor medium, but it must also be sufficient to transport reactant materials across the boundary layer surrounding the catalyst particles [176]. To eliminate the effect of external mass transport the conversion and product yield from furfural hydrogenation over Ni/biochar catalyst was studied as function of stirring speed. **Figure 6.3** shows the conversion of furfural as a function of batch reactor stirring rate using Ni/biochar(H_2SO_4) catalyst. The corresponding yield of desired product 2-methylfuran is shown in **Figure 6.4** plotted at different stirring rates.

Notably, the furfural conversion increases as stirring rate increases from 600 rpm to 800 rpm, and then plateaus between 800 rpm and 1200 rpm. Whereas the yield of 2-methylfuranincreases as the stirring speed increases from 600 rpm to1000 rpm (**Figure 6.4**). In other words, the rate of furfural hydrogenation increases as the stirring rate increases from 600 rpm to 1000 rpm.

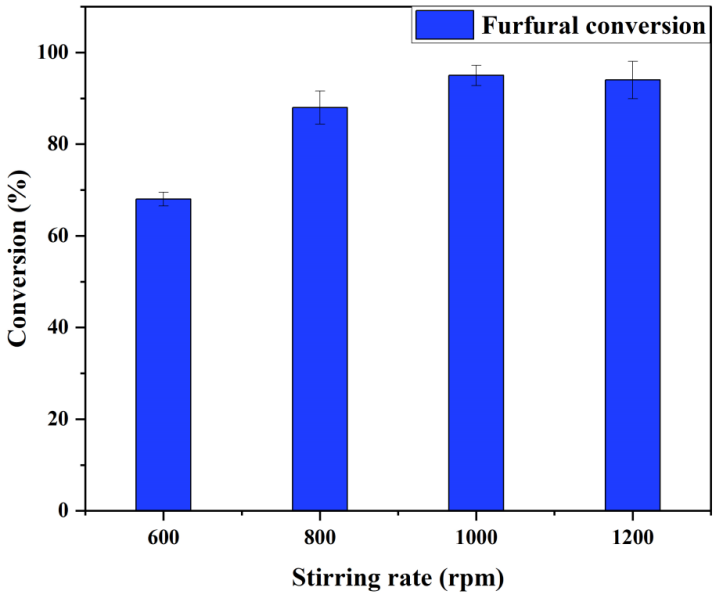

Figure 6.3. Conversion of furfural as a function of agitation over Ni/biochar(H_2SO_4) catalyst at reaction conditions: Initial concentration; 0.39M, solvent; tetralin, temperature; 240°C, catalyst loading; 0.3g, H_2 pressure; 50 bars, reaction time; 5 hours).

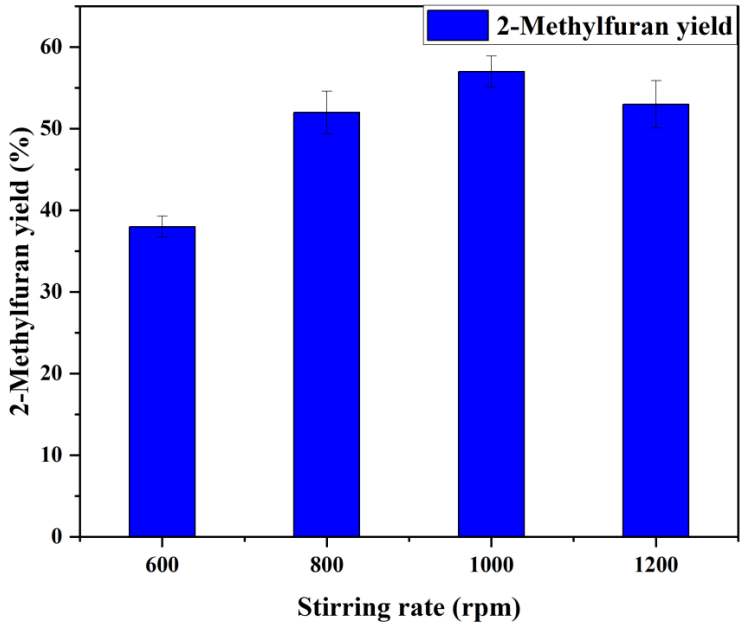

Figure 6.4. 2-methylfuran yield as a function of agitation over Ni/biochar(H_2SO_4) catalyst at reaction conditions: Initial concentration; 0.39M, solvent; tetralin, temperature; 240°C, catalyst loading; 0.3g, H_2 pressure; 50 bars, reaction time; 5 hours).

The conversion of furfural was not significantly altered by the further increase in stirring rate from 600 rpm to 1200 rpm. Based on this, it appears that the application of 1000 rpm stirring rate removes the external transport restrictions between the solid-liquid-gas phases in the reaction. Consequently, this outcome is consistent with stirring rates that are frequently cited in the literature as being adequate to cause negligible external transport limitations in batch reactors and related reaction investigations [115,177]. Therefore, subsequent data were collected from experiments carried out using stirring speed rate of 1000 rpm. It is noted that using a stirring rate of 1000 rpm can potentially achieve about 92% conversion and approximately 55% yield of 2-methylfuran, the product of interest in this study.

6.2.2 Intraparticle diffusion study

In addition to external diffusion considerations, internal mass transport restrictions, such as pore diffusion, or intraparticle diffusion can also have an impact on the overall reaction rate. To investigate this and eliminate its effects, the catalyst powder (Ni/biochar(H_2SO_4)) was sieved into the following particle size ranges: > 250 µm, 212 – 250 µm, 106 – 212 µm and < 106 µm, respectively. A similar approach has been published in the literature [91,161]. The aim is to investigate the catalyst particle size range that produces the shortest diffusion length by examining the conversion of furfural. It is believed that the shorter the diffusion length to the active sites of the catalyst particles, the higher the conversion achieved, which indicates negligible intraparticle diffusion, corresponding to intrinsic reaction rates.

The influence of catalyst particle size range on the conversion of furfural in shown in **Figure 6.5**. It can be observed that the furfural conversion increases as the catalyst particle size decreases from greater than or equal to 250 µm to less than 106 µm. The conversion approximately plateaus around 96% between 106 – 212 µm and < 106 µm catalyst particles sizes. It is shown that a change in catalyst particle size has an impact on the rate of furfural

hydrogenation reaction. In fact, **Figure 6.5** shows that the conversion of furfural was little affected by the additional reduction in particle size from 106 - 212 µm to less than 106 µm. The result suggests that the intraparticle diffusion or internal transport constraint is negligible by using catalyst particles smaller than 106 µm.

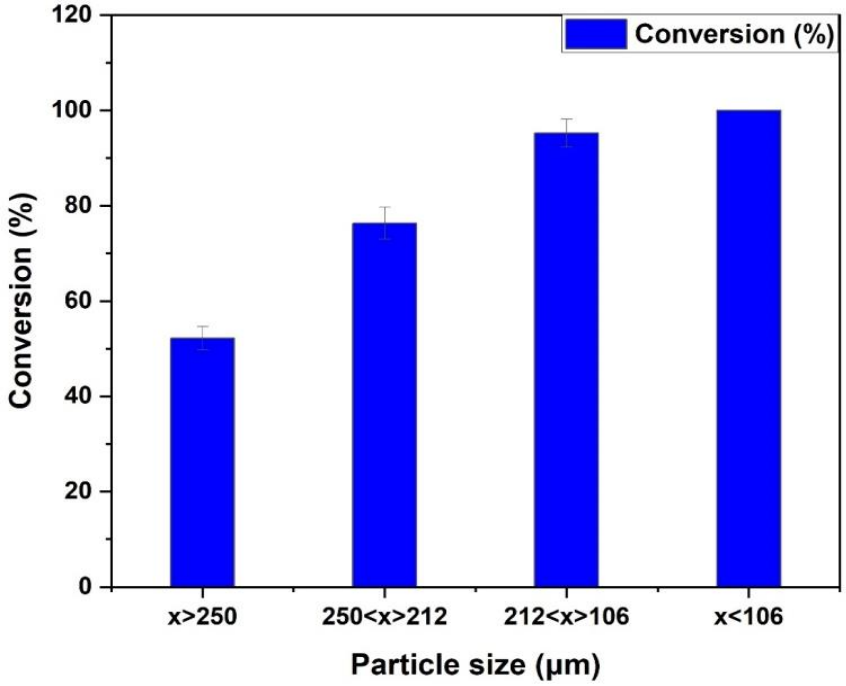

Figure 6.5. Furfural conversion against catalyst particle size over Ni/biochar (H_2SO_4) under reaction conditions: Initial concentration; 0.39M, solvent; tetralin, temperature; 240°C, catalyst loading; 0.3g, H_2 pressure; 50 bars, 1000 rpm, reaction time; 5 hours).

As the catalyst particle size decreases, the diffusion path length to the active sites also decreases. The dispersed catalysts are made up of finely divided particles (less than 106 µm), which gives them a very large surface area (as shown in **Chapter Four, Table 4.1**) and a high mass transfer rate for the catalytic hydrogenation of furfural into 2-methylfuran. Thus, under these conditions (i.e., 1000 rpm and catalyst particle size less 106 µm), rapid hydrogen adsorption is encouraged by the presence of the finely divided catalyst particles.

This finding led to the usage of catalyst particles smaller than 106 µm in subsequent studies for the gathering of experimental data for kinetic work and modelling using Ni/biochar(H_2SO_4) catalyst.

The identified products from the hydrogenation of furfural include furfuryl alcohol, 2-methyl furan, furan, and tetrahydrofuran. The result shows that the catalyst (Ni/biochar) is more selective toward 2-methyl furan, which is the desired product with the highest yield. It is worth noting that the gaseous products were not determined and quantified in this study.

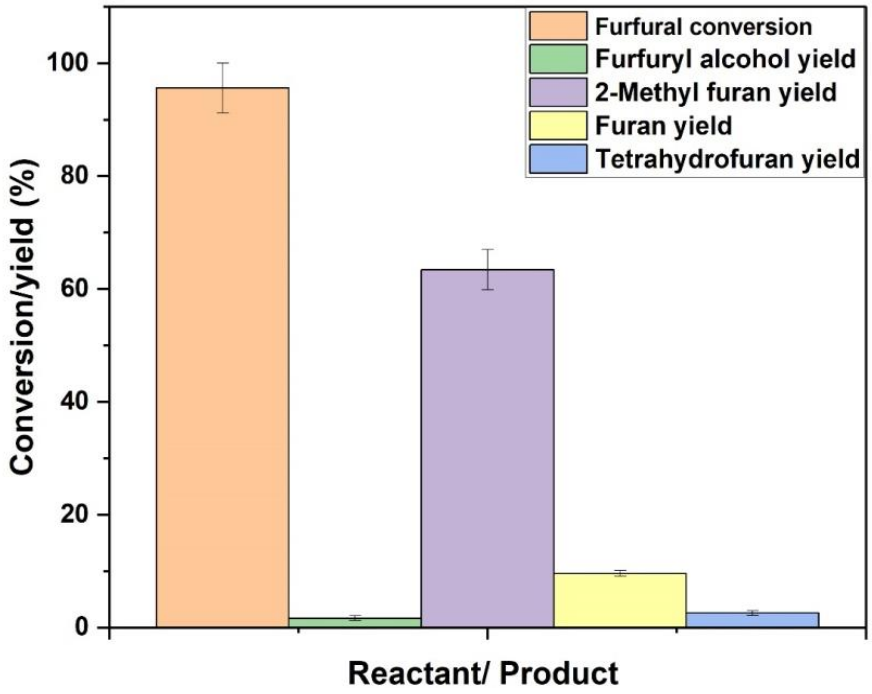

Figure 6.6. Conversion and products yield of Furfural hydrogenation over Ni/biochar (H_2SO_4) under reaction conditions: initial concentration 0.39M, tetralin as solvent, temperature 230°C, catalyst loading 0.3g, H_2 pressure 50 bar, stirring rate 1000 rpm, reaction time 4.5 hours).

6.3 Kinetic studies and model development

6.3.1 Catalyst activity, furfural conversion and products distribution

Furfural molecules have a carbonyl group and a furan ring with two C=C double bonds and one cyclic ether bond. As a result, the furfural molecule is very reactive and may be decarbonylated, hydrogenated, and hydrodeoxygenated to produce a variety of useful compounds such as furan, tetrahydrofuran, furfuryl alcohol, tetrahydrofurfuryl alcohol, and 2-methylfuran. **Figure 6.7** displays the catalytic activity trend for reactant and products as a

function of reaction time for the hydrogenation of furfural using 15 wt% Ni/biochar(H_2SO_4) catalyst. 2-Methylfuran is one of several products that can be formed from furfural by selectively removing oxygen from the formyl group via selective hydrodeoxygenation. The deoxygenation suppresses competitive ring hydrogenation and ring opening reactions from taking place [172]. It can be seen that as the concentration of furfural decreases, the concentration of 2-methylfuran increases with time on scream.

In comparison to comparable furfural hydrogenation products, the catalyst is shown to be more selective towards 2-methylfuran after 2 hours. There is a possibility of hydrogenolysis of C=O bonds, decarboxylation, or hydrogenation of C=O bond or furan ring of furfural during the reaction. The catalyst exhibited competence for the selective hydrogenation of C=O bond in furfural and deoxygenation capability for the cleavage of C−OH bond in furfuryl alcohol to further produce 2-methylfuran.

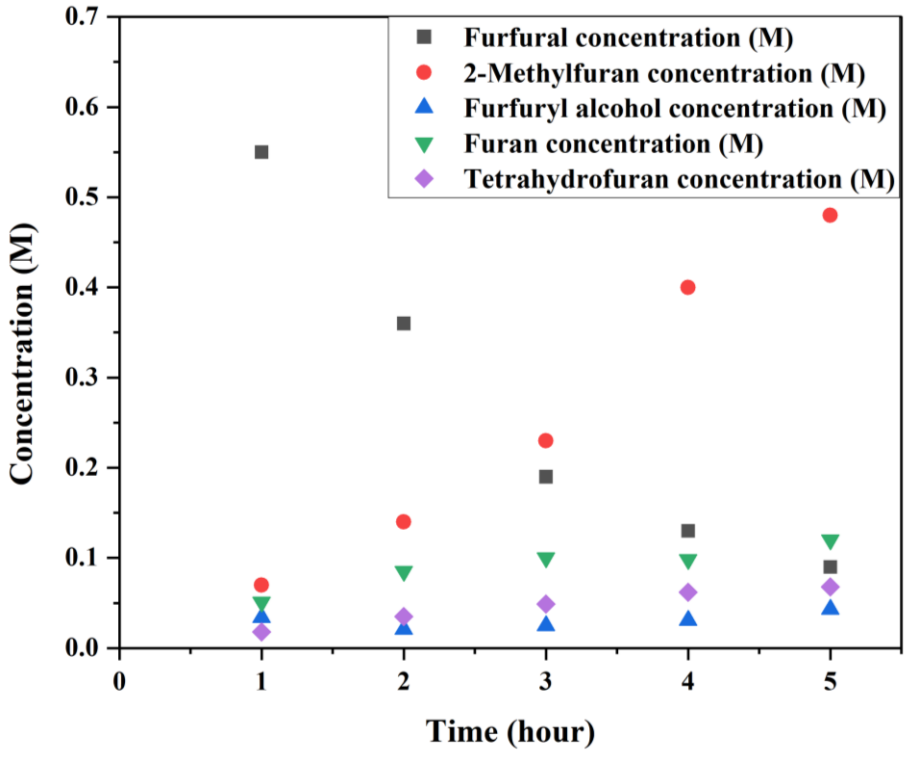

Figure 6.7. Concentration– time plot for furfural and products over Ni/biochar(H_2SO_4) reaction conditions: initial concentration 0.68M, tetralin as solvent, temperature 230°C, catalyst loading 0.35g, H_2 pressure 50 bar, and stirring rate 1000 rpm.

Other products such as furfuryl alcohol, furan and tetrahydrofuran also increase moderately as furfural concentration decreases. The formation of furan is due to the combination of dehydrogenation and decarbonylation of furfural [181]. Whereas furfuryl alcohol is basically formed from the hydrogenation of furfural, further hydrogenation of furan result in tetrahydrofuran. Based on the identified products 2-methylfuran, furfuryl alcohol, furan and tetrahydrofuran, the reaction scheme can be summarised as shown in **Figure 6.8**.

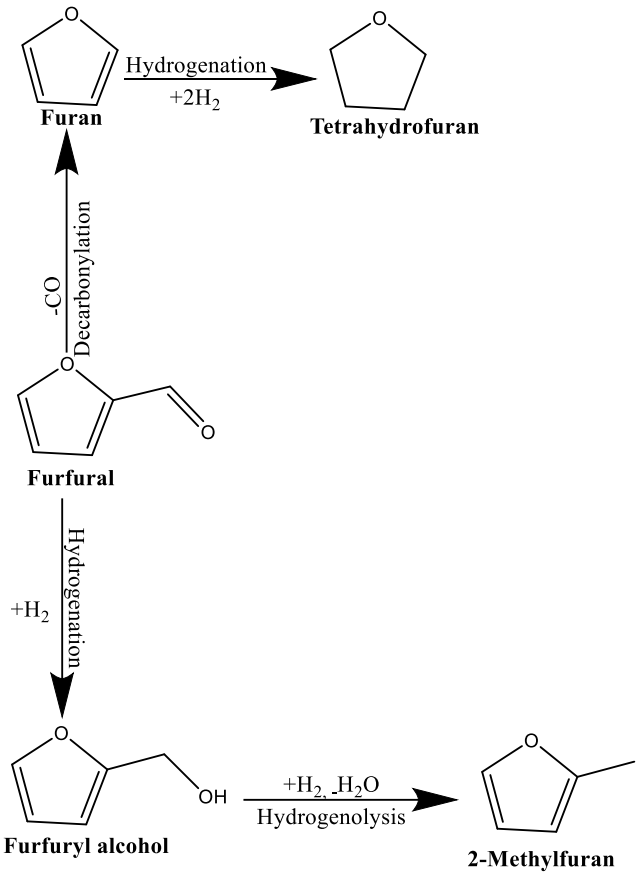

Figure 6.8. Reaction pathways for furfural hydrogenation.

Effect of furfural concentration on initial reaction rate

Preliminary studies were carried out to determine the effect of the various factors on the initial reaction rate of the furfural hydrogenation.

6.3.2 Effect of catalyst loading on initial reaction rate

Over the prepared Ni/biochar(H_2SO_4) catalyst, initial reaction rates (r_0) of furfural conversion into products were investigated as a function of catalyst loading. In **Figure 6.9**, the effect of catalyst loading on initial reaction rate of furfural hydrogenation is presented. It is obvious from the graph that initial rate of reaction increases as the amount of catalyst increases. This is because as the amount of catalyst for the reaction increase the number of active sites available for furfural and hydrogen adsorption and surface reaction increases likewise. Hence, a kinetically controlled regime should result in an increase in reaction rates in proportion to the number of catalytic active sites accessible [93].

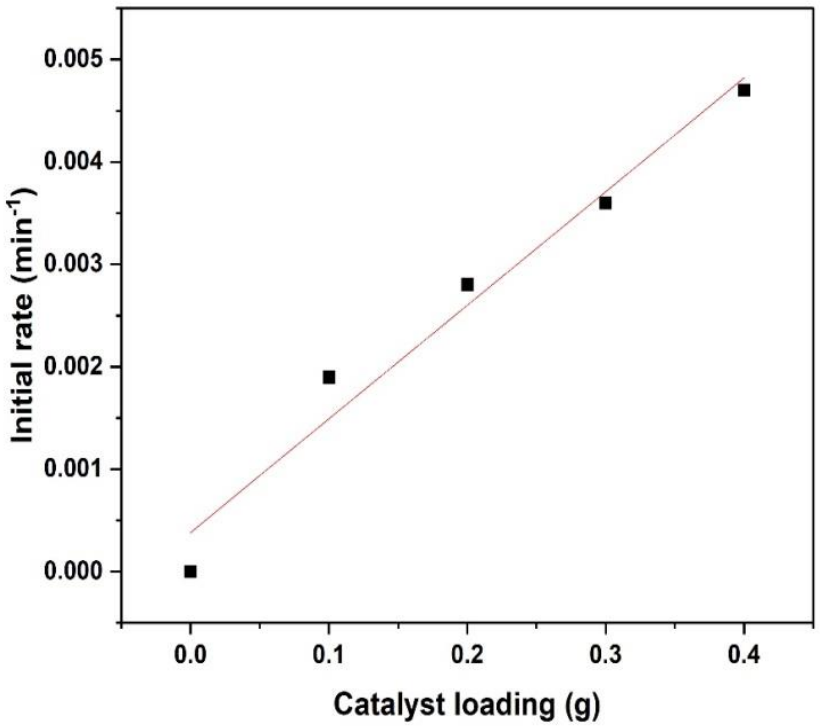

Figure 6.9. Effect of catalyst loading on furfural hydrogenation reaction over Ni/biochar(H_2SO_4) at temperature 190°C, stirring rate 1000 rpm, hydrogen pressure 50 bar, initial concentration 0.39M.

As a result, the findings support the idea that under the reaction conditions of catalyst particle size less 106 µm and stirring rate 1000 rpm (**Section 6.1**), both external and intraparticle diffusion transport limitations are negligible. **Figure 6.10** shows the Madon Boudart test for furfural hydrogenation over Ni/biochar(H_2SO_4) catalyst. The Madon Boudart test states that the plot of ln r_0 vs. ln (catalyst activity) will have a slope of 0.5 if reactions were conducted under internal transport restriction, while it will have a slope of zero when reactions were conducted under external transport limitation [93]. The reason for this is that when mass transport limitations are removed, the rate of the reaction is proportional to the number of active sites. It demonstrates a linear relationship between the reaction lnr_0 - ln (catalyst activity) due to the surface metal loadings on the catalyst. A critical factor is that the slope of the correlation line shown in **Figure 6.10** is greater than 0.5.

Based on the result there is no mass or heat transport resistance for stirring rate of 1000 rpm and catalyst particle size less than 106 µm. Also tested was the effect of catalyst loading on controlling resistance in a batch reactor using Ni/biochar(H_2SO_4) catalyst developed in-house.

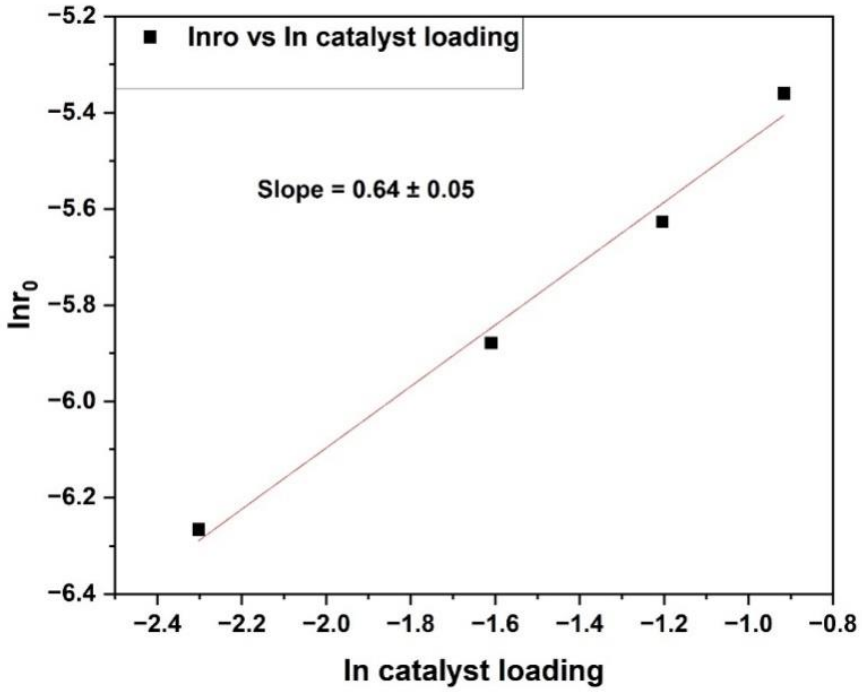

Figure 6.10. Madon Boudart test for furfural hydrogenation reaction over Ni/biochar(H_2SO_4). As detailed by Winterbottom and King (1999) [173], plotting (C_H/r_0) versus 1/(catalyst loading) can be utilised to determine the region of restriction in the gas-liquid interface within system. The slope signifies a combination of both external mass transfer and internal mass transport resistance at catalyst particles, while the intercept corresponds to the resistance to gas absorption at gas-liquid interfaces [182]. The resulting plot collected in this work is presented in **Figure 6.11**. It is important to note that the hydrogen pressure is constant (50 bar) for each experiment carried out. The resistance due to gas absorption through the liquid film at the gas-liquid interface is represented by the intercept of the plot, which is 0.78 min, while the combined external mass transport restriction and internal pore diffusion restriction at the catalyst particle is 0.022 min. Thus, using a finely divided Ni/biochar(H_2SO_4) catalyst particles reduced both the internal and external mass transport resistances at the catalyst particle. Due to the elimination of external and internal diffusional resistances described in **Section 6.1**, it

shows that resistance against absorption is negligible and surface reaction between furfural and hydrogen proceeds unhindered by transport limitations.

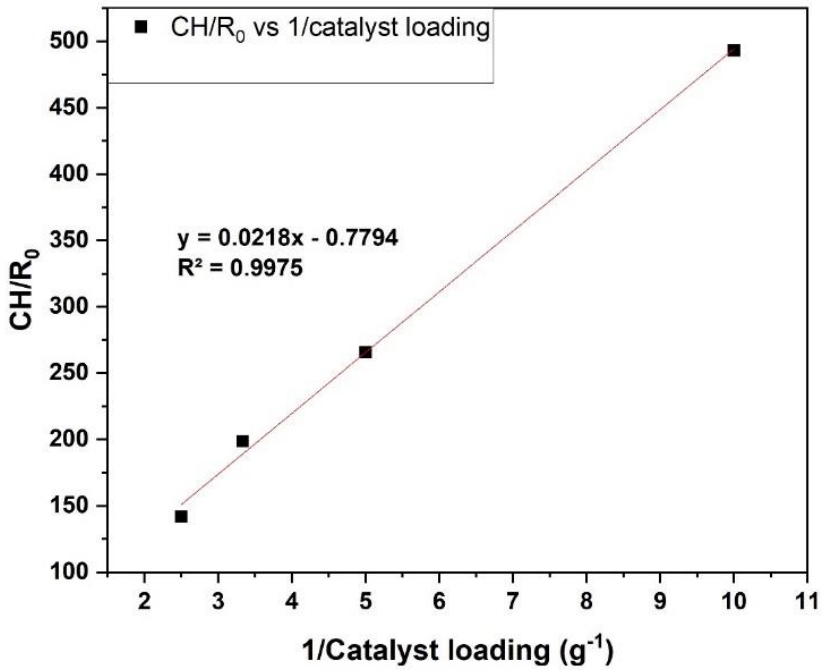

Figure 6.11. The plot of C_H/r_0 vs 1/catalyst loading

A reaction's activation energy and reaction rate are quantitatively described by the Arrhenius equation, a thermodynamic function. Using **equation (5.2)**, one can obtain the rate constant based on thermodynamic temperature. The plot of ln(k) versus 1/T to determine the activation energy (E_a) and pre-exponential factor (A) is shown in **Figure 6.12**. The graph shows that the rate constant increases as the reaction temperature increased from 200°C to 260°C. This suggests an increase in the rate of reaction with temperature.

6.1

Where R_{gas} denotes the universal gas constant 8.314J.K^{-1}mol^{-1}, E_a the activation energy (Jmol^{-1}), A the pre-exponential factor (1/s), and k the rate constant (M^{1-n}.min^{-1}).

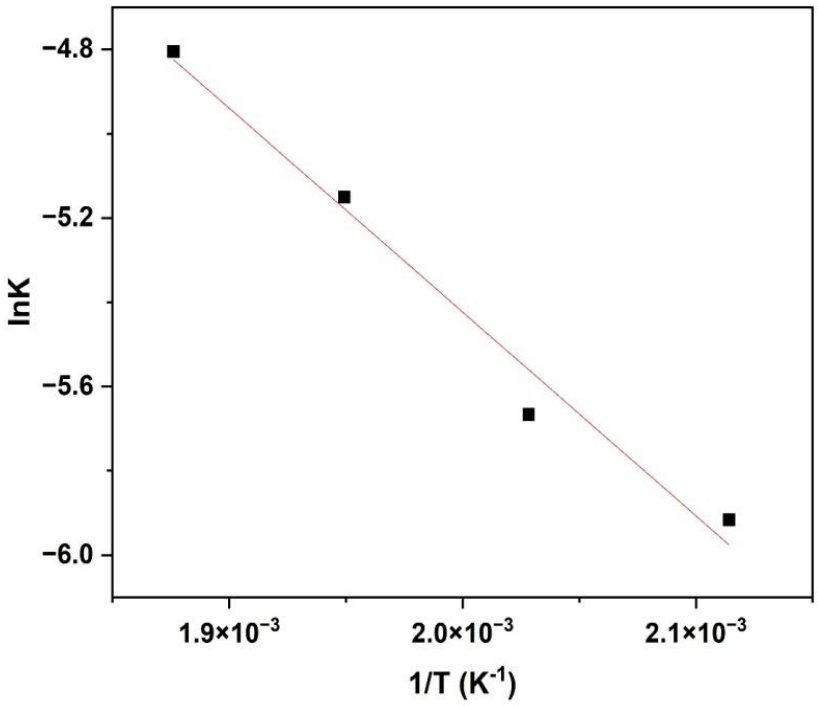

Figure 6.12. The Arrhenius equation plot of ln(k) versus 1/T.

Based on Arrhenius equation plot, the activation energy (E_a) is 40.22 kJmol^{-1} and pre-exponential factor (A) is 70.26min^{-1}. Similar activation energy values have been reported in the literature [183,184]; these are within 2.88kJmol^{-1} and 9.99 kJmol^{-1} respectively. On the contrary, the experimentally obtained activation energy here can be regarded as the true activation energy and the response might be said to be under kinetic control as a result.

6.4 Power-law model based on initial rate data

From **Figure 6.8**, the reaction pathway leading to the formation of 2-methylfuran (MF) through furfural (FAL) hydrogenation via furfuryl alcohol (FOL) can be expressed as follows: (*FAL→ FOL→ 2MF*) [170]. This suggests that furfuryl alcohol was produced right away from furfural and then converted into 2-methylfuran. In order to fit a kinetic model it is necessary to gather data for furfural concentration over time, but tracking the intermediate products can be problematic due to the intricacy of the reaction pathways and difficulties in measuring the

intermediate furfuryl alcohol during the hydrogenation process. The experimental data were collected at a constant hydrogen pressure of 5 bars. The effect of hydrogen pressure was not studied. Therefore, the rate of reaction terms of the concentration of furfural consumed per unit can be expressed using a Power Law, **equation (5.1)**.

6.2

The linearised form:

where, r denotes the reaction rate ($Mmin^{-1}$), k the rate constant ($M^{1-n}min^{-1}$), C the concentration (M) and n the order of reaction.

Based on the collected concentration data, a plot of concentration as a function of time is produced. The initial rates were calculated by polynomial fitting approach, then differentiated at time zero (t = 0). This approach has been used and reported in many studies [5,23,91,92]. In order to determine the reaction rate constant (k) and order (n), the plot of natural log of the initial rates ($\ln r_0$) against natural log of initial furfural concentration ($\ln C_0$) is produced for reaction temperatures 200°C (473 K), 220°C (493 K) and 240°C(513 K) as shown in **Figure 6.13**. The order of reaction is the slope of the plot at each experimental temperature, while the corresponding rate constant is determined from the intercept.

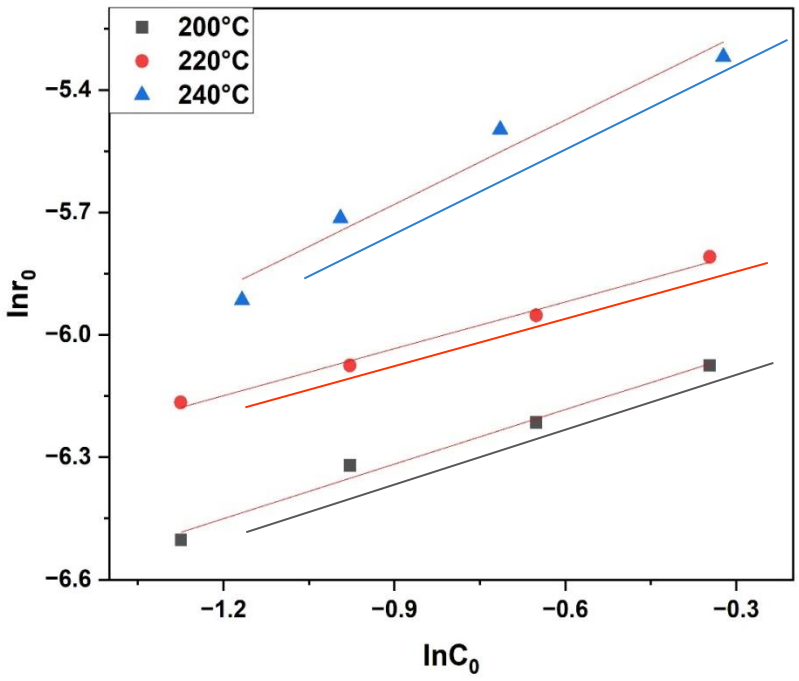

Figure 6.13. Plots of lnr_0 against ln$C_0$for reaction temperatures 200°C, 220°C, and 240°C under reaction conditions: catalyst loading 0.2g (< 106 µm), hydrogen pressure 50 bar, tetralin as solvent, and stirring rate 1000.

The respective order of reaction (n) at reaction temperatures 200°C, 220°C and 240°Care 0.42, 0.45 and 0.59, while the rate constants are as follows: 0.002695 $M^{0.58}min^{-1}$, 0.003462 $M^{0.55}min^{-1}$, and 0.005795 $M^{0.41}min^{-1}$. The order of reaction is less than 1, suggesting it is not first-order. The orders of reaction with regard to furfural concentration vary from 0.42 to 0.6, as can be seen from the slopes of the plot of ln (r_0) versus ln (C_0). If Langmuir-Hinshelwood kinetic type models are used instead of first-order rates, the resulting rate of reaction would be more complex. Therefore, due to the non-first-order dependency of the reaction on furfural initial concentration, the development of a model describing furfural hydrogenation reaction kinetics must take into account processes on the catalyst surface like adsorption, surface reaction, and desorption. Therefore, Langmuir - Hinshelwood (L - H) reaction rate model type equations would be more adequate to describe the reaction kinetics of furfural hydrogenation. This is

because the L – H type rate model will consider the active sites and the processes such as adsorption, surface reaction, and desorption occurring on the surface of the catalyst that controls the reaction.

6.5 Langmuir–Hinshelwood kinetic type model

The Langmuir-Hinshelwood kinetic type models could potentially be used to fit and explain the experimental data [91]. Based on previous works it was suggested a Langmuir−Hinshelwood−Hougen−Watson (LHHW) kinetic model for furfural hydrogenation over copper chromite that assumes a single type of adsorption site and a surface reaction between a partially hydrogenated furfural species and an adsorbed hydrogen [5,65,91].

On the catalyst, it is assumed that on S_1 sites, atoms of H are the predominant species, while furfural dominates on S_2 sites. Based on the assumption, the reaction mechanism is illustrated by reaction schemes 1 to 4. Typical Langmuir-Hinshelwood kinetic models (LH) can be derived, which involves hydrogen dissociatively adsorbed on dual active sites, and hydrogen chemisorbed on the same surface reacting with chemisorbed furfural.

Based on the experimental data, the most satisfactory fit was a dual-site mechanism with dissociative adsorption of hydrogen and surface reactions as rate-controlling steps [92]. The assumptions of the model may be summarised:

(i) Molecular adsorption of furfural (F), furfuryl alcohol (FOL), and 2-methyl furan (MF),

(ii) Dissociative adsorption of hydrogen on the catalyst active site,

(iii) During the reaction, the partial pressure of hydrogen can be considered constant due to the excess of hydrogen.

(iv) All adsorption sites are equivalent and independent of coverage, and

(v) Surface reaction is the rate-determining step.

It is believed that hydrogen adsorption onto the catalyst surface occurred dissociatively. Accordingly, **equations 6.3 to 6.6** represent the elementary steps taken in determining rate expressions for both competitive and non-competitive adsorption of dissociatively chemisorbed hydrogen (H_2) and furfural (F). Consequently, all adsorption and desorption sites of the catalysts are equivalent and independent of coverage [92].

$$H_2 + 2S_1 2H - S_1 \qquad 6.3$$

$$F + S_2 F - S_2 \qquad 6.4$$

$$F - S_2 + H - S_1 S_2 - F.H - S_1 \qquad 6.5$$

$$S_2 - F.H - S_1 + H - S_1\ Product + S_2 + 2S_1 \qquad 6.6$$

The following rate equations were derived to study the conversion of furfural (F) to furfuryl alcohol and 2-methyl furan and applied to the experimental data for parameter estimation. The derivation of these rate expressions has been provided in **Appendix II**. Based on dissociation of hydrogen, the following rate expressions are presented for the hydrogenation of furfural (F) and furfuryl alcohol:

Model-I Competitive adsorption of dissociative H_2 and furfural (F) during hydrogenation:

. 6.7

Model-II: the model assumed one type of adsorption site (competitive adsorption) and the rate-determining step as a surface reaction between an adsorbed H and a partially hydrogenated furfural species:

. 6.8

Model-III Non-competitive adsorption of dissociative H_2 and furfural during hydrogenation. Based on the assumption that H atoms dominate S1, and furfural dominates S2:

. 6.9

In literature, the two-sites' models, Model-II and Model-III, have been applied to study furfural hydrogenation over copper dispersed on three forms of carbon, namely activated carbon, diamond and graphitized fibres [65]. In 2018, the hydrogenation of furfural derived from biomass into 2-methylfuran, was studied over Cu–Co/Al_2O_3 catalyst using Model-I and Model-II [92].

In this work the sum of squared errors (SSE) function was used for non-linear regression fit of the model predictions. The objective function presented in **equation 6.10** was used to fit the proposed model and identify its parameters by minimising the residual sum of squares (RSS). The model parameters were estimated by using the optimization programme for a nonlinear generalized reduced gradient (GRG) solver in Microsoft Excel 2016. The RSS objective function was minimized to determine the model parameters that describe the experimental data:

6.10

In order to identify the appropriate model for the hydrogenation of furfural over Ni/biochar catalyst, the models were linearised to the format $y = mx + C$ as shown in the equations below:

Model-I

Model-II

Model-III

At constant hydrogen pressure of 50 bar (5 MPa) the concentration of dissolved hydrogen gas (C_H) will be constant and would follow Henry's law ($C_H = K_H P_H$). Therefore, the plot ofandshould be linear fits to the experimental data. Based on initial reaction rate obtained from the concentration-time plots of the experimental data, **Figure 6.14** shows the linear fits to the data.

(a)

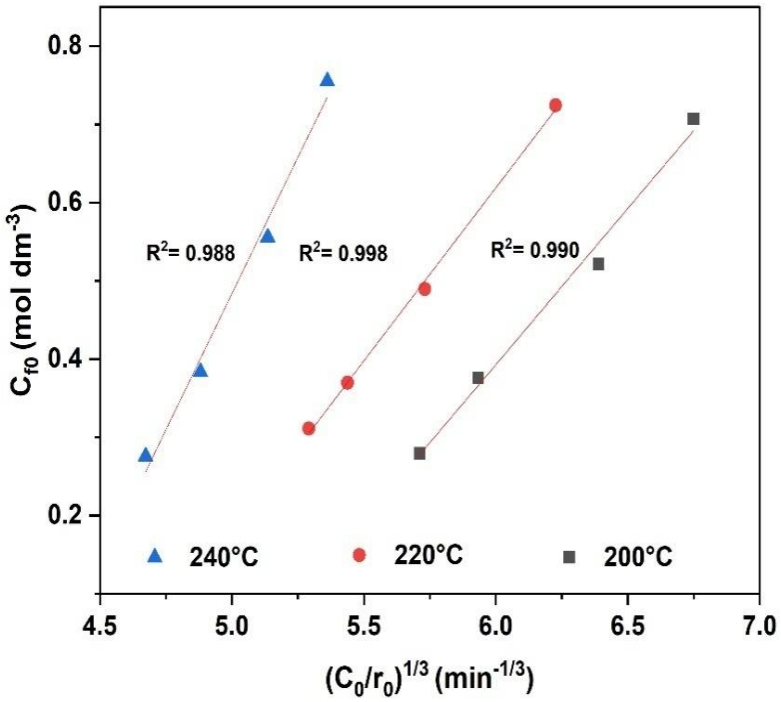

(b)

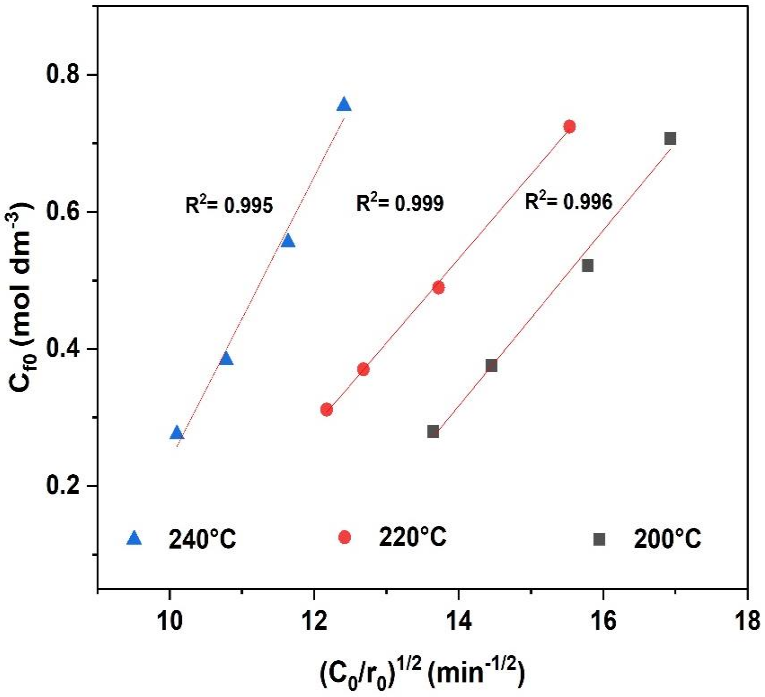

(c)

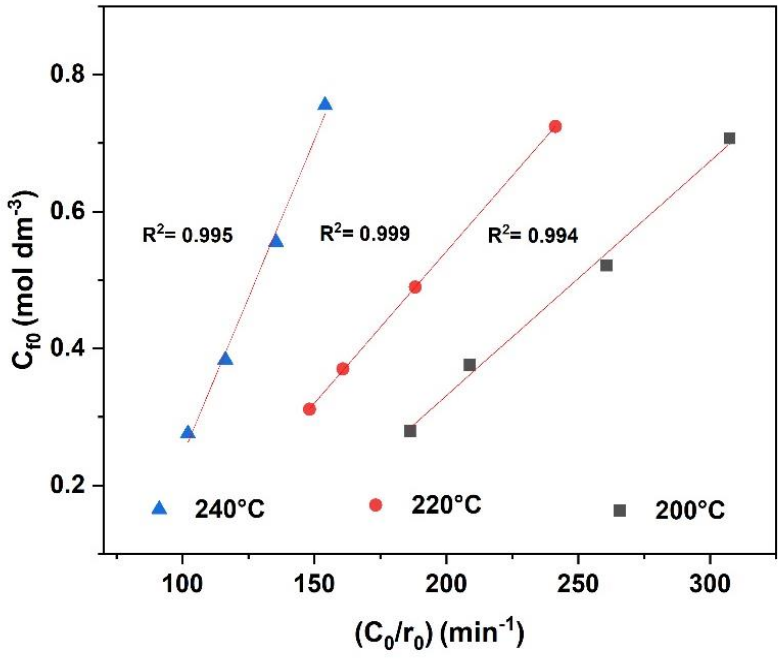

Figure 6.14. Fit of linearised version of models to experimental data using initial rates obtained from their concentration-time plots: (a) **Model-I**, (b) **Model-II**, and (c) **Model-III**.

The coefficient of determination (R^2) value, which represents the proportion of variation in the dependent variable that can be predicted completely from the independent variable, is used to evaluate the extent of linear fits to the initial reaction rates data. R^2 is a range of values between 0 and 1, and a value close to 1 implies the dependent variable can be predicted efficiently based on the independent variable with less error expected. Therefore, based on the linearised fits to the initial rates data, the R^2 values are as follows: Model-I [0.990 (200°C), 0.998 (220°C) and 0.988 (240°C)], Model-II [0.996 (200°C), 0.999 (220°C) and 0.995 (240°C)], and Model-III [0.994 (200°C), 0.999 (220°C) and 0.995 (240°C)]. Based on the R^2 values obtained through the linearised fits to the experimental data as shown in **Figures 6.14**, all three models predicted the experimental data with certain degrees of error, but Model-III has higher R^2 values and minimized errors compare to Model-I and Model-II. This suggests that both Model-II and Model-III are the more favourable kinetic model to describe the experimental data better than Model-I. Hence, the experimental data will be studied using Model-III. The conversion of furfural to furfuryl alcohol, and furfuryl alcohol to 2-methyl furan was found to match the experimental data obtained with reaction mechanism described by Model-II satisfactorily, according to published research [92].

In other studies, regarding the hydrogenation reaction of furfural model compound over Cu/activated carbon catalyst, Model-III has been reported to be the best fit to the experimental data [65]. It can be concluded therefore that the best match for the experimental data was a dual-site mechanism with hydrogen dissociative adsorption and surface reaction as the rate-controlling step. This is consistent with findings reported for copper-cobalt catalysed liquid phase hydrogenation of furfural to 2-methylfuran using the same kinetic model-II [92].

6.5.1 Model Parameter Estimation

By minimizing the residual sum of squares (RSS) objective error function using the Microsoft Excel's nonlinear generalized reduced gradient (GRG) solver optimization programme, the kinetic Model-III parameters such as surface reaction rate constant (k_S) and adsorption constants (K_H and K_F) was determined, including heat of adsorption (ΔH_H and ΔH_F) and intrinsic activation energy (EA). **Table 6.1** shows the estimated kinetic model parameters for furfural hydrogenation reaction over Ni/biochar(H_2SO_4) catalyst at a constant hydrogen pressure of 50 bar (5 MPa). With R^2 values beyond 99%, the proposed mechanistic model fit the data satisfactorily based on its kinetic model parameters (**Table 6.1**), as well as its correlation coefficients.

Table 6.1. Estimated Values of Kinetic Model Parameters for furfural Hydrogenation Reaction over Ni/biochar(H_2SO_4) Catalyst.

Temperature(°C)	k_S	K_H	K_F	RSS
200	0.018	0.235	1.353	7.913×10^{-8}
220	0.023	0.254	1.388	8.876×10^{-8}
240	0.030	0.299	1.521	7.717×10^{-9}
260	0.036	0.320	1.582	3.430×10^{-8}

Figure 6.15 shows the plot of experimental reaction rates against model predicted rates for Model-III, which indicates a strong agreement between experimental reaction rates and predicted reaction rates. This claim can be supported by a correlation coefficient greater than 99% between the experimental rates and the predicted rates from the model.

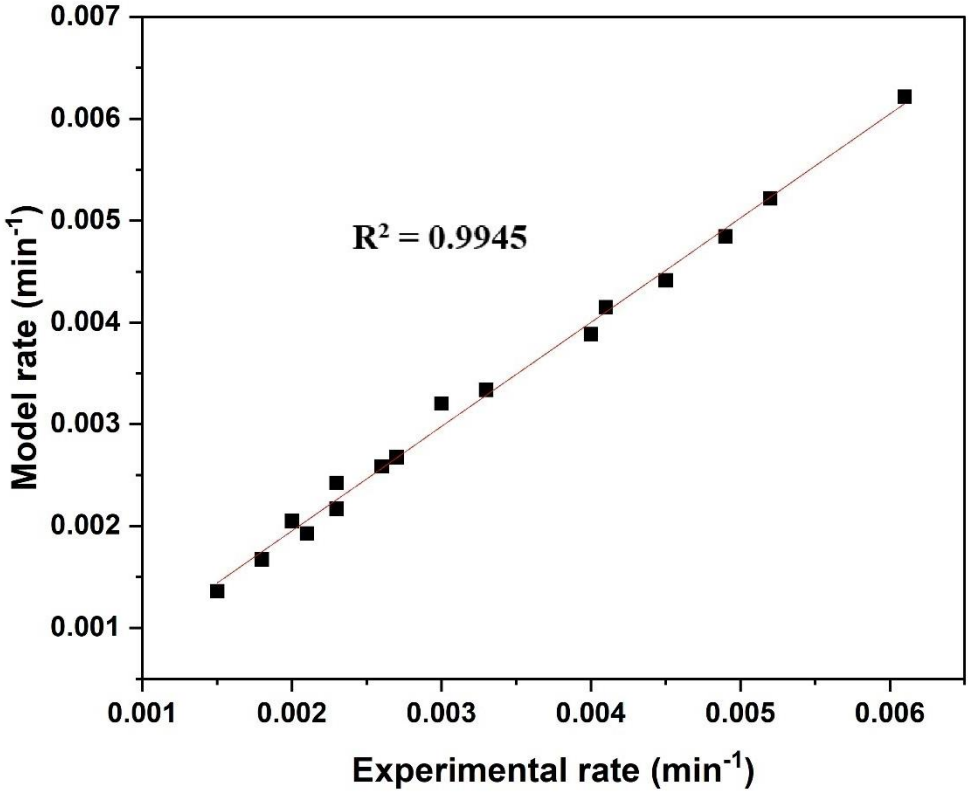

Figure 6.15. Parity plot of model-III to compare predicted rates by model and experimentally determined rates.

The activation energy for the hydrogenation reaction of furfural was determined using the Arrhenius **equation (6.1)**, which relates the reaction rate constant with temperature. This is the activation energy based on the LHHW kinetic model, which considers the dissociative adsorption of hydrogen and surface reaction. The activation energy of the surface reaction is considered here. The linearised Arrhenius equation is shown below, while the plot of ln k_S vs 1/T for reaction temperature from 200°C to 260°C at 20°C interval is shown in **Figure 6.16**.

However, the Van't Hoff isochore expression **(equation 6.11)** was used to estimate the enthalpy of adsorption as shown in **Figures 6.16** and **6.17** for both furfural and hydrogen.

Arrhenius equation (6.1):

Van't Hoff isochore equation: 6.11

Where, R denotes the universal gas constant 8.314 $JK^{-1}mol^{-1}$, E_a the activation energy ($J.mol^{-1}$), A the pre-exponential factor, K_{ads} the adsorption equilibrium constant, ΔH_{ads} the enthalpy changes due to adsorption, and ΔS the change in entropy of the system.

Based on the Arrhenius plot, the estimated activation energy is 24.39 $kJmol^{-1}$. It has been found that the apparent energy of activation for the surface reaction to be 16.36 $kcalmol^{-1}$ (68.45 $kJmol^{-1}$) for furfural hydrogenation reaction over Cu–Co/Al_2O_3 catalyst [92]. The difference in activation energy can be attributed to the different catalyst used in both studies and experimental conditions. But the activation energy obtained is significantly lower than that reported in the literature for other catalysts [65,92]. This shows that the developed catalyst in this study can lower the activation energy for furfural hydrogenation to 2-methylfuran.

On the other hand, the enthalpy of adsorption and entropy change for the adsorption of furfural on the active sites of the Ni/biochar (H_2SO_4) catalyst are -5.86 $kJmol^{-1}$and 14.81 $JK^{-1}mol^{-1}$, respectively. While for the adsorption of hydrogen enthalpy of adsorption and entropy change are -11.43 $kJmol^{-1}$ and 12.04 $JK^{-1}mol^{-1}$ [65].

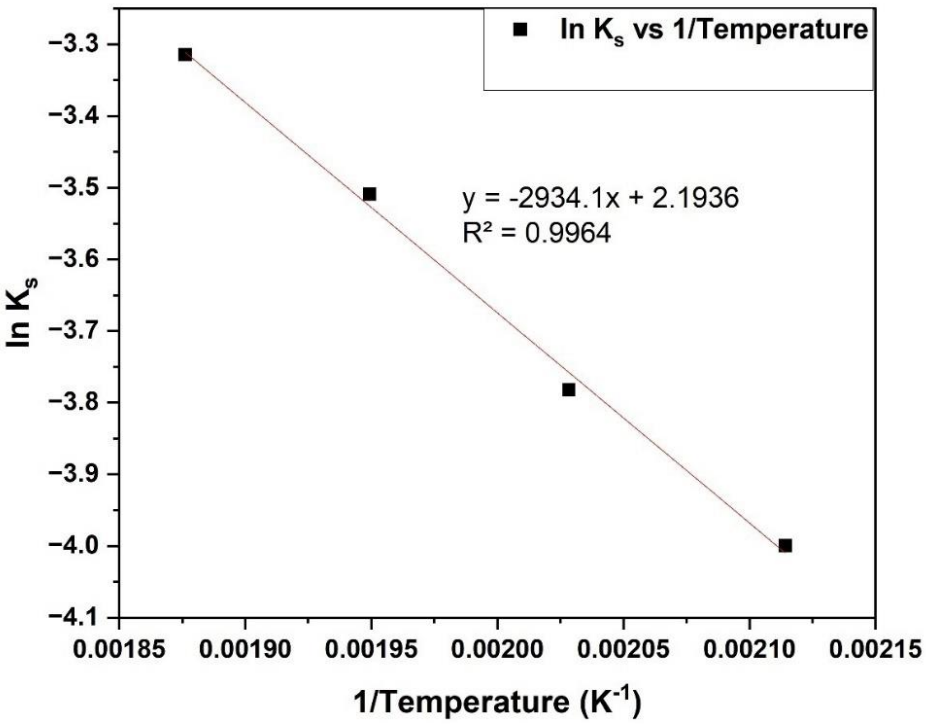

Figure 6.16. Arrhenius plot for furfural hydrogenation reaction.

a)

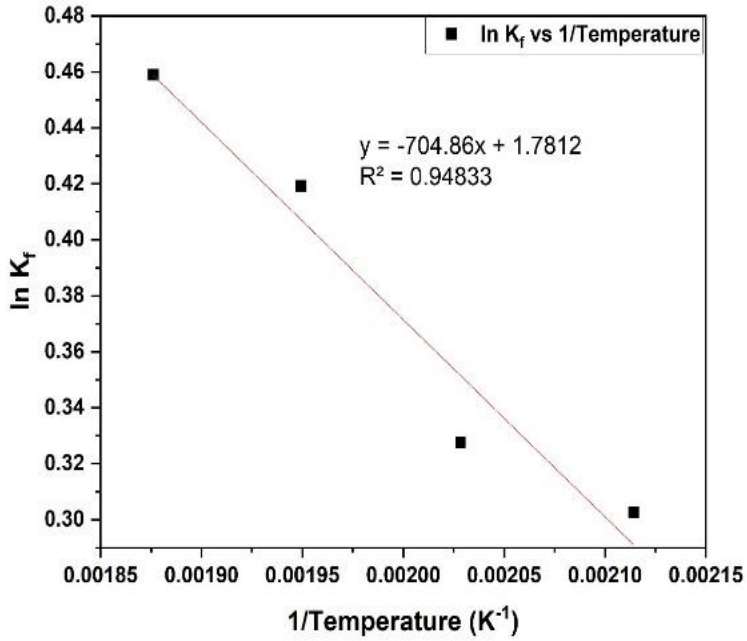

b)

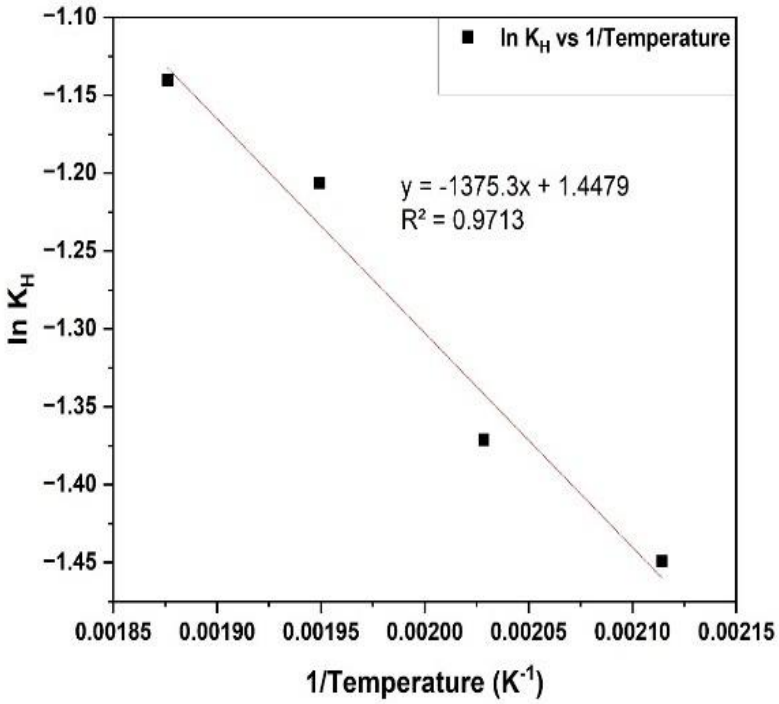

Figure 6.17. a) Van't Hoff isochore plot for furfural adsorption onto the catalyst. b) Van't Hoff isochore plot for hydrogen adsorption onto the catalyst.

6.6 Catalyst reusability

The reusability of Ni/biochar(H_2SO_4) catalyst was studied by recovering spent catalyst and reusing the catalysts for four successive furfural hydrogenation reaction cycles. The recovered catalysts were dried at 200°C for 30 mins to remove unreacted furfural, solvent, and products from the catalyst pores, before being used in the subsequent experiment. The reusability of Ni/biochar(H_2SO_4) catalyst was studied for four successive experimental cycles. **Figure 6.18** displays changes in conversion and products yields for each reaction cycle. As can be seen from the graph, there is no noticeable difference between the first and fourth cycles when it comes to the furfural conversion (99% to 96%) and the yield of 2-methyl furan (57% to 54%). Likewise, the yields of furan and tetrahydrofuran. On the other hand, the yield of furfuryl alcohol increases as the reaction cycle increase from first cycle to fourth cycle.

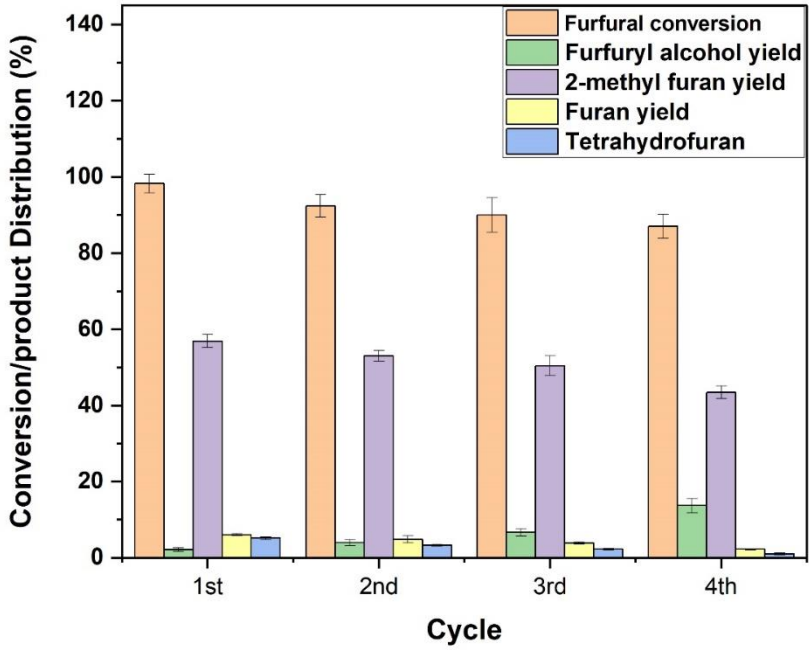

Figure 6.18. Effect of catalyst reusability on conversion and products yield from furfural hydrogenation over Ni/biochar (H_2SO_4) at reaction conditions: initial concentration 0.39M,

tetralin as solvent, temperature 230°C, catalyst loading 0.3g, stirring rate 1000 rpm, H_2 pressure; 50 bars, reaction time 5 hours.

Regarding the observed slight drop, the decline in furfural conversion and yield of 2-methyl furan is possibly due to the reduced strength in the catalyst active sites after successive reaction and drying steps [115]. This is further reaffirmed by the increasing yield of furfuryl alcohol from first cycle to fourth cycle, signifying that the hydrogenation of furfuryl alcohol to 2-methyl furan had been impacted. This can be attributed to the chemisorbed aromatic species (furfural, furan, 2-methyl furan, etc.) on the catalyst active sites after consecutive reaction, which could have adversely impacted on the strength, since no further regeneration of catalysts was performed before reuse. This explains the gradual decrease in the yield of 2-methyl furan and corresponding in the yield of furfuryl alcohol (**Figure 6.18**).

6.7 Effect of acidification time

It has been shown in **Chapter Four** that treating the biochar with sulfuric acid (H_2SO_4) significantly increased the surface area, pore volume and microporosity. The hypothesis therefore is that acid treatment of catalyst will increase rate of reaction by improving mass transport and providing more surface area for adsorption and surface reaction. It is believed that increasing acid time will produce a further increase in the catalyst surface area and porosity. **Figure 6.19** shows how the acid treatment time of the biochar impacted the catalytic performance of Ni/biochar(H_2SO_4) catalyst in terms of furfural conversion and product yields. It is obvious that the acid treated catalyst exhibited superior performance in comparison to the non-treated counterpart (NT) based on furfural conversion and 2-methyl furan yield. This is consistent with improvement in the catalyst physicochemical properties as demonstrated in **Chapters 4 and 5**.

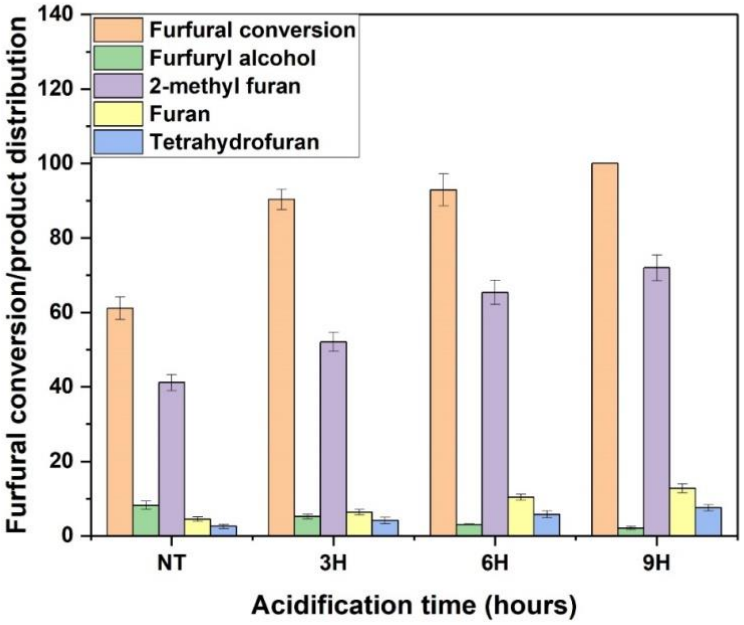

Figure 6.19. Conversion and product yield of Furfural hydrogenation over Ni/biochar (H_2SO_4) at reaction conditions: initial concentration 0.39M, tetralin as solvent, temperature 240°C, catalyst loading 0.3g, stirring rate 1000 rpm, H_2 pressure 50 bars, and reaction time 5 hours. [Note: NT denotes no acid treatment, and 3H, 6H, and 9H are 3-, 6- and 9-hours acid treatment].

Notably, the conversion of furfural and the yield of 2-methyl furan increases as the acid treatment time of the catalyst increases from 3 h to 9 h. Likewise, the yields of furan and tetrahydrofuran, while the yield of furfuryl alcohol decrease accordingly. At 9 h acid treatment, furfural conversion is approximately 100% and the yield of 2-methyl furan is about 71%. The improvement in the catalyst surface area and pore size distribution as a result of acid treatment favoured the reaction route and selectivity toward 2-methyl furan. This can further be confirmed from furfuryl alcohol which is a prerequisite product to produce 2-methyl furan, in which the yield decreases upon increasing acid treatment time. Consequently, since a high molecular weight hydrocarbon tetralin was used as solvent for HDO of furfural, the improvement in the catalyst pore size following 9 h acid treatment, could have further enhanced the intraparticle diffusion or pore diffusion.

6.8 Dual model compound system

In this section, the results of the mixture of vanillin and furfural over Ni/biochar(H_2SO_4) catalyst system is presented and discussed. It is expected, however, that the type of reactions displayed by the different classes of model compounds in a multi-component system and their competition for catalyst active sites would have a substantial effect on the reaction rate, compared to a system with just a single model compound. In this case, hydrogenation and hydrodeoxygenation of both furfural and vanillin will be occurring on the surface of the catalyst. **Figure 6.20** shows the conversions for both vanillin and furfural as a function of time. As expected, the conversion in both model compounds increases as the reaction time increased.

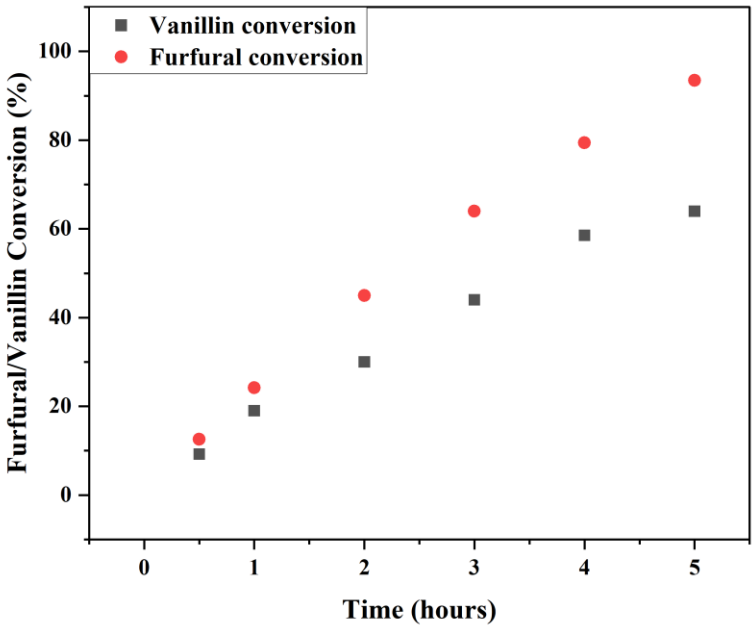

Figure 6.20. The conversion – time plot of vanillin due to HDO and furfural hydrogenation mixture over Ni/biochar(H_2SO_4) at reaction conditions: Initial concentration 0.38M, tetralin as solvent, temperature 240°C, catalyst loading 0.4g, H_2 pressure 40 bars, and stirring rate 1000 rpm.

Notably, at 4.5 hours reaction furfural conversion for as a single model compound system was around 95% (**Figure 6.6**), while in the dual system with vanillin the conversion is approximately 51% (**Figure 6.20**). Likewise, for a single HDO experiment of vanillin a conversion of about 43% for 5 h reaction time (**Chapter Five**, **Figure 5.4**), while for a dual system with furfural a conversion of around 35% was obtained. This can be attributed to the competitive adsorption for both furfural and vanillin for the catalyst active sites as well as hydrogen available in the system. As a result, the rate of hydrogenation of furfural to 2-methyl furan and HDO of vanillin to p-creosol is decreased. On the other hand, it can be observed that the conversion of furfural is significantly higher than that of vanillin. The plausible reason could be the molecular structure and size of both model compounds which plays a critical role in their diffusion through the catalyst pores to the active sites.

6.9 Bio-oil upgrading

For HDO of vanillin (**Chapter Five**), the sulfuric acid modified biochar catalyst outperformed both pristine biochar support and KOH modified catalysts, and it also displayed stability in the hydrogenation of furfural for four experimental cycles in this chapter. As a result, the sulfuric acid modified biochar catalyst (15wt% Ni/biochar(H_2SO_4)), was employed to catalyse the hydrodeoxygenation (HDO) of actual bio-oil itself. The rationale is that the improved mesoporosity of the acid modified biochar would enhance the mass transport of complex organic molecules present in the bio-oil itself, having demonstrated superior performance for both HDO of the phenolic compound vanillin and hydrogenation of the furfural platform molecule. The prove of improved pore structure and large surface area of the sulfuric acid modified biochar catalyst is shown in **Chapter Four**, while the performance on HDO using phenolic bio-oil model compound is demonstrated in **Chapter Five**. Thus, the rationale is to compare the catalytic performance of this study's developed catalyst (15 wt% Ni/biochar(H_2SO_4) catalyst) to that of a typical industrial catalyst (commercial TK-341

catalyst). Consequently, the effect of sulfiding the catalyst on the extent of HDO of actual bio-oil was also examined.

To demonstrate the application and effectiveness of the developed catalysts, they were tested with real bio-oil upgrading, to supplement the earlier work on model compound upgrading. Each system has advantages and disadvantages. For example, model compounds are easier to analyse and understand the reaction network and kinetics occurring. Whilst real bio-oils are representative of transport fuels but may have a complex mixture of compounds that are more difficult to quantify. Bio-oils consist of mixtures of unstable oxygenated compounds (phenolics, ketones, aldehydes, alcohols, carboxylic groups, and esters) that gradually react with each other to attain chemical equilibrium, leading to compositional changes and phase separation during storage. An important amount of the chemically attached oxygen in bio-oil will be removed by catalytic upgrading, creating a more hydrocarbon-like liquid with reduced viscosity, a high energy density, enhanced stability, and increased compatibility with petroleum fuels.

The multi-component nature of bio-oil causes several reactions to occur concurrently, including hydrocracking, hydrodeoxygenation, decarboxylation, decarbonylation, and hydrogenation [6]. Among these reactions, the quality of conversion is determined by the deoxygenation and cracking of non-volatile components. Therefore, catalytic upgrading is aimed at improving quality, H/C ratio via the oxygenate reduction in form water (H_2O), carbon dioxide (CO_2) and carbon monoxide (CO). The catalytic upgrading was carried out using a Parr 4848 batch reactor and catalyst (Ni/biochar (H_2SO_4) and commercial TK-341 catalysts). The commercial TK-341 catalyst is used to validate the catalyst developed in this work. **Figure 6.21** shows the photograph of the crude and upgraded bio-oil. The visual examination of displayed samples demonstrates that the upgraded oil is lighter in both colour and appearance than crude bio-oil. This suggests an improvement in quality. To confirm this, **Table 6.2** displays changes in the

bio-oil before and after catalytic upgrading. It is worth noting that the others include compounds containing heteroatoms such as sulfur, nitrogen, etc.

a) b)

Figure 6.21. Photograph of (a) raw bio-oil and (b) upgraded bio-oil

Table 6.2. Catalytic HDO of bio-oil produced by thermochemical reforming (TCR) of sewage sludge over Ni/biochar(H_2SO_4) and commercial TK-341 catalysts under reaction conditions: temperature 370°C, pressure 95 bar, and time 3 hours.

Catalyst	**Hydrocarbon (%)**	**Oxygenates (%)**	**Others (%)**
No treatment (Raw bio-oil)	71.26	13.02	14.7
Sulfided commercial TK-341	90.39	8.30	1.17
Sulfided Ni/biochar (H_2SO_4)	93.56	5.93	0.51
Ni/biochar (H_2SO_4)	87	9.27	4.15
NB: Others: Compounds with hetero-atoms other than Oxygen e nitrogen, iodine etc			

The results showed that during catalytic upgrading under hydrogen environment, the oxygenates decreased from 13.02% (crude bio-oil) to 8.3% (sulfided commercial TK-341 catalyst), 5.93% (sulfided Ni/biochar (H_2SO_4) catalyst) and 9.27% (Ni/biochar (H_2SO_4) catalyst). The reduction in oxygenates following catalytic upgrading are as follow: 4.72%,

7.09% and, 3.75% respectively. In terms of the hydrocarbon components the following was recorded: 90.39% (commercial TK-341 catalyst), 93.56% (sulfided Ni/biochar (H_2SO_4) catalyst) 87% and (Ni/biochar (H_2SO_4) catalyst) relative to 71.26% for the crude bio-oil. These respectively represent 19.13%, 22.3% and 15.74% improvement in hydrocarbon component over the crude bio-oil. This explains why the colour of the upgraded bio-oil is lighter as a result of reduction in the oxygenate via the removal of oxygen in the form H_2O, CO_2 and CO. The reactions occurring during bio-oil upgrading can be classified based on hydrocarbon products and oxygen removal products. A combination of decarbonylation, decarboxylation, direct deoxygenation (hydrogenolysis), dealkoxylation, cracking, hydrocracking, hydrogenation, dealkylation, methyl transfer, and hydrodeoxygenation have been observed during deoxygenation reaction. These reactions have been proven in both HDO of vanillin and the products (**Chapter Five**) and furfural hydrogenation and the products (**Section 6.2.1**). Likewise, the improvement in H/C atom ratio as indicated by the increase in the hydrocarbon component of the upgraded bio-oil.

Notably, the prepared Ni/biochar(H_2SO_4) catalyst sulfided provided a superior performance over a sulfided commercial TK-341 catalyst. It can be observed in **Table 6.2**, that pre-sulfiding the prepared Ni/biochar(H_2SO_4) catalyst outperformed the unsulfided counterpart. On the other hand, in terms of reduction in compounds containing sulfur and nitrogen, commercial TK-341 catalyst produced 1.17% and sulfided Ni/biochar (H_2SO_4) catalyst 0.51% relative to 14.7% for the raw bio-oil. This represents a significant decrease in sulfur and nitrogen containing compounds based on catalytic upgrading. However, sulfided Ni/biochar (H_2SO_4) catalyst provided a superior performance in comparison to commercial TK-341 catalyst.

6.10 Conclusion

Furfural hydrogenation to 2-methylfuran was studied. It is possible to produce 2-methylfuran by selectively removing oxygen from the formyl group through selective hydrodeoxygenation, suppressing competitive ring hydrogenation and ring opening. The results prove that the prepared Ni/biochar(H_2SO_4) catalyst selectively produced 2-methylfuran via furfural hydrogenation. The results show that using stirring rate 1000 rpm and catalyst particle size 106 μm both external and intraparticle mass transport limitations were negligible. A Langmuir-Hinshelwood type kinetic model could explain the experimental results mechanistically, in contrast to the power law method. A correlation coefficient better than 99% between the experimental rates and the predicted rate from the model supports this conclusion. Based on the experimental data, it can be concluded that a dual-site mechanism involving hydrogen dissociative adsorption and surface reaction gives the best fit. After successive reactions and drying steps, the active sites of the catalyst may have lost strength due to the decline in furfural conversion and yield of 2-methyl furan observed from first cycle to fourth cycle of catalyst reusability tests. This can be attributed to chemisorbed aromatic species from furfural and its products. On the basis of furfural conversion and 2-methyl furan yield, it was found that the acid-treated catalyst outperformed the non-treated counterpart. This can be explained by the increased surface area and mesopority with acidification time.

However, catalytic upgrading of bio-oil in a hydrogen environment reduced oxygenates from 13.02% (crude bio-oil) to 8.3% (commercial TK-341 catalyst) and 5.93% (sulfided Ni/biochar (H_2SO_4) catalyst. In terms of hydrocarbon components, the following level of catalytic upgrading was achieved: 90.39% (commercial TK-341 catalyst), and 93.56% (sulfided Ni/biochar (H_2SO_4) catalyst) relative to 71.26% for the raw bio-oil. It was found that the developed sulfided Ni/biochar (H_2SO_4) catalyst in this study outperformed commercial TK-

341 catalyst. The real bio-oil HDO was a limited study aimed to test the catalytic activity of the prepared Ni/biochar(H_2SO_4).

Chapter Seven

Conclusion and Recommendations

In this work, biochar was used as a catalyst carrier to develop a Ni/biochar catalyst for the HDO conversion of vanillin, an oxygenated phenolic compound present in bio-oil, into p-creosol, a future biofuel. The mesoporous structure of biochar was chemically improved before being impregnated with nickel metal to produce a novel, cost-effective, and renewable catalyst.

1. Through chemical activation with KOH and H_2SO_4 the biochar porous structure and specific surface area was tuned to improve the mesoporous structure network and increase specific surface area. It was hypothesised that this improvement in mesoporous structure and surface area would enhance the dispersion of Ni nanoparticles upon impregnation, improve mass transport of reactant molecules during HDO, and consequently increase catalytic activity and selectivity towards the desired biofuel products. The developed Ni/biochar and its chemically tuned counterparts' catalysts were characterised with the nitrogen adsorption-desorption technique, X-ray diffraction (XRD), scanning electron microscopy (SEM) coupled with energy dispersed X-ray analysis (EDX), carbon dioxide temperature-programmed desorption (CO_2-TPD), transmission electron microscopy (TEM), hydrogen gas temperature-programmed reduction (H_2-TPR), and Fourier-transform infrared spectroscopy (FT-IR). The surface area and pore size distribution were determined using the model equations proposed by Brunauer–Emmett–Teller (BET) and Barrett–Joyner–Halenda (BJH). The amount of Ni metal nanoparticles incorporated into the biochar was determined using inductively coupled plasma–optical emission spectroscopy (ICP-OES).

2. The actual Ni metal active phase impregnated in the developed 15 wt% Ni/biochar catalysts ranged from 14.7 to 15.3% wt%, according to ICP-OES analysis results. The adsorption–

desorption hysteresis patterns indicate that they are Type IV isotherms, indicating mesoporous structures, which is between 2 nm and 50 nm. As a result of leaching, dehydration, and oxidation, chemical treatment can create mesopores (pores that are 2 nm to 50 nm in size) within biochar support. It was found that 15 wt% Ni/biochar (H_2SO_4) mesopores (0.095 nm) were smaller than those discovered in 15 wt% Ni/biochar (KOH) catalyst (0.150 nm). The results of the chemical modification of the biochar showed that the surface area and pore volume of KOH treated biochar improved by 65.5% and 65.3%, while treatment with H_2SO_4 produced an enhancement of 372.3% in surface area and 256.8% increase in pore volume relative to the as-received biochar (74.84 m^2g^{-1} and 0.095 cm^3g^{-1}) (**Chapter four**). The FT-IR analysis results prove the presence of several typical functional groups, which includes phenolic -OH at 3400 cm^{-1}, carboxylic acids -COOH at 2330 cm^{-1}, -C-O stretching in cellulose at 1030 cm^{-1}, and C=C vibration for aromatic groups at 1580 cm^{-1}, respectively. The TEM results showed that nano-sized range of Ni active metal phase on the 15 wt% Ni/biochar was mostly between 6 nm to 11 nm, 15 wt% Ni/biochar (KOH) ranges from 4 nm to 12 nm and that of 15 wt% Ni/biochar (H_2SO_4) was between 4 nm and 10 nm. Based on this, it appears that chemical activation of the biochar support with KOH and H_2SO_4 has no significant effect on the particle size of the Ni metal phase nanoparticles dispersed on it.

3. The designed and developed active nickel-based and biochar support catalysts were experimentally tested for vanillin HDO to p-creosol, The optimisation study based on Ni/biochar demonstrated that for a 10 h experimental time, optimal conditions for vanillin HDO to p-creosol were determined by using response surface methodology (RSM) at 150°C, 50 bar, 0.6 g catalyst load and 1000 rpm. The experimental data demonstrated that as reaction temperature increased from 100°C to 150°C, vanillin conversion via HDO increases from 26% to 95%, likewise the yield of the desired product p-creosol increases from 15% to 90%, while vanillyl alcohol yield decreases from 8% to 2%. After four cycles of use, the catalyst also

showed a high degree of stability in vanillin HDO reaction to p-creosol. However, it was observed that the catalytic activity of the 15 wt% Ni/biochar catalyst decreased slightly after the third cycle, which might have been due to organic species (e.g., phenolic compounds) adsorbing onto the Ni/biochar surface during the first and second cycles. As a result, subsequent reaction cycles exhibited a decline in catalytic activity. Compared to as-received biochar prepared catalyst (15 wt% Ni/biochar), the catalyst prepared using the chemical activated biochar support with KOH- and H_2SO_4-treated demonstrated superior performance in terms of vanillin conversion and selectivity towards p-creosol yield in the order Ni/biochar (H_2SO_4) > Ni/biochar (KOH) > Ni/biochar. Generally, mesoporous biochar supports permit the Ni active phase to be located in within the pores, allowing the vanillin substrate and hydrogen molecule to be intimately contacted by the Ni active phase.

4.The Ni/biochar(H_2SO_4) was used for furfural hydrogenation to 2-methylfuran and kinetic modelling studies. In terms of the kinetic model study, it was discovered that the use of catalyst particles smaller than or equal to 106 μm and a stirring rate of 1000 rpm for experimental data collection for kinetic work and modelling eliminate both external and intraparticle mass transfer restrictions. The developed 15 wt% Ni/biochar(H_2SO_4) catalyst exhibited capability for the selective hydrogenation of C=O bond in furfural and deoxygenation ability for the cleavage of C−OH bond in furfuryl alcohol to further produce 2-methylfuran. 0.022 min represents the resistance against hydrogen gas absorption through the tetralin solvent at the gas-liquid interface at the experimental conditions. As opposed to the power law method, Langmuir−Hinshelwood−Hougen−Watson (LHHW) kinetic models can explain experimental results mechanistically. In support of this conclusion, a correlation coefficient better than 99% exists between the experimental and predicted rates. It was found that that the best model explains the experimental data by using a dual-site mechanism that involves dissociative adsorption of hydrogen and surface reactions. A decline in furfural conversion and yield of 2-

methyl furan observed between the first and fourth cycle of catalyst reusability tests could have resulted from chemisorbed aromatic species (e.g., furans) from furfural and its products, which may have weakened the active sites of the catalyst following successive reactions and drying steps.

5) The sulfuric acid tuned Ni/biochar(15 wt% Ni/biochar (H_2SO_4)) was)) was tested with actual bio-oil HDO for catalytic upgrading of actual bio-oil. The Ni/biochar(H_2SO_4) catalyst performance was validated against typical industrial catalyst used in catalytic upgrading of bio-oils. The oxygenates in crude bio-oil were reduced from 13.02% (as-received bio-oil) to 8.3% (commercial TK-341 catalyst) and 5.93% (sulfided Ni/biochar (H_2SO_4) catalyst) when catalytically upgraded in a hydrogen environment. This represents about 2.4% further reduction of oxygenates, confirming the robustness and superior catalytic activity of the developed catalyst in study relative to commercial TK-341 catalyst used in the industry. Correspondingly, the hydrocarbon components increased in this order of the tested catalysts: 93.56% (sulfided Ni/biochar (H_2SO_4) catalyst) > 90.39% (commercial TK-341 catalyst) >Ni/biochar (H_2SO_4) >71.26% (as-received raw bio-oil). This suggests that sulfiding the developed catalyst improved its HDO activity with bio-oil. Due to the reduction in ash content and oxygenate via the removal of oxygen in the form of H_2O, CO_2 and CO, the colour of the upgraded bio-oil is lighter.

Recommendations

The present study successfully developed a novel and low-cost catalyst based on recycled biochar from biomass pyrolysis, which is more economical compared to previous works on bio-oil upgrading and its model compounds HDO. As a result, it was tested with HDO of vanillin, hydrogenation of furfural, and HDO of bio-oil itself, demonstrating the robustness of the catalysts in the HDO process. Additionally, it contributes significantly

towards making HDO of bio-oil economically viable through robust and low-cost catalyst. This study is only an integral part of the collection of studies required to accomplish this goal. In this present work, monometallic Ni-based and biochar catalyst was developed. But it has been reported in the literature that bimetallic catalyst can achieve higher HDO activity and selectivity than their monometallic counterparts.

1. There is a large amount of research required in the field of developing catalysts for deoxygenating bio-oil and its model compounds, this needs a great deal of time and effort. Thus, biochar catalyst impregnated with bimetallics such as Ni-Cu, Ni-Fe, Ni-W, etc. represent a potentially attractive combination of metals to be investigated in future studies. Although for this monometallic study involving only Ni metal active phase 15 wt% metal loading was used, so in a bimetallic study there is potential for overall metal loading reduction following the incorporation of a second or third metal. The choice of metals should be based on their oxophilic tendency to form oxides or abstract oxygen from a molecule (i.e., model compounds), which makes them demonstrate excellent catalytic activity for oxygenate bio-oil model compounds.

2. Production costs, scalability, and yield are important factors in the successful commercialization of the catalyst and products from its HDO of model compounds or bio-oil. It is necessary to create a techno-economic model of HDO based on the recycled biochar from the pyrolysis of biomass as a catalyst support. This is necessary in evaluating the economic viability of using biochar and Ni metal to develop catalysts for HDO of bio-oil and its model compounds. Techno-economic analysis will incorporate elements such as process modelling, equipment sizing, capital cost estimation, and operating cost estimation. This study is critical for demonstrating the appropriateness of biochar and Ni metal for potential future commercial advancements of HDO of bio-oil.

3. In this study the thermal stability of the biochar support catalyst and its chemically modified counterparts have been studied with the aid of a thermogravimetric analyser, TGA (**Chapter four**). The results prove that they are thermally stable up to 800^{o}C temperature under nitrogen atmosphere. However, the deactivation of the catalyst due to HDO of actual bio-oil was not examined. Thus, a future study should include regeneration of Ni/biochar following its application in upgrading bio-oil via HDO. The different environments under which this can be achieved are nitrogen, hydrogen, and steam.

4. Most of the experiments reported in this study are based on batch reactor data. It may be difficult to extend these studies to large-scale applications due to the limited scope of batch reactors. Hence, it is necessary to study continuous reactor systems, which would provide practical data for industrial or pilot-scale reactors.

5. Different physical and/or chemical treatments can be applied to biochar to fine-tune its morphology, pore structure, and surface functionality. In this study only KOH and H_2SO_4 chemical activation was used. Physical methods using oxidising agents such as CO_2 and steam at high temperature. Also, other chemicals can be applied to tune the biochar pore structure. In addition, it is worthwhile to investigate what effect biochar functionalisation and incorporation of dopants would have on catalyst activity and selectivity.

6. As a result of the high market price of hydrogen, upgrading bio-oil using HDO is limited by its large usage and requirement for external hydrogen. This increases the operating cost of producing high quality fuel products. So, it will be of economic importance to focus on hydrogen-donor solvents such as cyclohexane and decalin in future research, as well as to validate the results using hydrogen gas.

7. Extensive study of real bio-oil HDO over Ni/iochar(H_2SO_4) could not be conducted in this research work due to limitation of time and as such is highly recommended for future research.

LIST OF REFERENCES

1. Isikgor, F.H.; Becer, C.R. Lignocellulosic biomass: a sustainable platform for the production of bio-based chemicals and polymers. *Polymer chemistry* **2015**, *6*, 4497-4559.
2. Graca, I.; Lopes, J.M.; Cerqueira, H.S.; Ribeiro, M.F. Bio-oils upgrading for second generation biofuels. *Industrial & Engineering Chemistry Research* **2013**, *52*, 275-287.
3. Bridgwater, A.V. Review of fast pyrolysis of biomass and product upgrading. *Biomass and bioenergy* **2012**, *38*, 68-94.
4. Czernik, S.; Bridgwater, A. Overview of applications of biomass fast pyrolysis oil. *Energy & fuels* **2004**, *18*, 590-598.
5. Aliu, E. Vanillin hydrodeoxygenation reaction kinetics over supported monometallic and bimetallic Pd-based catalysts in different solvents and binary environments. University of Birmingham, 2020.
6. Mortensen, P.M.; Grunwaldt, J.-D.; Jensen, P.A.; Knudsen, K.; Jensen, A.D. A review of catalytic upgrading of bio-oil to engine fuels. *Applied Catalysis A: General* **2011**, *407*, 1-19.
7. Shit, S.C.; Koley, P.; Joseph, B.; Marini, C.; Nakka, L.; Tardio, J.; Mondal, J. Porous organic polymer-driven evolution of high-performance cobalt phosphide hybrid nanosheets as vanillin hydrodeoxygenation catalyst. *ACS applied materials & interfaces* **2019**, *11*, 24140-24153.
8. Peters, J.E.; Carpenter, J.R.; Dayton, D.C. Anisole and guaiacol hydrodeoxygenation reaction pathways over selected catalysts. *Energy & Fuels* **2015**, *29*, 909-916.
9. Egorova, M.; Prins, R. The role of Ni and Co promoters in the simultaneous HDS of dibenzothiophene and HDN of amines over Mo/γ-Al2O3 catalysts. *Journal of Catalysis* **2006**, *241*, 162-172.
10. Prins, R.; Egorova, M.; Röthlisberger, A.; Zhao, Y.; Sivasankar, N.; Kukula, P. Mechanisms of hydrodesulfurization and hydrodenitrogenation. *Catalysis Today* **2006**, *111*, 84-93.
11. Bello, S.S.; Wang, C.; Zhang, M.; Gao, H.; Han, Z.; Shi, L.; Su, F.; Xu, G. A review on the reaction mechanism of hydrodesulfurization and hydrodenitrogenation in heavy oil upgrading. *Energy & Fuels* **2021**, *35*, 10998-11016.
12. Sorunmu, Y.; Billen, P.; Spatari, S. A review of thermochemical upgrading of pyrolysis bio-oil: Techno-economic analysis, life cycle assessment, and technology readiness. *Gcb Bioenergy* **2020**, *12*, 4-18.
13. Qu, L.; Jiang, X.; Zhang, Z.; Zhang, X.-g.; Song, G.-y.; Wang, H.-l.; Yuan, Y.-p.; Chang, Y.-l. A review of hydrodeoxygenation of bio-oil: model compounds, catalysts, and equipment. *Green Chemistry* **2021**, *23*, 9348-9376.
14. Lee, H.; Kim, H.; Yu, M.J.; Ko, C.H.; Jeon, J.-K.; Jae, J.; Park, S.H.; Jung, S.-C.; Park, Y.-K. Catalytic hydrodeoxygenation of bio-oil model compounds over Pt/HY catalyst. *Scientific reports* **2016**, *6*, 28765.
15. Mortensen, P.M.; Grunwaldt, J.-D.; Jensen, P.A.; Jensen, A.D. Screening of catalysts for hydrodeoxygenation of phenol as a model compound for bio-oil. *Acs Catalysis* **2013**, *3*, 1774-1785.
16. Sankaranarayanan, T.M.; Berenguer, A.; Ochoa-Hernández, C.; Moreno, I.; Jana, P.; Coronado, J.M.; Serrano, D.P.; Pizarro, P. Hydrodeoxygenation of anisole as bio-oil model compound over supported Ni and Co catalysts: Effect of metal and support properties. *Catalysis Today* **2015**, *243*, 163-172.

17. Tang, X.; Ding, W.; Li, H. Improved hydrodeoxygenation of bio-oil model compounds with polymethylhydrosiloxane by Brønsted acidic zeolites. *Fuel* **2021**, *290*, 119883.
18. Wang, X.; Zhang, Z.; Yan, Z.; Li, Q.; Zhang, Y. Catalysts with metal-acid dual sites for selective hydrodeoxygenation of lignin derivatives: Progress in regulation strategies and applications. *Applied Catalysis A: General* **2023**, 119266.
19. Laurenti, D.; Afanasiev, P.; Geantet, C. Hydrodeoxygenation of guaiacol with CoMo catalysts. Part I: Promoting effect of cobalt on HDO selectivity and activity. *Applied Catalysis B: Environmental* **2011**, *101*, 239-245.
20. Lin, Y.-C.; Li, C.-L.; Wan, H.-P.; Lee, H.-T.; Liu, C.-F. Catalytic hydrodeoxygenation of guaiacol on Rh-based and sulfided CoMo and NiMo catalysts. *Energy & Fuels* **2011**, *25*, 890-896.
21. Santos, J.; Alda-Onggar, M.; Fedorov, V.; Peurla, M.; Eränen, K.; Mäki-Arvela, P.; Centeno, M.Á.; Murzin, D.Y. Hydrodeoxygenation of vanillin over carbon supported metal catalysts. *Applied Catalysis A: General* **2018**, *561*, 137-149.
22. Nie, R.; Yang, H.; Zhang, H.; Yu, X.; Lu, X.; Zhou, D.; Xia, Q. Mild-temperature hydrodeoxygenation of vanillin over porous nitrogen-doped carbon black supported nickel nanoparticles. *Green Chemistry* **2017**, *19*, 3126-3134.
23. Aliu, E.; Hart, A.; Wood, J. Kinetics of vanillin hydrodeoxygenation reaction in an organic solvent using a Pd/C catalyst. *Industrial & Engineering Chemistry Research* **2019**, *58*, 15162-15172.
24. Aliu, E.; Hart, A.; Wood, J. Mild-Temperature hydrodeoxygenation of vanillin a typical bio-oil model compound to Creosol a potential future biofuel. *Catalysis Today* **2021**, *379*, 70-79.
25. Wang, C.; Guo, L.; Wu, K.; Li, X.; Huang, Y.; Shen, Z.; Yang, H.; Yang, Y.; Wang, W.; Li, C. Rational design of Ni–MoO3–x catalyst towards efficient hydrodeoxygenation of lignin− derived bio− oil into naphthenes. *Journal of Energy Chemistry* **2023**.
26. Xiong, K.; Wan, W.; Chen, J.G. Reaction pathways of furfural, furfuryl alcohol and 2-methylfuran on Cu (111) and NiCu bimetallic surfaces. *Surface Science* **2016**, *652*, 91-97.
27. Kiméné, A.; Wojcieszak, R.; Paul, S.; Dumeignil, F. Catalytic decarboxylation of fatty acids to hydrocarbons over non-noble metal catalysts: the state of the art. *Journal of Chemical Technology & Biotechnology* **2019**, *94*, 658-669.
28. Ouedraogo, A.S.; Bhoi, P.R. Recent progress of metals supported catalysts for hydrodeoxygenation of biomass derived pyrolysis oil. *Journal of Cleaner Production* **2020**, *253*, 119957.
29. Sharma, B.K.; Kohli, K. Slurry Phase Catalysts for Bio-Oil Upgradation. *TR Series (Illinois Sustainable Technology Center); TR-077* **2020**.
30. Wanmolee, W.; Sosa, N.; Junkaew, A.; Youngjan, S.; Geantet, C.; Afanasiev, P.; Puzenat, E.; Laurenti, D.; Faungnawakij, K.; Khemthong, P. Phase speciation and surface analysis of copper phosphate on high surface area silica support by in situ XAS/XRD and DFT: Assessment for guaiacol hydrodeoxygenation. *Applied Surface Science* **2022**, *574*, 151577.
31. Guo, X.; Wang, W.; Wu, K.; Huang, Y.; Shi, Q.; Yang, Y. Preparation of Fe promoted MoS2 catalysts for the hydrodeoxygenation of p-cresol as a model compound of lignin-derived bio-oil. *Biomass and Bioenergy* **2019**, *125*, 34-40.
32. Magalhães, B.C.; Checa, R.; Lorentz, C.; Prévot, M.; Afanasiev, P.; Laurenti, D.; Geantet, C. Catalytic Hydrotreatment of Algal HTL Bio-Oil over Phosphide, Nitride, and Sulfide Catalysts. *ChemCatChem* **2023**, *15*, e202300025.

33. Cheng, S.; Wei, L.; Julson, J.; Rabnawaz, M. Upgrading pyrolysis bio-oil through hydrodeoxygenation (HDO) using non-sulfided Fe-Co/SiO2 catalyst. *Energy Conversion and Management* **2017**, *150*, 331-342.
34. Jahangiri, H.; Bennett, J.; Mahjoubi, P.; Wilson, K.; Gu, S. A review of advanced catalyst development for Fischer–Tropsch synthesis of hydrocarbons from biomass derived syn-gas. *Catalysis Science & Technology* **2014**, *4*, 2210-2229.
35. Gupta, S.; Mondal, P.; Borugadda, V.B.; Dalai, A.K. Advances in upgradation of pyrolysis bio-oil and biochar towards improvement in bio-refinery economics: A comprehensive review. *Environmental Technology & Innovation* **2021**, *21*, 101276.
36. Quan, C.; Zhou, Y.; Wang, J.; Wu, C.; Gao, N. Biomass-based carbon materials for CO2 capture: A review. *Journal of CO2 Utilization* **2023**, *68*, 102373.
37. Jechan, L.; Ki-Hyun, K.; Eilhann, K. Biochar as a Catalyst. *Renew. Sustainable Energy Rev* **2017**, *77*, 70-79.
38. Yang, H.; Chen, Z.; Chen, W.; Chen, Y.; Wang, X.; Chen, H. Role of porous structure and active O-containing groups of activated biochar catalyst during biomass catalytic pyrolysis. *Energy* **2020**, *210*, 118646.
39. Nguyen, H.K.; Pham, V.V.; Do, H.T. Preparation of Ni/biochar catalyst for hydrotreating of bio-oil from microalgae biomass. *Catalysis Letters* **2016**, *146*, 2381-2391.
40. Bykova, M.; Ermakov, D.Y.; Kaichev, V.; Bulavchenko, O.; Saraev, A.; Lebedev, M.Y.; Yakovlev, V. Ni-based sol–gel catalysts as promising systems for crude bio-oil upgrading: Guaiacol hydrodeoxygenation study. *Applied Catalysis B: Environmental* **2012**, *113*, 296-307.
41. Li, X.; Jia, P.; Wang, T. Furfural: A promising platform compound for sustainable production of C4 and C5 chemicals. *ACS catalysis* **2016**, *6*, 7621-7640.
42. Wu, P.; Singh, B.P.; Wang, H.; Jia, Z.; Wang, Y.; Chen, W. Bibliometric analysis of biochar research in 2021: a critical review for development, hotspots and trend directions. *Biochar* **2023**, *5*, 6.
43. Cao, L.; Zhang, C.; Chen, H.; Tsang, D.C.; Luo, G.; Zhang, S.; Chen, J. Hydrothermal liquefaction of agricultural and forestry wastes: state-of-the-art review and future prospects. *Bioresource technology* **2017**, *245*, 1184-1193.
44. Tian, C.; Li, B.; Liu, Z.; Zhang, Y.; Lu, H. Hydrothermal liquefaction for algal biorefinery: A critical review. *Renewable and Sustainable Energy Reviews* **2014**, *38*, 933-950.
45. Zhang, M.; Hu, Y.; Wang, H.; Li, H.; Han, X.; Zeng, Y.; Xu, C.C. A review of bio-oil upgrading by catalytic hydrotreatment: Advances, challenges, and prospects. *Molecular Catalysis* **2021**, *504*, 111438.
46. Elliott, D.C. Historical developments in hydroprocessing bio-oils. *Energy & Fuels* **2007**, *21*, 1792-1815.
47. Elliott, D.C.; Biller, P.; Ross, A.B.; Schmidt, A.J.; Jones, S.B. Hydrothermal liquefaction of biomass: Developments from batch to continuous process. *Bioresource technology* **2015**, *178*, 147-156.
48. Fang, H.; Zheng, J.; Luo, X.; Du, J.; Roldan, A.; Leoni, S.; Yuan, Y. Product tunable behavior of carbon nanotubes-supported Ni–Fe catalysts for guaiacol hydrodeoxygenation. *Applied Catalysis A: General* **2017**, *529*, 20-31.
49. Bridgwater, T. Challenges and opportunities in fast pyrolysis of biomass: Part I. *Johnson Matthey Technology Review* **2018**, *62*, 118-130.
50. Park, H.J.; Jeon, J.-K.; Suh, D.J.; Suh, Y.-W.; Heo, H.S.; Park, Y.-K. Catalytic vapor cracking for improvement of bio-oil quality. *Catalysis surveys from Asia* **2011**, *15*, 161-180.

51. Chen, Z.; Wang, M.; Jiang, E.; Wang, D.; Zhang, K.; Ren, Y.; Jiang, Y. Pyrolysis of torrefied biomass. *Trends in biotechnology* **2018**, *36*, 1287-1298.
52. Yin, S.; Zhang, N.; Tian, C.; Yi, W.; Yuan, Q.; Fu, P.; Zhang, Y.; Li, Z. Effect of accumulative recycling of aqueous phase on the properties of hydrothermal degradation of dry biomass and bio-crude oil formation. *Energies* **2021**, *14*, 285.
53. Bridgwater, A.V.; Meier, D.; Radlein, D. An overview of fast pyrolysis of biomass. *Organic geochemistry* **1999**, *30*, 1479-1493.
54. Ren, S.; Lei, H.; Wang, L.; Bu, Q.; Chen, S.; Wu, J. Hydrocarbon and hydrogen-rich syngas production by biomass catalytic pyrolysis and bio-oil upgrading over biochar catalysts. *Rsc Advances* **2014**, *4*, 10731-10737.
55. Luterbacher, J.; Alonso, D.M.; Dumesic, J. Targeted chemical upgrading of lignocellulosic biomass to platform molecules. *Green Chemistry* **2014**, *16*, 4816-4838.
56. Ruddy, D.A.; Schaidle, J.A.; Ferrell III, J.R.; Wang, J.; Moens, L.; Hensley, J.E. Recent advances in heterogeneous catalysts for bio-oil upgrading via "ex situ catalytic fast pyrolysis": catalyst development through the study of model compounds. *Green Chemistry* **2014**, *16*, 454-490.
57. Khromova, S.A.; Smirnov, A.A.; Bulavchenko, O.A.; Saraev, A.A.; Kaichev, V.V.; Reshetnikov, S.I.; Yakovlev, V.A. Anisole hydrodeoxygenation over Ni–Cu bimetallic catalysts: The effect of Ni/Cu ratio on selectivity. *Applied Catalysis A: General* **2014**, *470*, 261-270.
58. Ahmad, M.M.; Nordin, M.F.R.; Azizan, M.T. Upgrading of bio oil into high value hydrocarbons via hydrodeoxygenation. *American journal of applied sciences* **2010**, *7*, 746-755.
59. Zhu, X.; Lobban, L.L.; Mallinson, R.G.; Resasco, D.E. Bifunctional transalkylation and hydrodeoxygenation of anisole over a Pt/HBeta catalyst. *Journal of Catalysis* **2011**, *281*, 21-29.
60. Yusuf, M.; Leeke, G.; Wood, J. Anisole hydrodeoxygenation over nickel-based catalysts: influences of solvent and support properties. *Energy & Fuels* **2023**, *37*, 1225-1237.
61. Zhang, X.; Wang, T.; Ma, L.; Zhang, Q.; Yu, Y.; Liu, Q. Characterization and catalytic properties of Ni and NiCu catalysts supported on ZrO2–SiO2 for guaiacol hydrodeoxygenation. *Catalysis Communications* **2013**, *33*, 15-19.
62. Ruiz, P.; Frederick, B.; De Sisto, W.; Austin, R.; Radovic, L.; Leiva, K.; García, R.; Escalona, N.; Wheeler, M. Guaiacol hydrodeoxygenation on MoS2 catalysts: Influence of activated carbon supports. *Catalysis Communications* **2012**, *27*, 44-48.
63. Duan, M.; Cheng, Q.; Wang, M.; Wang, Y. In situ hydrodeoxygenation of vanillin over Ni–Co–P/HAP with formic acid as a hydrogen source. *RSC advances* **2021**, *11*, 10996-11003.
64. Santos, J.L.; Mäki-Arvela, P.; Wärnå, J.; Monzon, A.; Centeno, M.A.; Murzin, D.Y. Hydrodeoxygenation of vanillin over noble metal catalyst supported on biochars: Part II: Catalytic behaviour. *Applied Catalysis B: Environmental* **2020**, *268*, 118425.
65. Rao, R.S.; Baker, R.T.K.; Vannice, M.A. Furfural hydrogenation over carbon-supported copper. *Catalysis letters* **1999**, *60*, 51-57.
66. Ya, K.; Wu, G. T. La fleur and C. Jarvis. *Renewable Sustainable Energy Rev* **2014**, *38*, 663-676.
67. Wang, Y.; Zhao, D.; Rodríguez-Padrón, D.; Len, C. Recent advances in catalytic hydrogenation of furfural. *Catalysts* **2019**, *9*, 796.
68. Pirmoradi, M.; Kastner, J.R. A kinetic model of multi-step furfural hydrogenation over a Pd-TiO2 supported activated carbon catalyst. *Chemical Engineering Journal* **2021**, *414*, 128693.

69. Fulajtárova, K.; Soták, T.; Hronec, M.; Vávra, I.; Dobročka, E.; Omastová, M. Aqueous phase hydrogenation of furfural to furfuryl alcohol over Pd–Cu catalysts. *Applied Catalysis A: General* **2015**, *502*, 78-85.
70. Liu, M.; Zhang, J.; Zheng, L.; Fan, G.; Yang, L.; Li, F. Significant promotion of surface oxygen vacancies on bimetallic CoNi nanocatalysts for hydrodeoxygenation of biomass-derived vanillin to produce methylcyclohexanol. *ACS Sustainable Chemistry & Engineering* **2020**, *8*, 6075-6089.
71. Popov, A.; Kondratieva, E.; Mariey, L.; Goupil, J.M.; El Fallah, J.; Gilson, J.-P.; Travert, A.; Maugé, F. Bio-oil hydrodeoxygenation: Adsorption of phenolic compounds on sulfided (Co) Mo catalysts. *Journal of Catalysis* **2013**, *297*, 176-186.
72. Barroso-Martín, I.; Ballesteros-Plata, D.; Infantes-Molina, A.; Guerrero-Pérez, M.O.; Santamaría-González, J.; Rodríguez-Castellón, E. An overview of catalysts for the hydrodeoxygenation reaction of model compounds from lignocellulosic biomass. *IET Renewable Power Generation* **2022**, *16*, 3009-3022.
73. Yan, P.; Tian, X.; Kennedy, E.M.; Stockenhuber, M. The role of Ni sites located in mesopores in the selectivity of anisole hydrodeoxygenation. *Catalysis Science & Technology* **2022**, *12*, 2184-2196.
74. Vo, T.A.; Koo, Y.; Kim, J.; Kim, S.-S. Non-precious metal catalysts supported by activated carbon and TiO2–SiO2: Facile preparation and application for highly effective hydrodeoxygenation of syringol–a lignin-derived model compound. *Journal of Industrial and Engineering Chemistry* **2023**, *122*, 138-151.
75. He, Z.; Wang, X. Hydrodeoxygenation of model compounds and catalytic systems for pyrolysis bio-oils upgrading. *Catalysis for sustainable energy* **2012**, *1*, 28-52.
76. Zhang, J.; Sun, J.; Wang, Y. Recent advances in the selective catalytic hydrodeoxygenation of lignin-derived oxygenates to arenes. *Green Chemistry* **2020**, *22*, 1072-1098.
77. Ali, H.; Vandevyvere, T.; Lauwaert, J.; Kansal, S.K.; Sabbe, M.K.; Saravanamurugan, S.; Thybaut, J.W. Enhancing the anisole hydrodeoxygenation activity over Ni/Nb 2 O 5− x by tuning the oxophilicity of the support. *Catalysis Science & Technology* **2023**, *13*, 1140-1153.
78. Laurent, E.; Delmon, B. Influence of water in the deactivation of a sulfided NiMoγ-Al2O3 catalyst during hydrodeoxygenation. *Journal of Catalysis* **1994**, *146*, 281-291.
79. Venderbosch, R.H.; Ardiyanti, A.R.; Wildschut, J.; Oasmaa, A.; Heeres, H. Stabilization of biomass-derived pyrolysis oils. *Journal of Chemical Technology & Biotechnology* **2010**, *85*, 674-686.
80. Popov, A.; Kondratieva, E.; Goupil, J.M.; Mariey, L.; Bazin, P.; Gilson, J.-P.; Travert, A.; Maugé, F. Bio-oils hydrodeoxygenation: Adsorption of phenolic molecules on oxidic catalyst supports. *The Journal of Physical Chemistry C* **2010**, *114*, 15661-15670.
81. Garcia-Perez, M.; Shen, J.; Wang, X.S.; Li, C.-Z. Production and fuel properties of fast pyrolysis oil/bio-diesel blends. *Fuel Processing Technology* **2010**, *91*, 296-305.
82. Lu, Q.; Chen, C.-J.; Luc, W.; Chen, J.G.; Bhan, A.; Jiao, F. Ordered mesoporous metal carbides with enhanced anisole hydrodeoxygenation selectivity. *ACS Catalysis* **2016**, *6*, 3506-3514.
83. Qian, K.; Kumar, A.; Zhang, H.; Bellmer, D.; Huhnke, R. Recent advances in utilization of biochar. *Renewable and Sustainable Energy Reviews* **2015**, *42*, 1055-1064.
84. Lee, J.; Kim, K.-H.; Kwon, E.E. Biochjar as a catalyst. *Renewable and Sustainable Energy Reviews* **2017**, *77*, 70-79.
85. Teles, C.A.; Rabelo-Neto, R.C.; de Lima, J.R.; Mattos, L.V.; Resasco, D.E.; Noronha, F.B. The effect of metal type on hydrodeoxygenation of phenol over silica supported catalysts. *Catalysis Letters* **2016**, *146*, 1848-1857.

86. Chadderdon, X.H.; Chadderdon, D.J.; Matthiesen, J.E.; Qiu, Y.; Carraher, J.M.; Tessonnier, J.-P.; Li, W. Mechanisms of furfural reduction on metal electrodes: Distinguishing pathways for selective hydrogenation of bioderived oxygenates. *Journal of the American Chemical Society* **2017**, *139*, 14120-14128.
87. Wang, B.; He, Z.; Zhang, B.; Duan, Y. Study on hydrothermal liquefaction of spirulina platensis using biochar based catalysts to produce bio-oil. *Energy* **2021**, *230*, 120733.
88. Figueiredo, J.L.; Pereira, M.F.R. The role of surface chemistry in catalysis with carbons. *Catalysis Today* **2010**, *150*, 2-7.
89. Ranga, C.; Alexiadis, V.I.; Lauwaert, J.; Lødeng, R.; Thybaut, J.W. Effect of Co incorporation and support selection on deoxygenation selectivity and stability of (Co) Mo catalysts in anisole HDO. *Applied Catalysis A: General* **2019**, *571*, 61-70.
90. Yang, Y.; Ochoa-Hernández, C.; Pizarro, P.; Coronado, J.M.; Serrano, D.P. Effect of metal–support interaction on the selective hydrodeoxygenation of anisole to aromatics over Ni-based catalysts. *Applied catalysis B: environmental* **2014**, *145*, 91-100.
91. Maccarrone, M.J.; Torres, G.; Lederhos, C.; Betti, C.; Badano, J.M.; Quiroga, M.; Yori, J. Kinetic study of the partial hydrogenation of 1-heptyne over Ni and Pd supported on alumina. *Hydrogenation* **2012**, 159-184.
92. Srivastava, S.; Jadeja, G.; Parikh, J. Copper-cobalt catalyzed liquid phase hydrogenation of furfural to 2-methylfuran: An optimization, kinetics and reaction mechanism study. *Chemical Engineering Research and Design* **2018**, *132*, 313-324.
93. Singh, U.K.; Vannice, M.A. Kinetics of liquid-phase hydrogenation reactions over supported metal catalysts—a review. *Applied Catalysis A: General* **2001**, *213*, 1-24.
94. Lawal, A.M.; Hart, A.; Daly, H.; Hardacre, C.; Wood, J. Kinetics of hydrogenation of acetic acid over supported platinum catalyst. *Energy & Fuels* **2019**, *33*, 5551-5560.
95. Vázquez-Fuentes, L.F.; Cortés-Jácome, M.A.; Lopez-Salinas, E.; Sanchez-Valente, J.; Toledo-Antonio, J.A. Vanillin hydrodeoxygenation kinetics on takovite derived NiAlOx mixed oxides. *Catalysis Today* **2022**, *394*, 103-109.
96. Cha, J.S.; Park, S.H.; Jung, S.-C.; Ryu, C.; Jeon, J.-K.; Shin, M.-C.; Park, Y.-K. Production and utilization of biochar: A review. *Journal of Industrial and Engineering Chemistry* **2016**, *40*, 1-15.
97. Kannan, M. Transmission electron microscope—Principle, components and applications. *A textbook on fundamentals and applications of nanotechnology* **2018**, 93-102.
98. Mohammed, A.; Abdullah, A. Scanning electron microscopy (SEM): A review. In Proceedings of the Proceedings of the 2018 International Conference on Hydraulics and Pneumatics—HERVEX, Băile Govora, Romania, 2018; pp. 7-9.
99. Abd Mutalib, M.; Rahman, M.; Othman, M.; Ismail, A.; Jaafar, J. Scanning electron microscopy (SEM) and energy-dispersive X-ray (EDX) spectroscopy. In *Membrane characterization*; Elsevier: 2017; pp. 161-179.
100. Pavia, D.L.; Lampman, G.M.; Kriz, G.S.; Vyvyan, J.A. *Introduction to spectroscopy*; Cengage learning: 2014.
101. Bacsik, Z.; Mink, J.; Keresztury, G. FTIR spectroscopy of the atmosphere. I. Principles and methods. *Applied spectroscopy reviews* **2004**, *39*, 295-363.
102. Dollimore, D.; Spooner, P.; Turner, A. The BET method of analysis of gas adsorption data and its relevance to the calculation of surface areas. *Surface Technology* **1976**, *4*, 121-160.
103. Lowell, S.; Shields, J.E.; Thomas, M.A.; Thommes, M.; Lowell, S.; Shields, J.E.; Thomas, M.A.; Thommes, M. Surface area analysis from the Langmuir and BET theories. *Characterization of porous solids and powders: surface area, pore size and density* **2004**, 58-81.

104. Ooi, L.-l. *Principles of X-ray Crystallography*; Oxford University Press: 2010.
105. Pope, C.G. X-ray diffraction and the Bragg equation. *Journal of chemical education* **1997**, *74*, 129.
106. Copeland, L.E.; Bragg, R.H. Quantitative X-ray diffraction analysis. *Analytical Chemistry* **1958**, *30*, 196-201.
107. Bhatia, S.; Beltramini, J.; Do, D. Temperature programmed analysis and its applications in catalytic systems. *Catalysis Today* **1990**, *7*, 309-438.
108. Boaro, M.; Vicario, M.; De Leitenburg, C.; Dolcetti, G.; Trovarelli, A. The use of temperature-programmed and dynamic/transient methods in catalysis: characterization of ceria-based, model three-way catalysts. *Catalysis Today* **2003**, *77*, 407-417.
109. Hurst, N.W.; Gentry, S.J.; Jones, A.; McNicol, B.D. Temperature programmed reduction. *Catalysis Reviews Science and Engineering* **1982**, *24*, 233-309.
110. Falconer, J.L.; Schwarz, J.A. Temperature-programmed desorption and reaction: applications to supported catalysts. *Catalysis Reviews Science and Engineering* **1983**, *25*, 141-227.
111. Pirola, C.; Galli, F.; Patience, G.S. Experimental methods in chemical engineering: Temperature programmed reduction—TPR. *The Canadian Journal of Chemical Engineering* **2018**, *96*, 2317-2320.
112. Reiche, M.; Maciejewski, M.; Baiker, A. Characterization by temperature programmed reduction. *Catalysis today* **2000**, *56*, 347-355.
113. Zhang, H.; Li, M.; Xiao, P.; Liu, D.; Zou, C.-J. Structure and catalytic performance of Mg-SBA-15-supported nickel catalysts for CO2 reforming of methane to syngas. *Chemical Engineering & Technology* **2013**, *36*, 1701-1707.
114. Rodrigues, A.C.C. Extension of the modified Sanderson method to ternary mixed oxides derived from hydrotalcite-like compounds and its correlation to CO 2 (TPD-CO 2) desorption peak maxima. *Journal of mathematical chemistry* **2006**, *39*, 541-549.
115. Lawal, A.M.; Hart, A.; Daly, H.; Hardacre, C.; Wood, J. Catalytic hydrogenation of short chain carboxylic acids typical of model compound found in bio-oils. *Industrial & Engineering Chemistry Research* **2019**, *58*, 7998-8008.
116. Larson, M.G. Analysis of variance. *Circulation* **2008**, *117*, 115-121.
117. Sudarsanam, P.; Peeters, E.; Makshina, E.V.; Parvulescu, V.I.; Sels, B.F. Advances in porous and nanoscale catalysts for viable biomass conversion. *Chemical Society Reviews* **2019**, *48*, 2366-2421.
118. Dehkhoda, A.M.; West, A.H.; Ellis, N. Biochar based solid acid catalyst for biodiesel production. *Applied Catalysis A: General* **2010**, *382*, 197-204.
119. Zhang, C.; Sun, S.; Xu, S.; Wu, C. CO2 capture over steam and KOH activated biochar: Effect of relative humidity. *Biomass and Bioenergy* **2022**, *166*, 106608.
120. Zhang, P. Adsorption and desorption isotherms. *KE Group* **2016**.
121. Zhang, F.-S.; Nriagu, J.O.; Itoh, H. Mercury removal from water using activated carbons derived from organic sewage sludge. *Water research* **2005**, *39*, 389-395.
122. Chen, W.; Gong, M.; Li, K.; Xia, M.; Chen, Z.; Xiao, H.; Fang, Y.; Chen, Y.; Yang, H.; Chen, H. Insight into KOH activation mechanism during biomass pyrolysis: Chemical reactions between O-containing groups and KOH. *Applied Energy* **2020**, *278*, 115730.
123. Luo, Y.; Street, J.T.; Steele, P.H.; Entsminger, E.D.; Guda, V.K. Activated Carbon Derived from Pyrolyzed Pinewood Char using Elevated Temperature, KOH, H3PO4, and H2O2. *BioResources* **2016**, *11*, 10433.
124. Bear, J. *Dynamics of fluids in porous media*; Courier Corporation: 2013.
125. Batchelor, G. The effect of Brownian motion on the bulk stress in a suspension of spherical particles. *Journal of fluid mechanics* **1977**, *83*, 97-117.

126. Nilabh, S. Numerical modelling of the dynamics of chlorinated solvent pollution in aquifers and their remediation with engineered nano-particles: An integrated approach. **2021**.
127. Deen, W. Hindered transport of large molecules in liquid-filled pores. *AICHE journal* **1987**, *33*, 1409-1425.
128. Somorjai, G.A.; Li, Y. *Introduction to surface chemistry and catalysis*; John Wiley & Sons: 2010.
129. Wahi, R.; Zuhaidi, N.F.Q.a.; Yusof, Y.; Jamel, J.; Kanakaraju, D.; Ngaini, Z. Chemically treated microwave-derived biochar: An overview. *Biomass and Bioenergy* **2017**, *107*, 411-421.
130. Waqas, M.; Aburiazaiza, A.; Miandad, R.; Rehan, M.; Barakat, M.; Nizami, A. Development of biochar as fuel and catalyst in energy recovery technologies. *Journal of cleaner production* **2018**, *188*, 477-488.
131. Chausali, N.; Saxena, J.; Prasad, R. Nanobiochar and biochar based nanocomposites: Advances and applications. *Journal of Agriculture and Food Research* **2021**, *5*, 100191.
132. Sajjadi, B.; Zubatiuk, T.; Leszczynska, D.; Leszczynski, J.; Chen, W.Y. Chemical activation of biochar for energy and environmental applications: a comprehensive review. *Reviews in Chemical Engineering* **2019**, *35*, 777-815.
133. Sano, E.E.; Rodrigues, A.A.; Martins, E.S.; Bettiol, G.M.; Bustamante, M.M.; Bezerra, A.S.; Couto Jr, A.F.; Vasconcelos, V.; Schüler, J.; Bolfe, E.L. Cerrado ecoregions: A spatial framework to assess and prioritize Brazilian savanna environmental diversity for conservation. *Journal of environmental management* **2019**, *232*, 818-828.
134. Spokas, K.A.; Reicosky, D.C. Impacts of sixteen different biochars on soil greenhouse gas production. **2009**.
135. Li, S.; Chen, G. Thermogravimetric, thermochemical, and infrared spectral characterization of feedstocks and biochar derived at different pyrolysis temperatures. *Waste Management* **2018**, *78*, 198-207.
136. Bakshi, S.; Banik, C.; Laird, D.A. Estimating the organic oxygen content of biochar. *Scientific reports* **2020**, *10*, 1-12.
137. Reisser, M.; Purves, R.S.; Schmidt, M.W.; Abiven, S. Pyrogenic carbon in soils: a literature-based inventory and a global estimation of its content in soil organic carbon and stocks. *Frontiers in Earth Science* **2016**, *4*, 80.
138. Cheng, C.H.; Lehmann, J.; Thies, J.E.; Burton, S.D. Stability of black carbon in soils across a climatic gradient. *Journal of Geophysical Research: Biogeosciences* **2008**, *113*.
139. Zhang, S.; Wang, J. Removal of chlortetracycline from water by immobilized Bacillus subtilis on honeysuckle residue–derived biochar. *Water, Air, & Soil Pollution* **2021**, *232*, 236.
140. Wang, Y.; Shao, Y.; Zhang, L.; Zhang, S.; Wang, Y.; Xiang, J.; Hu, S.; Hu, G.; Hu, X. Co-presence of hydrophilic and hydrophobic sites in Ni/biochar catalyst for enhancing the hydrogenation activity. *Fuel* **2021**, *293*, 120426.
141. Mohan, D.; Abhishek, K.; Sarswat, A.; Patel, M.; Singh, P.; Pittman, C.U. Biochar production and applications in soil fertility and carbon sequestration–a sustainable solution to crop-residue burning in India. *RSC advances* **2018**, *8*, 508-520.
142. Aftab, Z.-e.-H.; Aslam, W.; Aftab, A.; Shah, A.N.; Akhter, A.; Fakhar, U.; Siddiqui, I.; Ahmed, W.; Majid, F.; Wróbel, J. Incorporation of engineered nanoparticles of biochar and fly ash against bacterial leaf spot of pepper. *Scientific Reports* **2022**, *12*, 8561.
143. Gale, M.; Nguyen, T.; Moreno, M.; Gilliard-AbdulAziz, K.L. Physiochemical properties of biochar and activated carbon from biomass residue: influence of process conditions to adsorbent properties. *ACS omega* **2021**, *6*, 10224-10233.

144. Wang, Y.; Zhang, Y.; Pei, L.; Ying, D.; Xu, X.; Zhao, L.; Jia, J.; Cao, X. Converting Ni-loaded biochars into supercapacitors: Implication on the reuse of exhausted carbonaceous sorbents. *Scientific reports* **2017**, *7*, 41523.
145. Zhang, P.; Duan, W.; Peng, H.; Pan, B.; Xing, B. Functional biochar and its balanced design. *ACS Environmental Au* **2021**, *2*, 115-127.
146. Behazin, E.; Ogunsona, E.; Rodriguez-Uribe, A.; Mohanty, A.K.; Misra, M.; Anyia, A.O. Mechanical, chemical, and physical properties of wood and perennial grass biochars for possible composite application. *BioResources* **2016**, *11*, 1334-1348.
147. Zhang, K.; Sun, P.; Zhang, Y. Decontamination of Cr (VI) facilitated formation of persistent free radicals on rice husk derived biochar. *Frontiers of Environmental Science & Engineering* **2019**, *13*, 1-9.
148. Reza, M.S.; Afroze, S.; Bakar, M.S.; Saidur, R.; Aslfattahi, N.; Taweekun, J.; Azad, A.K. Biochar characterization of invasive Pennisetum purpureum grass: effect of pyrolysis temperature. *Biochar* **2020**, *2*, 239-251.
149. Sanchis, R.; García, T.; Dejoz, A.M.; Vázquez, I.; Llopis, F.J.; Solsona, B. Easy method for the transformation of levulinic acid into gamma-valerolactone using a nickel catalyst derived from nanocasted nickel oxide. *Materials* **2019**, *12*, 2918.
150. Cheng, F.; Li, X. Temperature-Programmed Reduction of NiO/Al2O3 by Biochar In Situ Generated from Citric Acid. *Processes* **2022**, *10*, 1542.
151. Cheng, F.; Dupont, V.; Twigg, M.V. Temperature-programmed reduction of nickel steam reforming catalyst with glucose. *Applied Catalysis A: General* **2016**, *527*, 1-8.
152. Liu, N.; Song, X.; Wang, C.; Li, K.; Ning, P.; Sun, X.; Wang, F.; Ma, Y. Surface characterization study of corn-straw biochar catalysts for the simultaneous removal of HCN, COS, and CS 2. *New Journal of Chemistry* **2020**, *44*, 13565-13575.
153. Eltaweil, A.S.; Abdelfatah, A.M.; Hosny, M.; Fawzy, M. Novel biogenic synthesis of a Ag@ Biochar nanocomposite as an antimicrobial agent and photocatalyst for methylene blue degradation. *ACS omega* **2022**, *7*, 8046-8059.
154. Li, T.; Li, H.; Li, C. Hydrodeoxygenation of vanillin to creosol under mild conditions over carbon nanospheres supported palladium catalysts: Influence of the carbon defects on surface of catalysts. *Fuel* **2022**, *310*, 122432.
155. Inglezakis, V.; Poulopoulos, S. *Adsorption, ion exchange and catalysis*; Elsevier: 2006; Volume 3.
156. Chen, T.; Kwon, O.; Huang, R.; Lin, C.; Vohs, J.M. WOx promoted nickel catalyst for hydrodeoxygenation of m-cresol. *Journal of Catalysis* **2021**, *400*, 294-300.
157. Zhu, Z.; Tan, H.; Wang, J.; Yu, S.; Zhou, K. Hydrodeoxygenation of vanillin as a bio-oil model over carbonaceous microspheres-supported Pd catalysts in the aqueous phase and Pickering emulsions. *Green Chemistry* **2014**, *16*, 2636-2643.
158. Zhang, F.; Jin, Y.; Fu, Y.; Zhong, Y.; Zhu, W.; Ibrahim, A.A.; El-Shall, M.S. Palladium nanoparticles incorporated within sulfonic acid-functionalized MIL-101 (Cr) for efficient catalytic conversion of vanillin. *Journal of Materials Chemistry A* **2015**, *3*, 17008-17015.
159. Vázquez-Fuentes, L.F.; Cortés-Jacome, M.; López-Salinas, E.; Valente, J.S.; Gil, P.M.; Hernández-Cortez, J.; Toledo-Antonio, J.A. Selective Vanillin Hydrodeoxygenation on Synthetic Takovite Derived NiAlO x Mixed Oxide. *Topics in Catalysis* **2020**, *63*, 428-436.
160. Kayalvizhi, J.; Pandurangan, A. Hydrodeoxygenation of vanillin using palladium on mesoporous KIT-6 in vapour phase reactor. *Molecular Catalysis* **2017**, *436*, 67-77.
161. Aliu, E.; Hart, A.; Wood, J. Reaction kinetics of vanillin hydrodeoxygenation in acidic and nonacidic environments using bimetallic PdRh/Al2O3 catalyst. *Energy & Fuels* **2019**, *33*, 11712-11723.

162. Yang, X.; Liang, Y.; Cheng, Y.; Song, W.; Wang, X.; Wang, Z.; Qiu, J. Hydrodeoxygenation of vanillin over carbon nanotube-supported Ru catalysts assembled at the interfaces of emulsion droplets. *Catalysis Communications* **2014**, *47*, 28-31.
163. Arun, J.; Gopinath, K.P.; SundarRajan, P.; Shyam, S.; Mayuri, N.; Sivaramakrishnan, R.; Pugazhendhi, A. Upgradation of Nostoc punctriforme under subcritical conditions into liquid hydrocarbons (bio-oil) via hydro-deoxygenation: Optimization and engine tests. *Journal of Environmental Chemical Engineering* **2021**, *9*, 105230.
164. Varala, S.; Dharanija, B.; Satyavathi, B.; Rao, V.B.; Parthasarathy, R. New biosorbent based on deoiled karanja seed cake in biosorption studies of Zr (IV): Optimization using Box–Behnken method in response surface methodology with desirability approach. *Chemical Engineering Journal* **2016**, *302*, 786-800.
165. Kristensen, T.; Hulteberg, C.; Blomberg, S.; Tunå, P.; Abdelaziz, O. Parametric Analysis and Optimization of Vanillin Hydrodeoxygenation Over a Sulfided Ni-Mo/δ-Al2O3 Catalyst Under Continuous-Flow Conditions. *Topics in Catalysis* **2022**, 1-12.
166. Baş, D.; Boyacı, I.H. Modeling and optimization I: Usability of response surface methodology. *Journal of food engineering* **2007**, *78*, 836-845.
167. Pipitone, G.; Zoppi, G.; Bocchini, S.; Rizzo, A.M.; Chiaramonti, D.; Pirone, R.; Bensaid, S. Aqueous phase reforming of the residual waters derived from lignin-rich hydrothermal liquefaction: Investigation of representative organic compounds and actual biorefinery streams. *Catalysis Today* **2020**, *345*, 237-250.
168. Butler, E.; Devlin, G.; Meier, D.; McDonnell, K. A review of recent laboratory research and commercial developments in fast pyrolysis and upgrading. *Renewable and sustainable energy reviews* **2011**, *15*, 4171-4186.
169. Yan, K.; Wu, G.; Lafleur, T.; Jarvis, C. Production, properties and catalytic hydrogenation of furfural to fuel additives and value-added chemicals. *Renewable and sustainable energy reviews* **2014**, *38*, 663-676.
170. Niu, H.; Luo, J.; Li, C.; Wang, B.; Liang, C. Transfer hydrogenation of biomass-derived furfural to 2-methylfuran over CuZnAl catalysts. *Industrial & Engineering Chemistry Research* **2019**, *58*, 6298-6308.
171. Chen, X.; Zhang, L.; Zhang, B.; Guo, X.; Mu, X. Highly selective hydrogenation of furfural to furfuryl alcohol over Pt nanoparticles supported on g-C3N4 nanosheets catalysts in water. *Scientific reports* **2016**, *6*, 1-13.
172. Date, N.S.; Hengne, A.M.; Huang, K.-W.; Chikate, R.C.; Rode, C.V. Single pot selective hydrogenation of furfural to 2-methylfuran over carbon supported iridium catalysts. *Green Chemistry* **2018**, *20*, 2027-2037.
173. Winterbottom, J.M.; King, M. *Reactor design for chemical engineers*; CRC Press: 1999.
174. GHERIB, H. Préparation, Caractérisation et Activité Catalytique de Nanoparticules de Rhodium. 2022.
175. Perego, C.; Peratello, S. Experimental methods in catalytic kinetics. *Catalysis Today* **1999**, *52*, 133-145.
176. Chen, Y.; Miller, D.J.; Jackson, J.E. Kinetics of aqueous-phase hydrogenation of organic acids and their mixtures over carbon supported ruthenium catalyst. *Industrial & engineering chemistry research* **2007**, *46*, 3334-3340.
177. Zhang, Z.; Jackson, J.E.; Miller, D.J. Kinetics of aqueous-phase hydrogenation of lactic acid to propylene glycol. *Industrial & engineering chemistry research* **2002**, *41*, 691-696.
178. Cornils, B.; Herrmann, W.A.; Xu, J.-H.; Zanthoff, H.-W. *Catalysis from A to Z: a concise encyclopedia*; John Wiley & Sons: 2020.

179. Vannice, M.A.; Joyce, W.H. *Kinetics of catalytic reactions*; Springer: 2005; Volume 134.
180. Quitian, A.; Ancheyta, J. Experimental methods for developing kinetic models for hydrocracking reactions with slurry-phase catalyst using batch reactors. *Energy & Fuels* **2016**, *30*, 4419-4437.
181. Shi, Y. Theoretical study of the mechanism of furfural conversion on the NiCuCu (111) surface. *ACS omega* **2019**, *4*, 17447-17456.
182. Joseph, W. Three-phase catalytic reactors for hydrogenation and oxidation reactions. *Physical Sciences Reviews* **2016**, *1*, 20150019.
183. Yang, H.; Chen, H.; Zhou, W.; Fan, H.; Chen, C.; Sun, Y.; Zhang, J.; Wang, S.; Guo, T.; Fu, J. Construction of N, O co-doped carbon anchored with Co nanoparticles as efficient catalyst for furfural hydrodeoxygenation in ethanol. *Journal of Energy Chemistry* **2023**, *78*, 195-202.
184. Sitthisa, S.; Sooknoi, T.; Ma, Y.; Balbuena, P.B.; Resasco, D.E. Kinetics and mechanism of hydrogenation of furfural on Cu/SiO2 catalysts. *Journal of catalysis* **2011**, *277*, 1-13.

APPENDICES

Appendix A1: DOE matrix and results obtained from Hydrodeoxygenation of Vanillin to p-creosol

Exp. no	Temperature (ºC)	Pressure (bar)	Catalyst (g)	VL Conv. (%)	P-creosol yield (%)
1	100	30	0.6	11.80	5.11
2	150	30	0.6	71.80	62.61
3	100	50	0.6	26.30	12.48
4	150	50	0.6	97.00	91.17
5	100	40	0.4	20.60	13.28
6	150	40	0.4	87.70	83.15
7	100	40	0.8	23.70	15.30
8	150	40	0.8	95.10	87.30
9	125	30	0.4	25.50	18.23
10	125	50	0.8	48.20	33.78
11	125	30	0.8	35.50	22.29
12	125	50	0.8	52.66	44.46
13	125	40	0.6	41.40	32.70
14	125	40	0.6	40.19	34.44
15	125	40	0.6	44.80	35.15

Appendix B: GC Calibration Curves

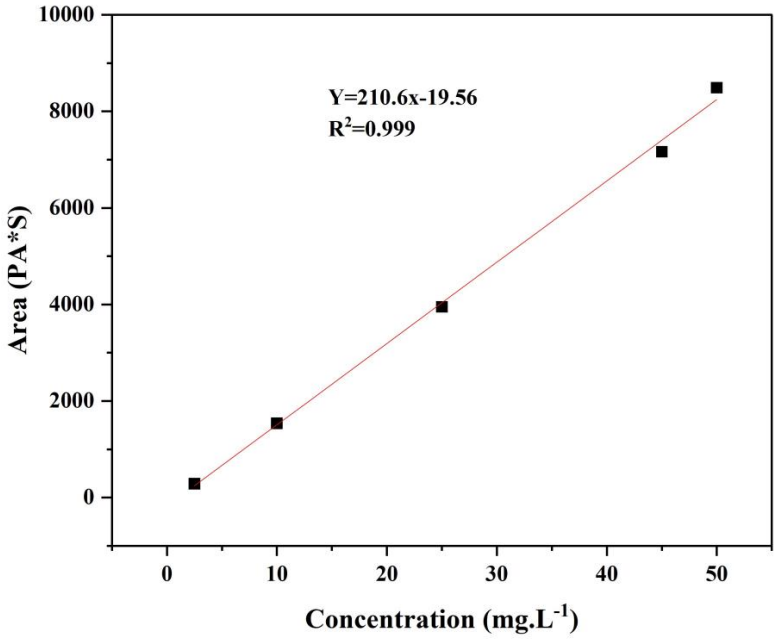

Figure B1: Vanillin calibration curve

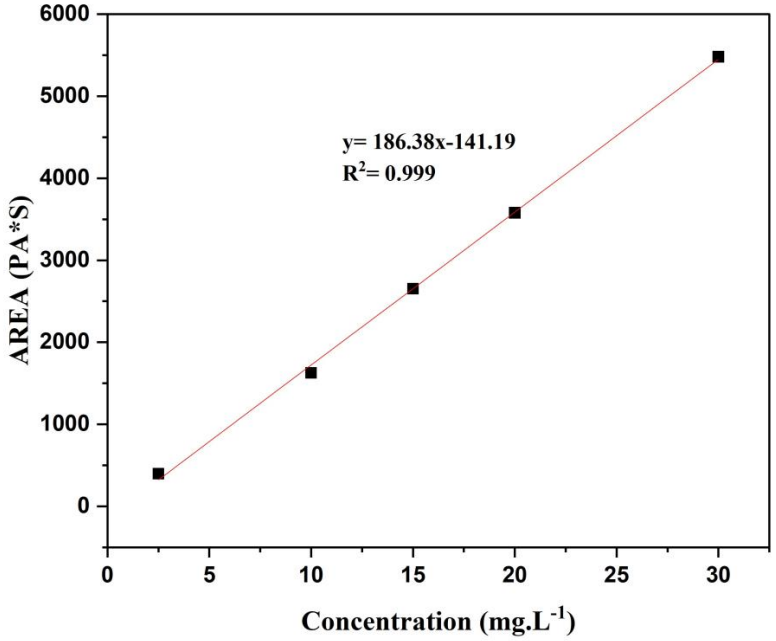

Figure B2: Vanillyl alcoholVanillin calibration curve

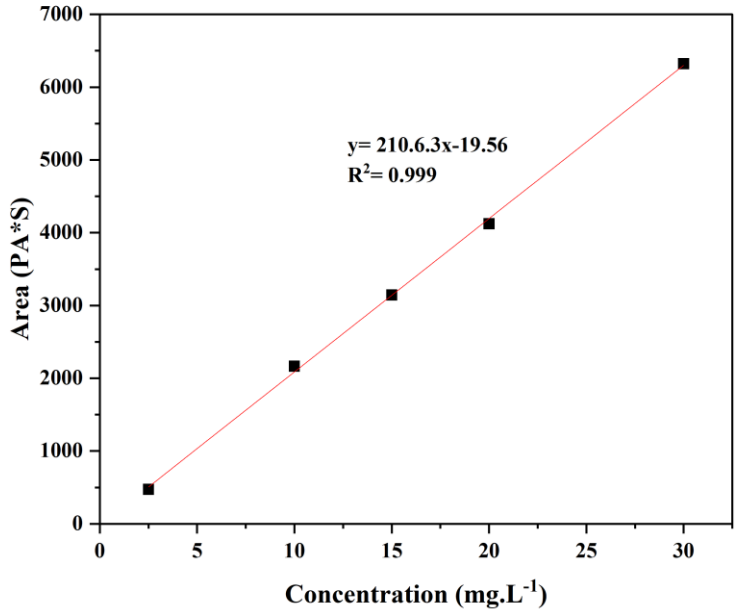

Figure B3: P-creosol calibration curve

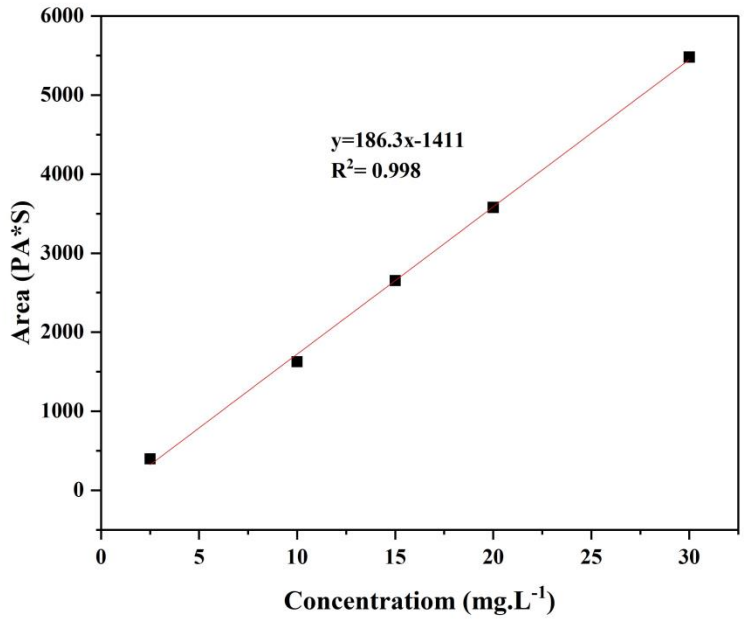

Figure B4: Furfural calibration curve

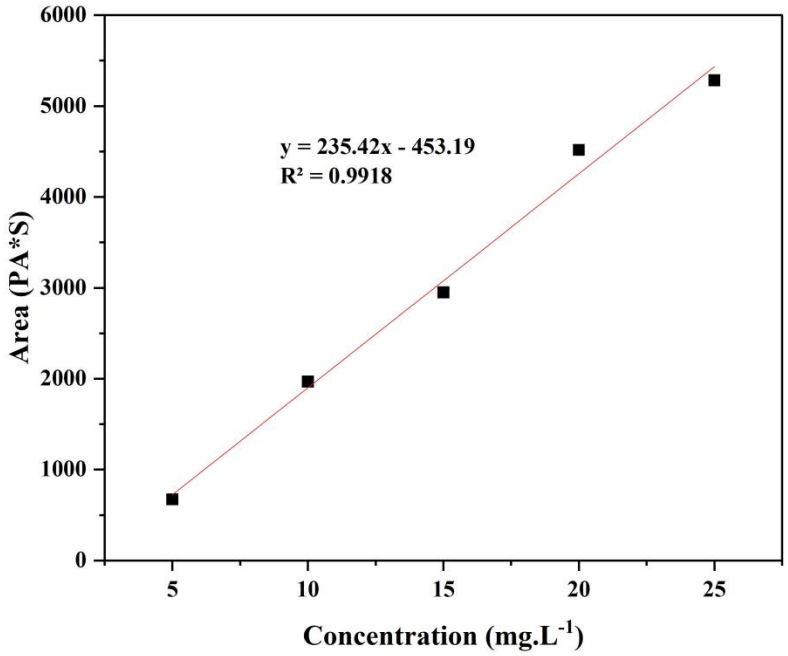

Figure B5: Furan calibration curve

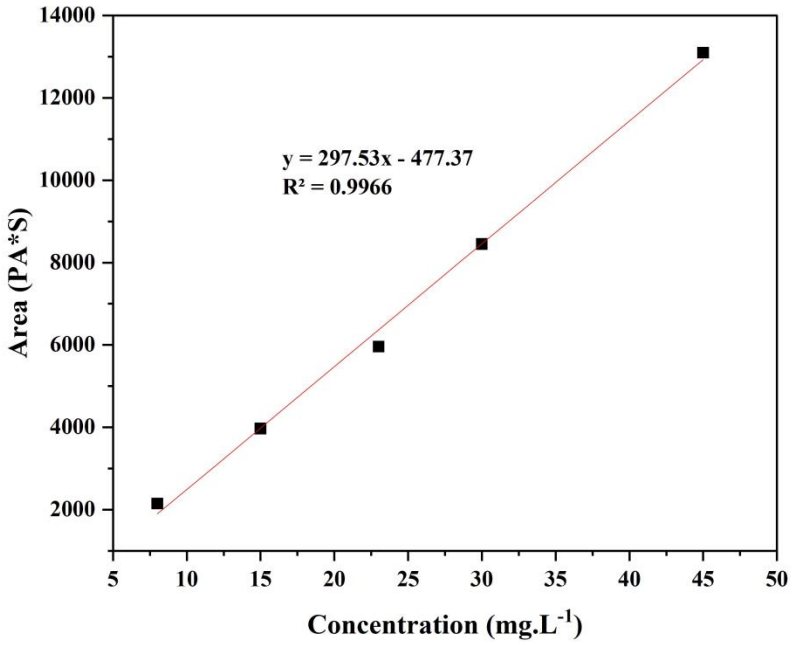

Figure B6: 2-Methylfuran calibration curve

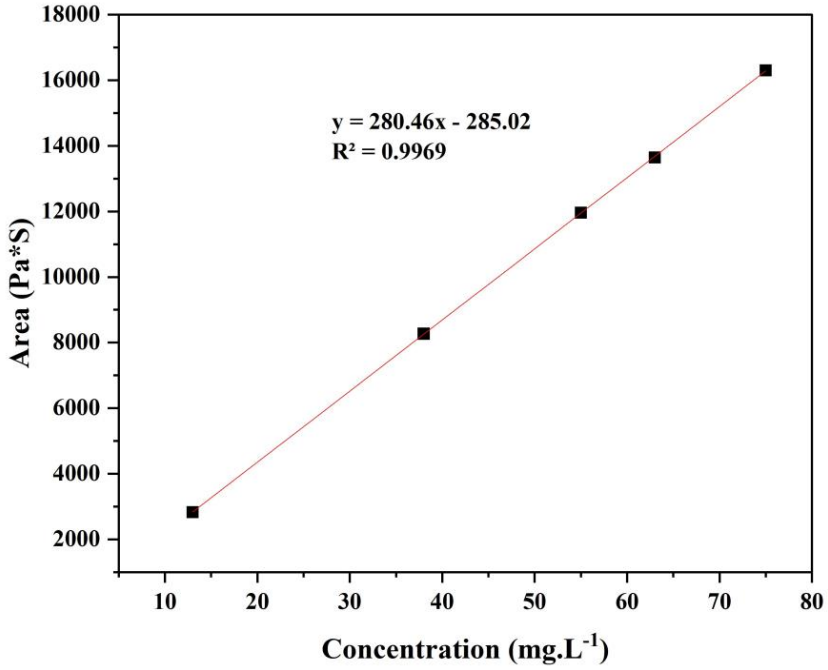

Figure B7: Tetrahydrofuran calibration curve.

Appendix C: Preliminary Analysis for the HDO of Vanillin

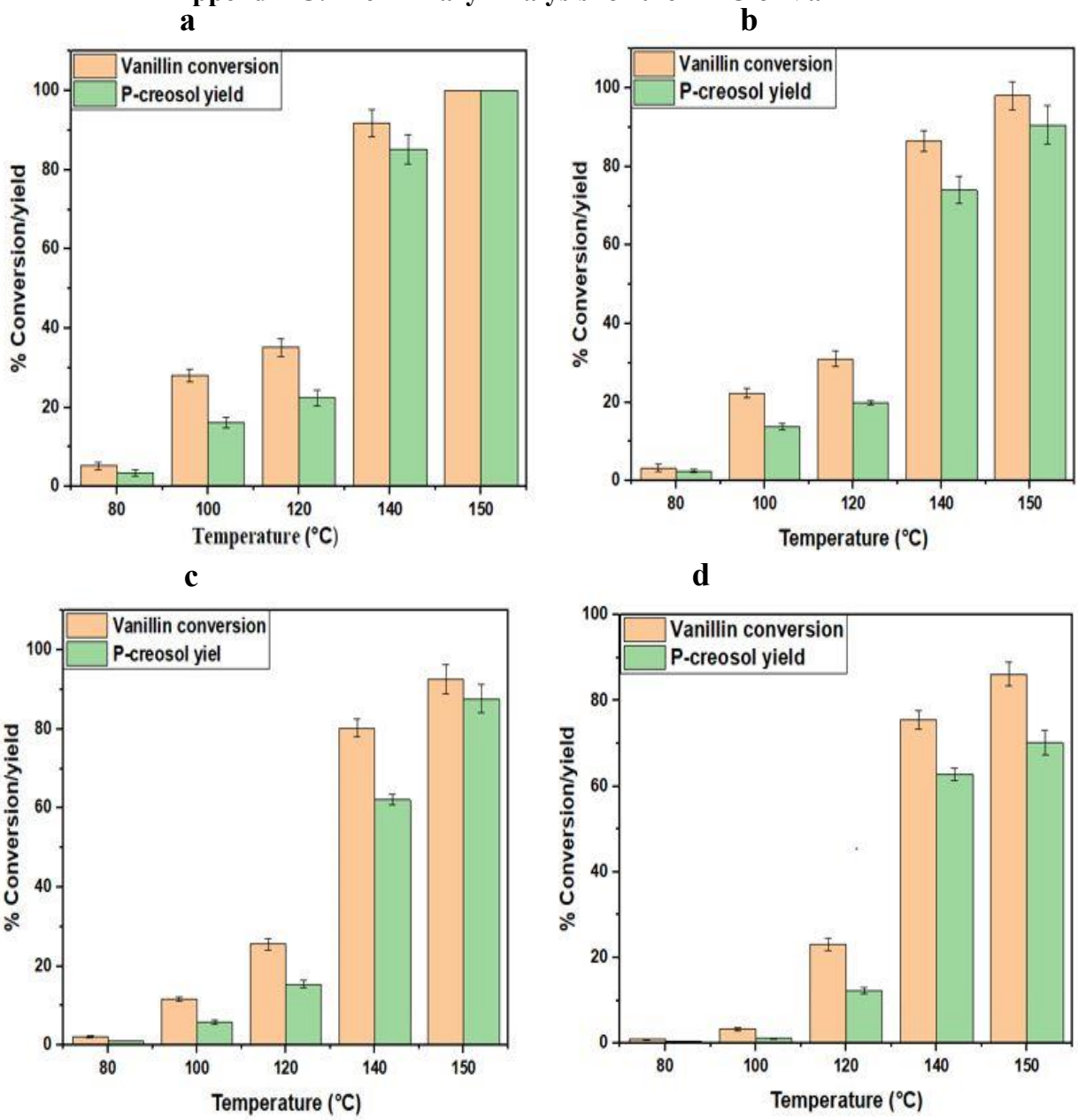

Figure C1: Preliminary study, showing vanillin conversion and p-creosol yield (reaction conditions: initial substrate concentration 0.33 M, **50 bar** agitation speed 1000 rpm) a) 0.8 g catalyst loading b) 0.6 g catalyst loading c) 0.4 g catalyst loading and d) 0.2g catalyst loading.

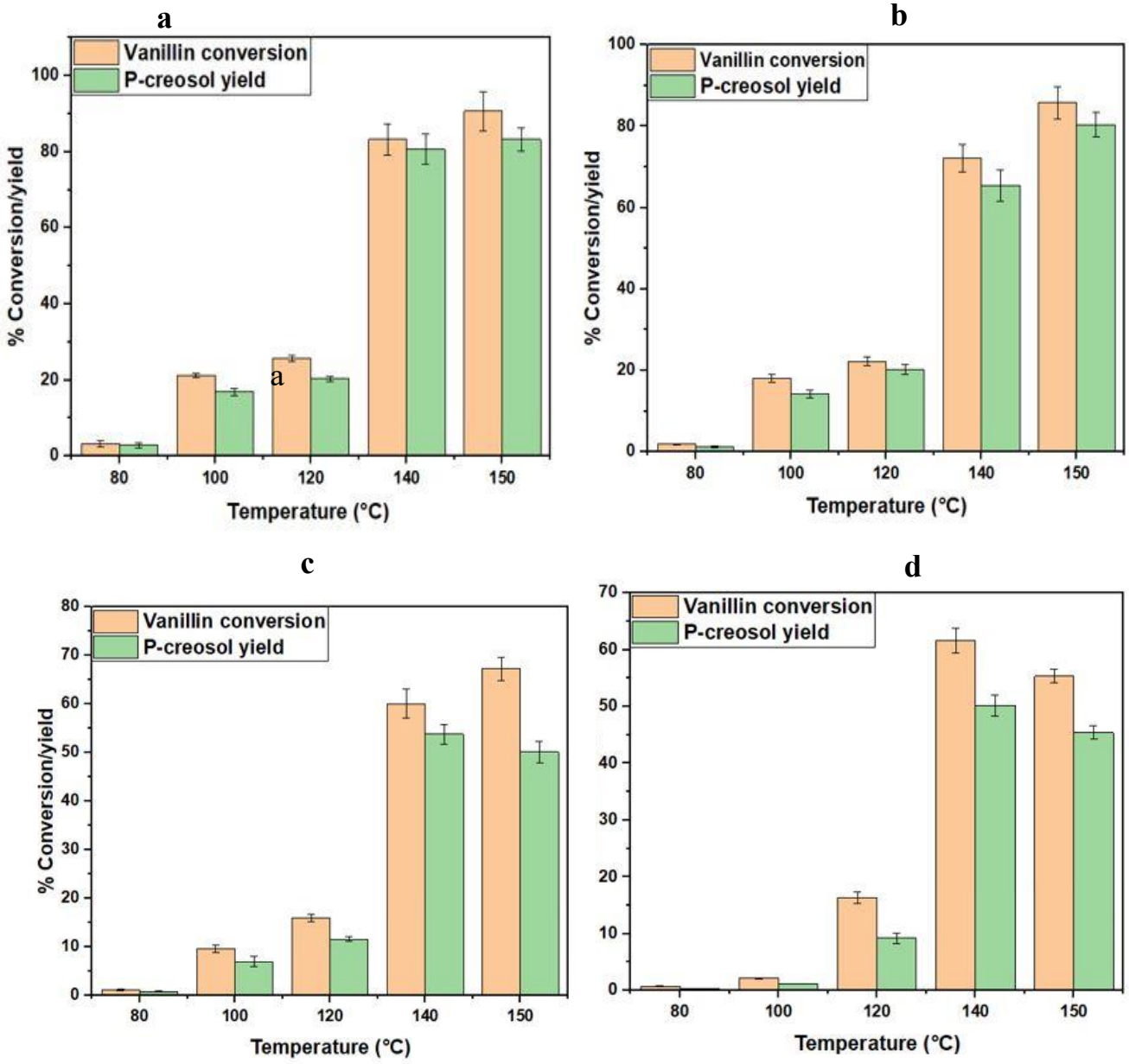

Figure C2: Preliminary study, showing vanillin conversion and p-creosol yield (reaction conditions: initial substrate concentration 0.33 M, **40 bar** agitation speed 1000 rpm) a) 0.8 g catalyst loading b) 0.6 g catalyst loading c) 0.4 g catalyst loading and d) 0.2g catalyst loading.

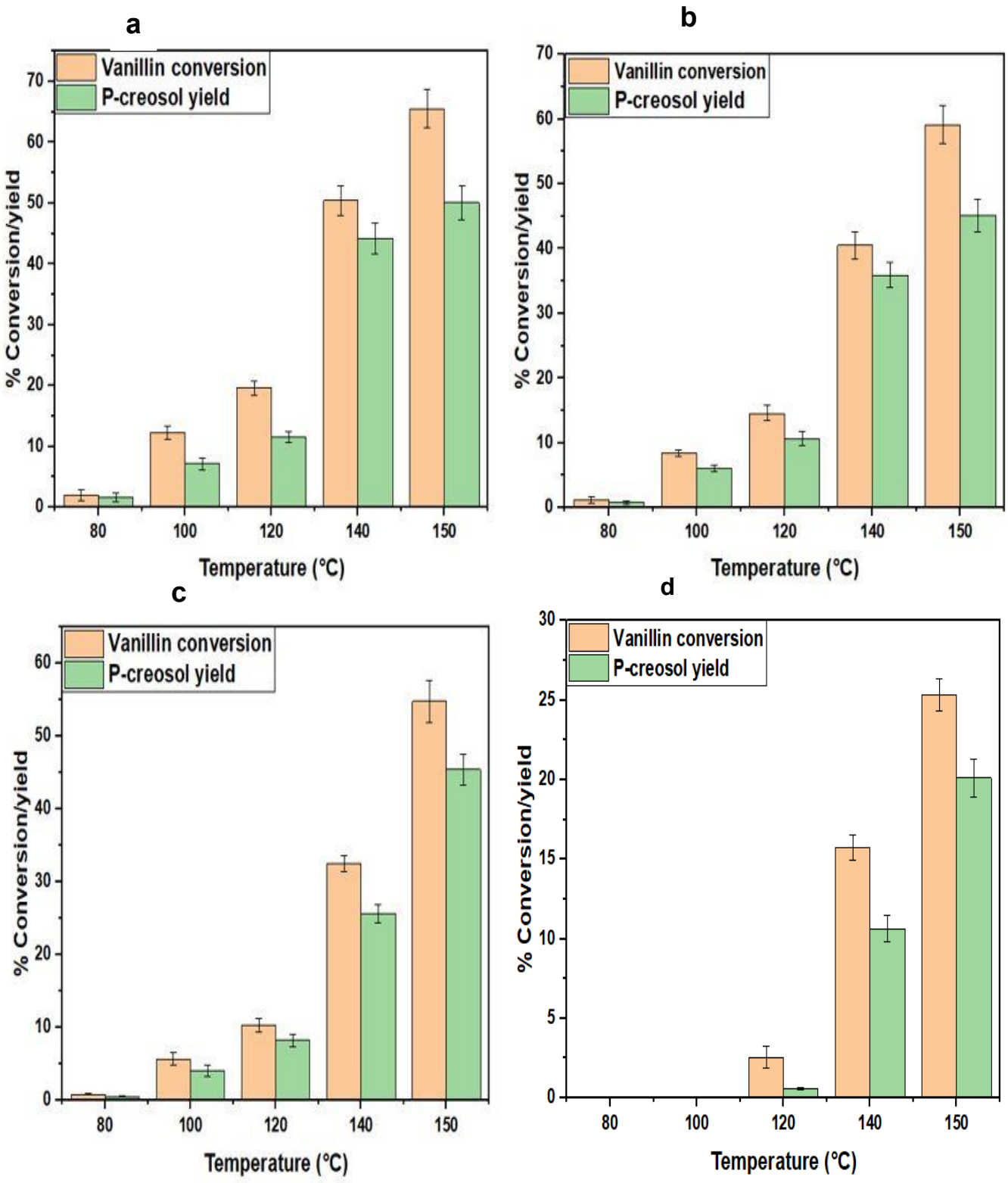

Figure C3: Preliminary study, showing vanillin conversion and p-creosol yield (reaction conditions: initial substrate concentration 0.33 M, **30 bar** agitation speed 1000 rpm) a) 0.8 g catalyst loading b) 0.6 g catalyst loading c) 0.4 g catalyst loading and d) 0.2g catalyst loading.